Ph.D. Dissertation

MODIFICATION OF THE ACTIVITY OF HYDROLYTIC ENZYMES BY THE NATURE OF THE NON-ENDOGENOUS/NON-NATIVE METAL IONS

By

ZEYAD HASAN ABDULLAH NAFAEE

Supervised by

Associate Professor Dr. BÉLA GYURCSIK

Doctoral School of Chemistry

Department of Molecular and Analytical Chemistry

Faculty of Science and Informatics, University of Szeged, Hungary

2024

Table of contents

1. INTRODUCTION 1
2. LITRETURE REVIEW 3
2.1. β-lactamases 3
2.1.1. Class A β-lactamases 4
2.1.2. TEM-1 β-lactamase 5
2.1.2.1. Structure of TEM-1 β-lactamases 6
2.1.2.2. Expression and purification of TEM-1 β-lactamases 7
2.1.2.3. Possible interaction of metal ions with TEM-1 β-lactamases 8
2.1.2.4. Catalytic mechanism of TEM-1 β-lactamases 9
2.1.2.5. Kinetics of TEM-1 β-lactamases 10
2.2. Metal ions in biocatalysis 13
2.2.1. Metallonuclease Colicins 15
2.2.2. Nuclease domain of colicin E7 15
2.2.3. Metal ion binding of NColE7 19
2.2.4. NColE7 interaction with DNA 20
2.2.5. Catalytic mechanism of NColE7 21
3. AIMS AND OBJECTIVES 24
4. REAGENTS AND METHODS 28
4.1. Reagents 28
4.2. Production of proteins 28
4.2.1. Gene amplification and mutation by PCR 29
4.2.2. Cleavage of the gene and carrier DNA and their ligation 31
4.2.3. Transformation of the bacterial cells for DNA cloning 32
4.2.4. Expression of proteins 32
4.3. Methods of protein purification 33
4.3.1. Affinity chromatography 34
4.3.2. Anion exchange chromatography 36
4.4. Detection of proteins by SDS-PAGE 37

4.5. Detection of DNA by agarose gel electrophoresis 39
4.6. Study of proteins by mass spectrometry 40
4.7. Study of proteins by circular dichroism spectroscopy 43
4.8. Determination of protein concentration 45
4.9. Study of TEM-1 β-lactamase by PAC spectroscopy 46
4.10. Catalytic activity of enzymes 47
4.10.1. Catalytic activity of NColE7 mutants 47
4.10.2. Kinetic investigation of TEM-1 β-lactamase 48
4.11. Bacterial viability assays 48
5. RESULTS AND DISCUSSION 50
5.1. TEM-1 β-lactamase 50
5.1.1. TEM-1 β-lactamase expression 50
5.1.2. TEM-1 β-lactamase purification strategy 52
5.1.3. Characterization of the purified TEM-1 β-lactamase 56
5.1.3.1. Mass spectrometric measurements 56
5.1.3.2. Circular dichroism spectroscopic measurements 58
5.1.3.3 Catalytic activity of TEM-1 β-lactamase 59
5.1.4. Catalytic activity of metallized TEM-1 β-lactamase 69
5.1.5. Interaction of TEM-1 β-lactamase with Ni(II) 73
5.1.5.1. CD spectroscopic measurements 73
5.1.5.2. Mass spectrometric measurements 74
5.1.6. Interaction of TEM-1 β-lactamase with Cd(II) and Hg(II) ions 76
5.1.6.1. CD spectroscopic measurements 76
5.1.6.2. Mass spectrometric measurements 77
5.1.6.3. PAC spectroscopic measurements 78
5.1.7. The effect of metal ions on bacterial cells expressing TEM-1 β-lactamase 80
5.2. NColE7 nuclease and its mutants 83
5.2.1. Expression and purification of NColE7 mutants 84
5.2.2. Solution structural studies of NColE7 mutants 86
5.2.2.1 CD spectroscopic measurements 86
5.2.2.2. Mass spectrometric measurements 91
5.2.3. Catalytic activity of KGNK 96

5.2.3.1 Catalytic activity in presence of Zn(II) ion and EDTA 96
5.2.3.2 Catalytic activity in the presence of non-native metal ions 98
5.2.3.3. The effect of metal ion competition on the catalytic activity 99
5.2.4. Catalytic activity of KGNK-His in the presence of non-native metal ions 100
6. SUMMARY AND FUTURE OUTLOOK 102
7. REFERENCES 107
ACKNOWLEDGEMENTS 113
PUBLICATION LIST 115
APPENDIX 116
Section A1. Role of metal ions in metallo-β-lactamases 116
Section A2. The steps of the catalytic mechanism of TEM-1 β-lactamases 116
Section A3. The domains structure of colicins 117
Tables A1-A3 119
Schemes A1-A3 123
Figures A1-A12. 125
Protocols A1-A6 131
References related to the Appendix 135
Abbreviations 136

1. INTRODUCTION

Proteins may require metal ions of specific properties and structure to perform their functions associated with life. A protein that binds a metal ion in complex form is called a metalloprotein, and a metal ion is called a cofactor. It is estimated that 50% of all proteins contain metal ions, and 30% of all proteins require metal ions in for their functions. Metal ions play important and essential roles in biological systems, particularly in association with the proteins, such as catalytic, electron-transfer, structural and storage roles. Metal ions are coordinated by nitrogen, oxygen, or sulfur donor atom containing functional groups of the side chains of amino acid residues of the proteins. These groups are mainly the imidazoles of histidine residues, thiolates of cysteine residues, and carboxylates of aspartates and glutamates. In addition, many organic cofactors function as ligands, such as tetradentate N4 macrocyclic compounds incorporated into the *e.g.*, heme proteins. Metalloproteins that perform a catalytic function are called metalloenzymes, promoting chemical transformations in a molecule (substrate). All proteins offering sites for potential metal ion binding, may be affected by non-native/non-endogenous metal ions found in the environment. Metal ion contamination therefore, may change the behavior of biological systems *e.g.*, bacteria by modification of the structural properties of cellular proteins and enhancing or repressing their function.

In this PhD thesis, the two main topics include the study of the interaction of non-endogenous/non-native metal ions with two types of bacterial enzymes: TEM-1 β-lactamase and NColE7 nuclease mutants are common targets of scientific research due to their relationship to antibacterial action and resistance, as well as to the design of artificial metallonucleases for gene therapy. Both enzymes are hydrolases and part of the defense systems of the bacteria. TEM-1 β-lactamase protects bacteria from β-lactam antibiotics, while NColE7 is the nuclease domain of colicin E7 that cleaves chromosomal DNA of the other bacteria under stress conditions and in case of lack of the nutrients. TEM-1 β-lactamase hydrolyzes the β-lactam ring, while NColE7 cleaves the phosphodiester bond of DNA non-specifically. Furthermore, the human body is usually infected by different kinds of bacteria and some of these may carry the genes of either TEM-1 β-lactamase or colicin E7 or both. The availability of the metal ions in surroundings may result in the change of the behaviour of these bacteria. We hypothesize that the TEM-1 β-lactamase interacts with toxic borderline metal ions, such as Ni(II) and soft metal ions, such as Hg(II) and Cd(II), leading to

changes in its function. The Zn(II)-binding site of NColE7 or its mutants is suggested to be able to accommodate other metal ions such as Ni(II), Cu(II), and Cd(II) ions. This can lead to changes in the structural properties and function of these enzymes. The results presented here are expected to contribute to the development of new strategies for protein purification, to better understanding of the kinetic behavior of β-lactamase and the metal ion-protein interaction, and antibiotic development, as well as the regulation of the nuclease activity of artificial nucleases.

2. LITRETURE REVIEW

2.1. β-lactamases

β-Lactam derivatives are the most common antibiotics targeting penicillin-binding enzymes, such as bacterial carboxy-transpeptidases, which are involved in synthesis of the bacterial cell wall. β-Lactam antibiotics are used to target a broad spectrum of both Gram-positive and negative pathogenic bacteria. However, β-lactamases, produced by bacteria, pose a grave threat to the efficacy of β-lactam drugs [1]. β-Lactamase enzymes protect bacteria by hydrolyzing the β-lactam ring of the antibiotics before they can interact with bacterial target proteins thus, providing resistance toward β-lactam antibiotics [2]. β-Lactamases are produced by both Gram-positive and Gram-negative bacteria, [3], and the enzymes are secreted when the antibiotics appear in the environment [4]. β-Lactam antibiotic rings are present in several antibiotics (**Fig. 2.1**) developed continuously, such as penicillins, some cephalosporins (early-generation cephalosporin), cephamycins, monobactams and carbapenes.

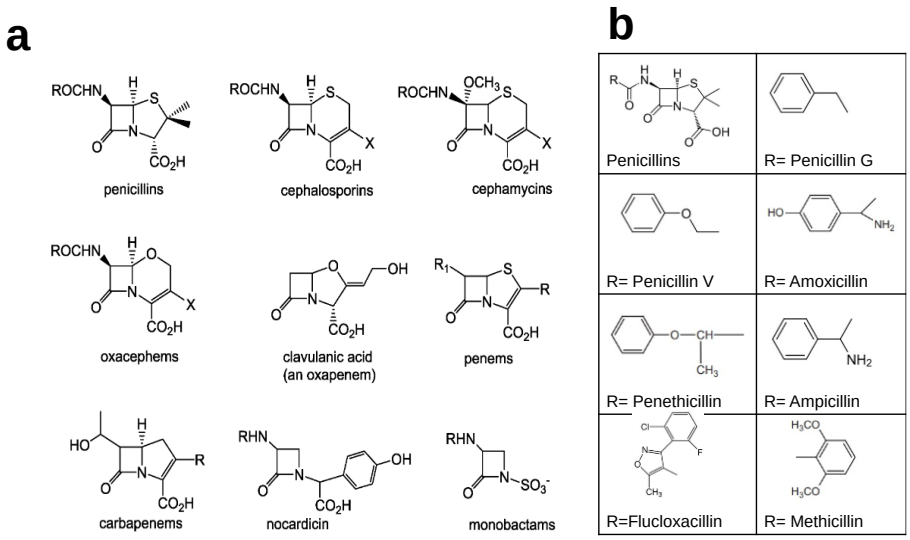

Figure 2.1. a) The chemical structures of the β-lactam antibiotics. **b**) The chemical structures of some penicillin antibiotics.

Nevertheless, bacteria evolve new β-lactamases in response to the new antibiotics called extended-spectrum β-lactamases (ESBLs). [1;5] β-Lactamases form a large family of enzymes as demonstrated by their database (www.bldb.eu) that contains over 4300 members [6]. Two systems of β-lactamase classification evolved: (i) the Bush–Jacoby–Medeiros classification is based on

their catalytic activity [3] and the (ii) Ambler system [7] is based on the sequence information. The latter divides β-lactamases into four distinct classes, termed A, B, C, and D that are identified based on the specific sequence motifs, while it also distinguishes the enzymes by fundamental differences in hydrolytic mechanism. Classes A, C and D are serine enzymes possessing the active-site with a characteristic Ser-Xaa-Xaa-Lys (SXXK) motif. Serine β-lactamases (SBLs) are distantly related to penicillin-binding proteins (PBPs) [8] having the same structure around the active center, and mechanism towards the β-lactam targets. Ser in the active center is employed as a nucleophile to attack β-lactams forming a covalent acylenzyme intermediate [3;9;10;11;12 The class A, C and D β-lactamases share structural similarities with the target of β-lactam antibiotics which are bacterial penicillin-binding proteins [13;14], and with transpeptidases in the residues around the active center [15]. Class B enzymes comprise a heterogeneous group of Zn(II) metalloenzymes known as metallo-β-lactamases (MBLs) containing a His-Xaa-His-Xaa-Asp (HXHXD) motif that is a metal ion binding site for Zn(II) at the interface of two β-sheets, building up the active center [10;16;17]. MBLs utilize a Zn(II) ion-activated water nucleophile for the hydrolytic reaction [3;9;10;12;18].

2.1.1. Class A β-lactamases

Class A β-lactamases include some familiar enzyme groups such as TEM, SHV, CTX-M, PER, VEB, GES, IBC (the abbreviations are detailed in Appendix), and others. Class A β-lactamases in Gram-positive bacteria are called penicillinases [19]. Penicillinase is a specific type of β-lactamase hydrolyzing the β-lactam ring of penicillins. The first β-lactamase to be identified was a penicillinase. Even before penicillin was used in medicine, Abraham and Chain isolated penicillinase from Gram-negative *E. coli* in 1940 [20].

Temoniera β-lactamase (TEM β-lactamase) was isolated from Temoniera (Athenian patient) feces culture in 1963 [21]. This type of enzymes catalyze most of β-lactam antibiotics such as penicillins, some generations of cephalosporins (early cephalosporins), carbapenems but they are ineffective catalysts for extended spectrum cephalosporin [22;23]. Currently, there are more than 250 types of TEM β-lactamases. The amino acid substitutions or mutations around the active site of the enzyme are responsible for the extended-spectrum phenotype. TEM β-lactamases show certain similarities in their amino acid sequences (**Fig. 2.2**) with sulfhydryl variant β-lactamases (SHV β-lactamases) [24] found in the *K. pneumoniae* (~ 68%), and with cefotaximases (CTX-M) found mainly in strains of *S. enterica, S. typhimurium, E. coli*, and other enterobacteriaceae (~ 40%).

Figure 2.2. Sequence alignment of different types of class A β-lactamase representatives. All these enzymes have the same active site, which is SXXK highlighted by yellow. All these enzymes share also the residues Ser130, Glu166, and Asn170 (highlighted by green, blue and grey respectively) (numbering of amino acids according to ref. [25]) in the same positions. In addition, the omega loop (underlined residues) sequence of these enzymes is almost identical in the majority of class A β-lactamases.

Even though the PER, VEB, GES, and IBC class A β-lactamases are uncommon ESBLs, they also share the same SXXK active site, and the Ser130, Glu166, and Asn170 residues that are responsible for the hydrolysis of the β-lactam molecules (**Fig. 2.2**). This suggests that these enzymes apply the same hydrolytic mechanism in spite of the other part of their amino acid sequences are rather different.

2.1.2. TEM-1 β-lactamase

TEM-1 β-lactamase is responsible for the ampicillin and penicillin resistance in *H. influenzae* and *N. gonorrhoeae*, and about 90% of ampicillin resistance in *E. coli* [26]. Over 170 natural and even more *in vitro* established catalytically active mutants of TEM-1 β-lactamases were reported. [27-29]. TEM-1 β-lactamase and its mutants, as the source of the extended spectrum serine β-lactamases and development of bacterial antibiotic resistance are frequent targets of the scientific

research [23;30-37]. Mutagenesis is also a useful research tool, that provides information about the interactions between the enzyme and the antibiotics. Such studies revealed that 220 residues of TEM-1 β-lactamase could be substituted, while maintaining the hydrolytic activity against ampicillin. Thus, only 43 out of the 263 amino acid residues are essential for function [23].

The gene of TEM-1 β-lactamase is incorporated into various DNA vectors to be applied as a selectable marker in biochemistry research. Bacteria for laboratory purposes *e.g.*, for DNA cloning or protein expression, gain ampicillin resistance by expressing this enzyme and therefore, can be selected against non-desired bacteria in the presence of antibiotic.

2.1.2.1. Structure of TEM-1 β-lactamases

Extensive investigations were carried out to determine the TEM-1 β-lactamase structure and function. The full-length *E. coli* TEM-1 β-lactamase sequence consists of 286 amino acids but only the 24-286 residues were detected by the X-ray diffraction method, consistent with the mature protein. The N-terminal 1-23 residues form a signal peptide sequence required for export of the protein in a locally unfolded state via the secretory system through the cytoplasmic membrane into the periplasm. In parallel, the signal sequence is cleaved, resulting in the mature TEM-1 β-lactamase that is able to fold into its functionally correct conformation [38;39]. The secondary structure of the enzyme is composed of 35% α-helix, 16% β-sheets, 49% turn, and others (**Fig. 2.3**) as obtained from the analysis of the crystal structures by BeStSel online tool [40-43].

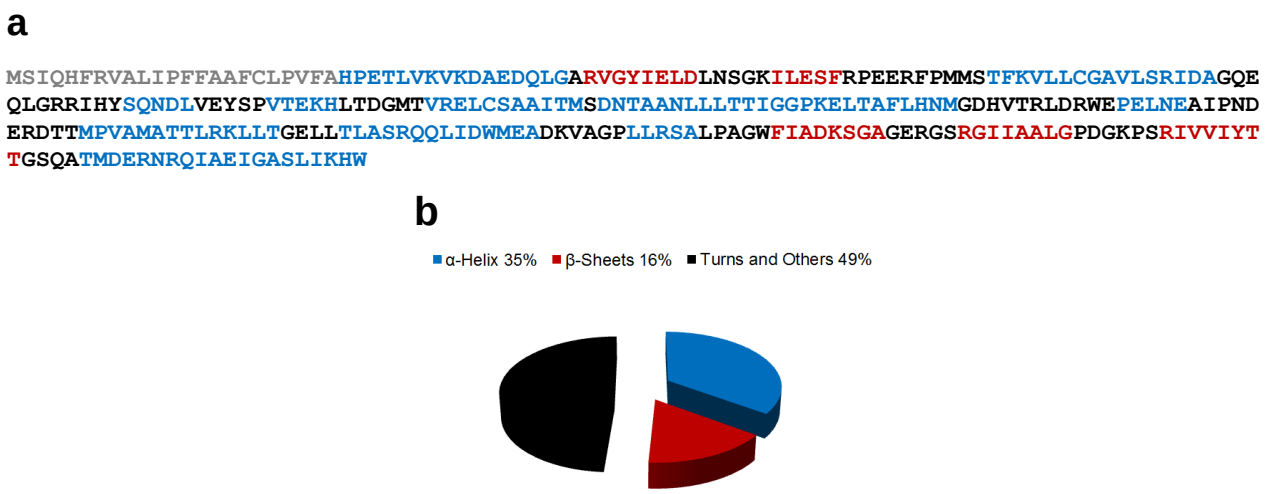

Figure 2.3. a) The 1-286 amino acid sequence of the *E. coli* TEM-1 β-lactamase (PDB code: 1ZG4) including the 1-23 signaling peptide in grey. **b**) The 3-D pie chart represents the composition of the secondary structure elements of the 24-286 mature protein sequence. The colors of the secondary structures are consistent with the colors in panel a).

Examples of crystal structures of TEM-1 β-lactamases solved so far, are the wild-type TEM-1 β-lactamase at 1.55 Å (PDB ID: 1ZG4), 6α-hydroxymethyl-penicillanate complexed to the TEM-1 β-lactamase (PDB ID: 1TEM), TEM-1 β-lactamase in complex with a designed boronic acid inhibitor (PDB ID: 1ERM), and the most stable TEM-1 β-lactamase variant (PDB ID: 3DTM). While few mutations can be revealed by comparing the amino acid sequences (**Fig. A1** in Appendix), these crystal structures can be considered identical based on the alignment of the structures (**Fig. 2.4**).

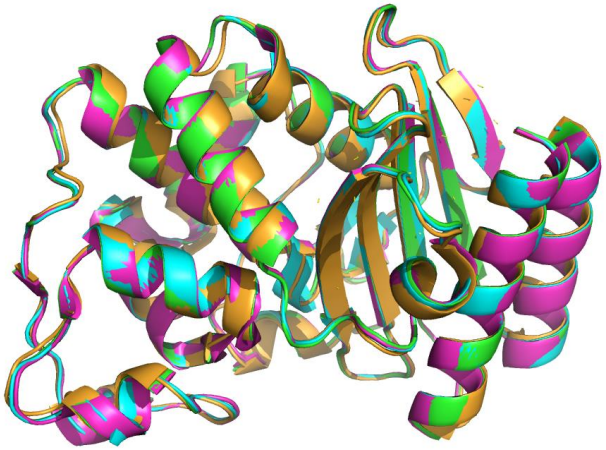

Figure 2.4. Alignment of selected crystal structures of TEM-1 β-lactamases (PDB ID: 1ZG4, 1TEM, 1ERM, 3DTM). From ref. [P1] (P1-3 are publications related to this dissertation).

2.1.2.2. Expression and purification of TEM-1 β-lactamases

Since TEM and closely related β-lactamases are soluble proteins, found in the periplasmic space, they are usually obtained from the large volume of the bacterial culture. Therefore, the first step of the purification is usually the concentration of the protein by precipitation using 20-65% (*w/v*) ammonium sulfate. Then the protein is renatured usually by dialysis. The native protein is purified is diferrent subsequent ion-exchange and gel filtration chromatographic steps. Examples of this purification method were *e.g.*, the *E. coli* strain W3310 R-factor-mediated penicillinase [44] and the wild-type TEM-2 β-lactamase and its mutant [45]. The ptac11K plasmid TEM-1 β-lactamase and its mutants were urified in native conditions using anion exchange chromatography, although the enzyme is weakly bound to this column. This was followed by a gel filtation, and a second strong anion-exchange step [46].

β-Lactamases were also purified by affinity methods. For this the β-lactam antibiotics substrate is bound to agarose support were applied for *N. gonorrhoeae* β-lactamase [47]. Affinity chromatography based on boronic acid-agarose linked either hydrophilic (type L) or hydrophobic (type B) spacer arms can be used to purify β-lactamases that are inhibited by boronic acid. This technique is rapid, selective, and single-step purification that is resulted a high yield of *P. maltophilia* β-lactamase [48]. The initial eluate of anion exchange step of TEM-1 β-lactamase was further purified using immunoaffinity chromatography on a Sepharose 4B column containing monoclonal antibody B3, which is a specific ligand to TEM-1 β-lactamase. The target protein was eluted by benzylpenicillin or cloxacillin. The drawback of this method that benzylpenicillin is hydrolyzed quickly and this causes losing its ability to elute the enzyme, while cloxacillin probably inhibit the enzyme irreversibly [49].

TEM-1 β-lactamase was also purified on a Zn(II)-bound chelating Sepharose column elutedby a gradual decrease of pH from 7.5 to 4.0 [50]. Yang et al., purified the enzyme using Ni(II)-bound NTA resin in a batch method, followed by size exclusion chromatography [51]. These experiments indicated that TEM-1 β-lactamase has an intrinsic affinity to bind a metal ion.

2.1.2.3. Possible interaction of metal ions with TEM-1 β-lactamases

TEM-1 β-lactamase is not a metalloenzyme, but the amino acid sequence offers a large number of possible metal ion binding sites in the sidechains of seven His residues, three Cys residues, ten Met residues, and several Asp and Glu residues (**Fig. 2.5**). These are the nitrogen donors of imidazole groups in the His7, His26, His96, His112, His153, His158, and His289 residues; the sulfur donor atoms of thiol and thioether groups in Cys20, Cys77, Cys123 residues; the Met3, Met68, Met69, Met117, Met129, Met155, Met182, Met186, Met211, Met272 residues, respectively; according to the standard numbering of enzyme by [25] as well as the negatively charged oxygen containing donor groups of Asp and Glu amino acids.

MSIQHFRVALIPFFAAFCLPVFAHPETLVKVKDAEDQLGARVGYIELDLNSGKILESFRPEERFP
MMSTFKVLLCGAVLSRIDAGQEQLGRRIHYSQNDLVEYSPVTEKHLTDGMTVRELCSAAITMSDN
TAANLLLTTIGGPKELTAFLHNMGDHVTRLDRWEPELNEAIPNDERDTTMPVAMATTLRKLLTGE
LLTLASRQQLIDWMEADKVAGPLLRSALPAGWFIADKSGAGERGSRGIIAALGPDGKPSRIVVIY
TTGSQATMDERNRQIAEIGASLIKHW

Figure 2.5. The amino acid sequence of the *E. coli* TEM-1 β-lactamase. The amino acids containing potential donor groups for metal ion coordination are colored: His-blue, Cys and Met-orange and Asp and Glu-red, the underlined residues represent the active site.

While a 23 amino acid long N-terminal sequence, constituting the signal peptide, is cleaved off to form the mature enzyme, metal ion chelation of the protein may still occur by several amino acid side-chains. The His residues offer binding sites for borderline transition metal ions such as e.g., Cu(II), Ni(II), Co(II) and Zn(II). The Cys thiolates can bind mainly soft metal ions (*e.g.*, Hg(II), Ag(I), Cu(I)) with high affinity. Although Hg(II) can also bind to His side chains, but in general, its affinity towards the imidazole nitrogen is low [52].

The sulfur donor atoms of the thioether groups are able to bind Hg(II) and more weakly Cd(II) in various amino acids, peptides and proteins [53-56]. Crystal structure studies of Hg(II) bis-methioninate complex, revealed that the Hg(II)-ion interacts with two thioether groups with the Hg-S distances of 2.5 Å [57]. The apparent stability constant (*K'*) for a monodentate thioether coordinated Hg(II) is in the order of ~10^5 M^{-1} in ternary complexes [58]. Methionine based turn-on sensors have been successfully applied for the selective detection of Hg(II) [59;60]. The apparent dissociation constant (K_d) obtained for the methionine sidechain of peptide models of the Ctr1 copper transport protein coordinated Cu(I) ion was found to be between 2 and 10 μM [61], reflecting a similar binding strength of the soft Cu(I) to that of the Hg(II)-methionine mentioned above. Furthermore, Delangle and coworkers showed that Cu(I) ion interacts strongly with a preorganized binding site consisting of methionines with an increased metal binding affinity by several orders of magnitude [62]. The presence of carboxyl groups of aspartic and glutamic acid units, carboxamide groups of asparagine and glutamine residues, as well as hydroxy groups of serine and threonine residues near to N or S donor containing groups may increase the binding affinity of the metal ions by offering further O donor atoms for coordination [63-66].

We highlight the possible roles of metal ions in the hydrolysis of β-lactam antibiotics by including a short summary of metallo-β-lactamases in **Section A1** in Appendix.

2.1.2.4. Catalytic mechanism of TEM-1 β-lactamases

Class A β-lactamase mechanism is similar to serine proteases, therefore class A β-lactamases are called serine β-lactamases [67]. The active sites of TEM-1 β-lactamases contain a SXXK motif with Ser functioning as a nucleophile in β-lactam hydrolysis by forming a covalent acylenzyme intermediate [6;10]. The class-A β-lactamase catalytic mechanism includes two main stages: acylation and de-acylation (**Scheme 2.1**) [68]. The mechanism is still under debate, which is described briefly in **Section A2** in Appendix. However, the different descriptions agree in the important role of the activated Ser70 as a nucleophile attacking the β-lactam carbonyl carbon in

the acylation step [69], in which the acyl-enzyme intermediate (tetrahedral oxyanion transition state) is formed (**Scheme 2.1**) [70;71].

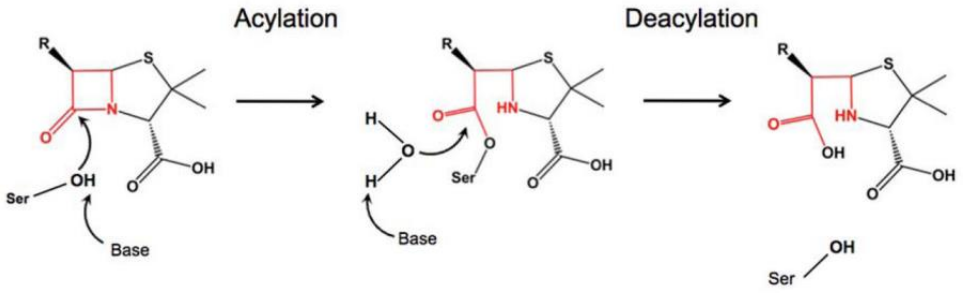

Scheme 2.1. The general catalytic mechanism of serine β-lactamases. The β-lactam ring is red. In the acylation step, the alcoholic oxygen of Ser is activated via a general base and attacks the carbonyl carbon atom of the β-lactam ring, resulting in a covalent acyl-enzyme complex. In the deacylation step, the enzyme-β-lactam antibiotic complex is dissociated by a catalytic water molecule, which is activated by a general base.

Glu166 is crucial for de-acylation step of the β-lactams hydrolysis, so substitution of Glu166 with other residues results in the formation of a stable acyl-enzyme intermediate [72;73], which can not be hydrolyzed. The crystal structure of the acyl-enzyme form of the Glu166Asn mutant covalently bonded to penicillin-G could be determined [69]. The reason of the poor catalytic activity of Glu166Ala TEM-1 β-lactamase with ampicillin or penicillin-G (substrates) is the inefficient activation of the water molecule for de-acylation step [69;72-75].

2.1.2.5. Kinetics of TEM-1 β-lactamases

Various techniques were applied to monitor the products of β-lactamase in hydrolysis of β-lactam antibiotics such as penicillins and cephalosporins. pH-static alkalimetric titration [76;77], acid base indicators [78], and iodometric titration including the formation of colorless iodine-penicilloic acid complex [79-81] were used to monitor the acidic carboxylic group formed upon β-lactam ring cleavage such as penicilloic acid of the pencillins hydrolysis. However, these methods are not applicable in the study of kinetics of the enzymatic hydrolysis [82;83]. Generally, the catalytic activity of a β-lactamase could be monitored by spectrophotometry using the peak of the differential absorbance spectrum of the product and the substrate. The direct spectrophotometric technique is used to monitor the hydrolysis of natural and semisynthetic penicillins. The most commonly used substrates for TEM-1 β-lactamase are cephalosporins and penicillins, such as penicillin G and ampicillin [84]. In the catalytic activity experiments of TEM-1 β-lactamase using ampicillin as a substrate, 235 nm is generally accepted to be the optimal wavelength for monitoring

the hydrolysis process. However, there are fluctuations in the molar absorbance values of ampicillin ranging between 1710 and 2160 M^{-1} cm^{-1}, while for the hydrolysis product of ampicillin to be between 1040 and 1260 M^{-1} cm^{-1} [85-88]. Cephalosporins have maximum UV-light absorption at about 260 nm. However, a cephalosporin derivative (chromogenic cephalosporin) known as nitrocefin containing a reactive β-lactam ring, can be monitored by visible absorption, since it changes color (from 380 to 500 nm *i.e.*, from yellow to red) in the presence of β-lactamase or bacteria-producing β-lactamase due to its breakdown (**Scheme. 2.2**) [89]. It is applicable for the serum, urine and tissues (from animals), since even in small concentrations it can be measured quantitatively [89].

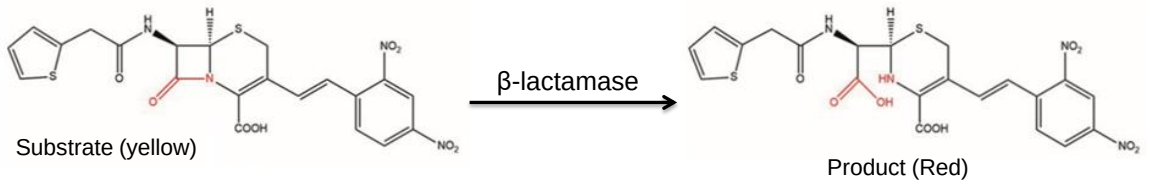

Scheme 2.2. Hydrolysis of nitrocefin by β-lactamase, it turns the chemical reaction mixture from yellow to red.

There are four major types of techniques to study the kinetics of enzyme-catalyzed reactions [90-92] (i) initial rate; (ii) progress curve; (iii) transient kinetics; and (iv) relaxation experiments. In the initial rate method, the enzyme is mixed with a large excess of a substrate for a short period of time, the enzyme-substrate intermediate forms as the fast initial transient state, and then the reaction achieves a quasi-steady state (QSS), in which the concentration of the intermediate remains mostly constant over time and the reaction rate changes slowly. In the progress curve method, the signal proportional to the concentration of the substrate or product is recorded in the time after the initial fast transient state. The kinetic parameters are determined by expressing the species (substrate or product) concentrations as a function of time. The obtained data are analyzed and evaluated by utilizing a computer program for determining the kinetic parameters. The reaction rate equation is integrated to evaluate the enzyme activity. In transient kinetics, which requires rapid mixing and observation techniques, the reaction is monitored at the initial fast transient when the intermediate reaches the QSS time. In relaxation method, an equilibrium mixture of substrate, enzyme, and product is perturbed by a jump in temperature, pressure, or pH and then returns to equilibrium. This technique is not used for mechanism identification because it is relatively insensitive to mechanistic details.

The efficiency of TEM-1 β-lactamase is often characterized by the specific activity, which is defined as millimoles ampicillin hydrolyzed per minute per mg total enzyme or mg of enzyme (expressed in mmole min^{-1} mg^{-1}). However, the unit of enzyme activity can be defined in a different ways and more precise definition is the amount of enzyme that hydrolyzes 1 μmol of substrate in 1 min at 30ºC in 0.05 M phosphate buffer, pH 7.0 [87;88;93].

In a majority of the publications, the catalytic activity of enzyme is evaluated through the V_{max} and/or turnover number (k_{cat}) depending on the rates of interconversion of the intermediates. The affinity or half-saturation constant is referred to as the Michaelis-Menten constant (K_M), the apparent second-order rate constant (k_{cat}/K_M) is referred to the catalytic efficiency, which is used instead of the specific activity. These kinetic parameters are determined by the initial rate kinetic analysis by using the Michaelis-Menten formalism (**Fig. A2** in Appendix), which is still a common procedure for TEM-1β-lactamase kinetic activity evaluation due to the comparability of the results [1;94;95].

Table 2.1. k_{cat} and K_M values of TEM-1 β-lactamase using ampicillin as a substrate [P2].

k_{cat} (s^{-1})	K_M (μM)	k_{cat}/K_M ($\mu M^{-1}s^{-1}$)	Medium	Temp.	Ref.
1428±24	50±2	28.6±5.5	50 mM phosphate buffer (pH 7.0)	30 °C	[23]
1460	60	24	50 mM phosphate buffer (pH 7.0)	37 °C	[50]
1085±137	38 ± 18	29	50 mM phosphate buffer (pH 7.0)	30 °C	[96]
1653±370	63±14	26	50 mM phosphate buffer (pH 7.2)	30 °C	[97]
830±30	58±1	14	50 mM phosphate buffer (pH 7.0)	30 °C	[98]
1428	50	28.58	50 mM phosphate buffer (pH 7.0)	30 °C	[99]
960	65.2	14.8	50 mM phosphate buffer (pH 7.0); 1 mg/ml BSA	30 °C	[100]

However, there are relatively large deviations in kinetic parameters of TEM-1β-lactamase in the literature. TEM-1 β-lactamase sequences can be potentially slightly different and partially different reaction conditions were applied in these studies, which may account for these differences. The kinetic parameters for the TEM-1 β-lactamase catalyzed hydrolysis of ampicillin as a substrate are collected in **Table 2.1**.

Class A β-lactamases undergo several conformational changes by binding and reactions with substrates resulting in other reaction pathways (**Scheme 2.3**) and complex kinetic mechanism.

Such a reaction cascade could be described by several microscopic species, which may provide deep insight into the mechanism of action [101].

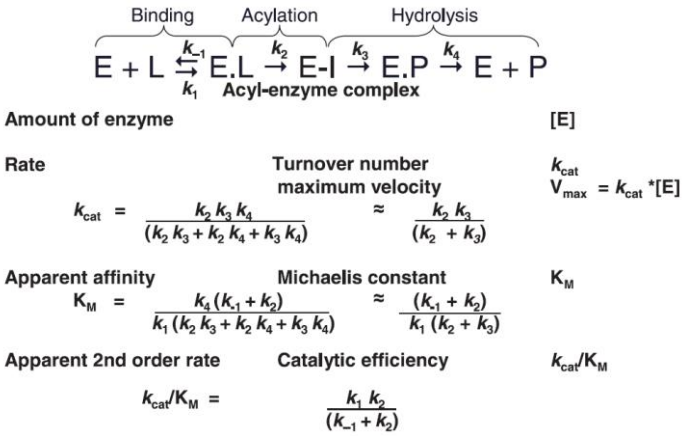

Scheme 2.3. An example of a complex mechanism of β-lactamase hydrolysis process. [102]

Fast kinetic methods such as the flow and relaxation experiments may contribute to determine further rate constants even in complicated branched catalytic pathways of β-lactam hydrolysis [101;103]. Single turnover kinetic conditions were used to determine the rate of the covalent enzyme-substrate complex formation, and/or of its decomposition rate constant [104;105].

2.2. Metal ions in biocatalysis

Mg(II) and Ca(II) ions are the most abundant divalent cations in the living systems [106;107]. Other metal ions such as Fe(II), Zn(II) and Cu(II) are widespread in the living organism, while Mn(II) and Ni(II) ions as trace elements are essential for the living system at low concentrations. [107] These divalent cations are frequently involved in enzymatic catalysis. Those, being able to easily change their oxidation states, such as Fe(II), Cu(II) and Mn(II) participate mainly in redox catalysis, while Mg(II) and Zn(II) mainly in hydrolytic enzymes. Few examples are Fe(II) ion in oxygenases and demethylases [108], Zn(II) ion in deacetylases and proteases [109;110], Ni(II) ion in urease [111], and the Mg(II) ion nucleases and polymerases [106]. These metal cations have advantageous properties, which can promote their active participation in catalysis. These are, *e.g.*, the high positive charge density for efficient charge neutralization of phospholipids and nucleic acids; hydration; specific ligand requirements; and preferred geometries, which are most commonly octahedral, square planar or tetrahedral [112].

Metal ions rarely exist without a coordinated bioligand in the biological systems. The coordination of a metal ion with macromolecules as ligands largely depends on the chemical properties, while the 3D structure of the macromolecules, stabilized by large number of intramolecular interactions, such as hydrogen bonds, salt bridges and hydrophobic interactions is also a crucial factor. Mg(II) and Fe(II) ions prefer to bind six ligands arranged in an octahedral configuration [112]. Mg(II) ion has rigid coordination geometry compared to other divalent cations [106]. Ca(II) ion binds six ligands in an octahedral geometry and it could bind seven or even more ligands [113]. Water molecules accomplishing the coordination sphere of the protein-bound metal ions in the active site provide opportunity for acid-base catalysis.

The solubility, redox stability compared with Mn(II), Fe(II) and Cu(II), and rigid geometry of Mg(II) ion [106;114] renders it as an ideal metal ion for participating in hydrolytic processes. As a hard Lewis acid, Mg(II) ion preferentially binds hard donor atoms, such as oxygen atoms of Asp or Glu sidechains. Mg(II) ion is coordinated only partially to donor atoms of the protein and thus, there is always place for one or more water molecules is the complex with octahedral geometry. These coordinated water molecules may be involved in various steps of the catalytic process. Either they are activated and transformed into OH^- ion, which as a strong nucleophile attacks the scissile phosphodiester bond, or they can protonate the leaving group after the cleavage of the P-O bond.

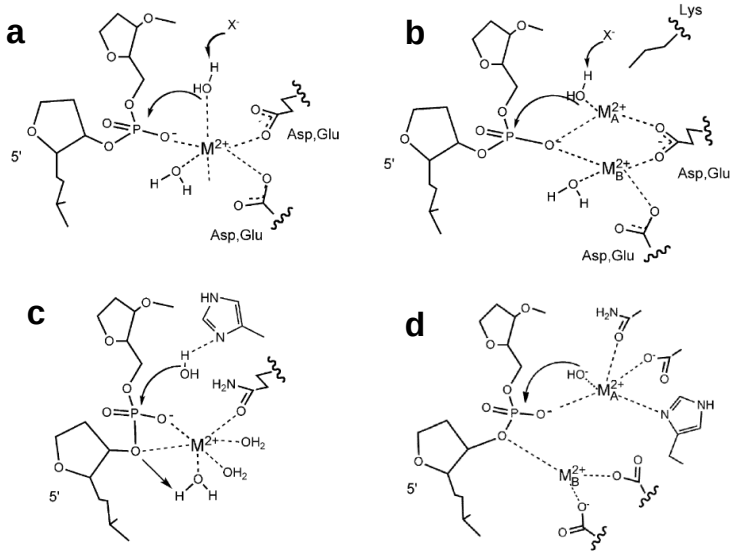

Scheme 2.4. Examples of metallonuclease mechanisms driven by metal ions. **a**) Single-metal ion mechanism in EcoRI. **b**) Two-metal ion mechanism in EcoRV. **c**) Single-metal ion mechanism with His as a general base in I-PpoI. **d**) Two-metal ion mechanism in APE-1 [115].

Therefore, nucleases (enzymes hydrolyzing nucleic acids) often use Mg(II) in their active center. Beside Mg(II), Zn(II) ions are most commonly found in nuclease active sites. ucleases are diverse regarding their active sites and mechanisms. Below we collected examples of metallonucleases, which utilize one or more metal ions as cofactors for stabilizing/activating their structures and for fulfilling their catalytic roles (**Scheme 2.4**). Metal ions generally participate in binding and electrostatic activation of the substrate, the transition state stabilization, and the activation of a water molecule either for nucleophilic attack or for the protonation of the leaving group [116].

2.2.1. Metallonuclease Colicins

Colicins are protein antibiotics acting as SOS-induced protein toxins. They are produced by strains of *E. coli* as a part of the defense system in cases of intense competition between bacteria for nutrient or during environmental stress [117]. Colicin-producing bacteria are resistant to their own colicin action via a small specific immunity protein (Im) that binds and inactivates the cytotoxic domain of colicin until the toxin is released into the environment. The immunity proteins have very high affinities (K_d < pM) for the cytotoxic domain of the recognized colicins [118]. Colicin endonucleases (colicins Es) are ~60 kDa proteins consisting of three domains: translocation, receptor binding, and nuclease (cytotoxic) domains, the detailed function of which is described in **Section A3** in Appendix.

Colicin Es are further classified into three groups based on their cytotoxic activities. Colicin E1 is not a nuclease but forms a pore ion channel that depolarizes the inner membrane of the cells [119]. Colicins E2, E7, E8, and E9 with non-specific DNase activity, degrade chromosomal DNA [120;121] Colicins E3, E4, and E6 with ribonuclease activity, specifically cleave the 16S ribosomal RNA [122;123], while colicin E5 cleaves the transfer RNA [124].

2.2.2. Nuclease domain of colicin E7

The C-terminal nuclease domain of colicin E7 (abbreviated NColE7), responsible for cytotoxicity, is a ~15 kDa protein consisting of 131 amino acid (a.a.) residues. The NColE7 sequence shows 70% identity to the NColE9 sequence (**Fig. 2.6**), while nucleases E2, E7, E8, and E9 are also structural homologues. The core of the NColE7 active site is the so called HNH motif comprising ~30 amino acids at the C-terminus of the enzyme. The HNH name originates from the three conserved residues (His-Asn-His) in the sequence GluXHisHisX_{14}AsnX_8HisX_3His.

The HNH motif contains four His residues as putative metal ion binding sites, suggesting that metal ions may play an important role in the catalysis. Nevertheless, one of the histidines (His545 in NColE7) was shown to be involved in the nuclease activity, while the other three His residues mediate the metal ion binding via their imidazole side-chains [125-128]. In addition, the HNH motif of colicins is structurally homologous to the other endonuclease active sites found in e.g., homing endonuclease I-PpoI, His-Cys box enzyme, and the non-specific nuclease from Serratia, rendering them to be members of the HNH nuclease family [129].

Figure 2.6 Sequence alignment of the nuclease domains of Colicins E2, E7, E8, and E9.

NColE7 is a very efficient toxin, even a single molecule is able to kill a bacterial cell. The DNase domain therefore, should be co-expressed together with the immunity protein 7 (Im7) in the host cell under laboratory conditions. Im7 protein interacts with the DNA binding site of NColE7 in order to protect the host cells (bacteria) from the nuclease action [130]. **Fig. 2.7** shows the interference between the binding sites of NColE7 with Im7 protein and with a short DNA.

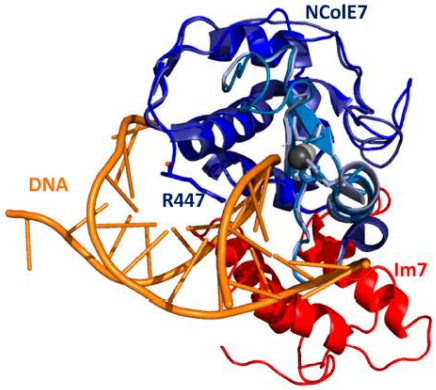

Figure 2.7. Crystal structures of two NColE7 complexes either with the Im7 protein (PDB ID: 7CEI) or with a short substrate DNA (PBD ID: 1ZNS) aligned through the two NColE7 proteins. The HNH motif is shown in light blue, NColE7 (PDB ID: 7CEI) in dark blue, the second NColE7 (PBD ID: 1ZNS) in gray, DNA in orange, while Im7 in red [P3].

The interaction between NColE7 and Im7 can be broken up by decreasing the pH to ~3.0, which leads to the apo-protein [131;132]. NColE7 was previously purified by immobilized Ni(II) ion chromatography through oligohistidine tag (6×His residues sequence) [126;132]. However, an oligohistidine tag may coordinate to the fourth binding site of Zn(II) ion instead of the water molecule, the phosphate group or the substrate, leading to inhibition of the nuclease action. Note that the imidazole of His residue has a higher affinity for the Zn(II) ion than the oxygen atom of the phosphodiester group in the DNA.

Table 2.2. List of the published crystal structures of NColE7 and its mutants. It shows the terminal sequences of the proteins, and any mutation is also indicated. The purification affinity tags, if they were available, or the remaining residues after the removal of the affinity tags are usually missing from the crystal structures due to their overly flexibility.

PDB ID/Ref.	Mutation	Complex	Sequence in PDB	Tag-NColE7
1M08/ [126]	K446M	Protein-Zn(II)-PO_4^{3-}	446 MRNK-HRGK 576	non tagged
7CEI/ [133]	-	Protein-Zn(II)-Im7	447 RNKP-IDIH 573	N-term. His-tag
2JB0/ [134]	H573A	Protein-Zn(II)-Im7	449 KPGK-HIDI 572	non tagged
3GJN/ [135]	H545A	Protein-Zn(II)-Im7 (mut.)	450 PGKA- HRGK 576	cleaved N-term. His-tag
3GKL/ [135]	H545A	Protein-Zn(II)-Im7 (mut.)	450 PGKA- HRGK 576	cleaved N-term. His-tag
1UJZ/ [136]	K528Q/T539R/H569A	Protein-Im	446 MRNK-IDIH 573	His-tag
2JAZ/ [134]	N560D	Protein-Zn(II)-PO_4^{3-}-Im7	450 PGKA- HRGK 576	non tagged
1MZ8/ [125]	-	Protein-Zn(II)-PO_4^{3-}-Im7	447 RNKP-IDIH 573	C-term. His-tag
1ZNV/[137]	K443M/H545E	Protein-Ni(II)-PO_4^{3-}-Im7	450 PGKA- HRGK 576	non tagged
3FBD/ [138]	D493Q	Protein-DNA(18bp)	445 SKRN- HRGK 576	non tagged
1PT3/ [130]	-	Protein-DNA (8 bp)	449 KPGK - HRGK 576	non tagged
1ZNS/ [137]	K443M/H545E	Protein-Zn(II)-DNA(12bp)	450 PGKA-DIHR 574	non tagged
2IVH/ [139]	H545Q	Protein-Zn(II)-DNA(18bp)	449 KPGK -IDIH 573	non tagged

Several crystal structures of wild-type and mutant NColE7 proteins have been published so far (**Table 2.2**). These structures, as well as computational modelling [131] revealed that the first 25 N-terminal residues of NColE7 exert unordered secondary structure. The HNH motif has a ββα

structure, which binds to the minor grove of the DNA, while other two helices of NColE7 are responsible for the DNA binding within the neighboring major grove (**Fig. 2.7**). From the crystal structures of NColE7 it can also be seen that the N-terminus of the protein is close to the C-terminal catalytic site in the folded protein. The amino acids positioned at the two termini thus, may interact with each other and/or with the substrate DNA (**Fig. 2.8**). The crystal structures of the wild-type or mutant NColE7 proteins bound to a metal ion and DNA or Im7 show high similarity in the overall structures of NColE7 with only minor differences in the conformation of side-chains of some residues. The termini of the NColE7 sequences and the loop between the β-strands of the HNH motif remained in some cases unresolved by X-ray crystallography. However, it would be difficult to crystalize the wild-type NColE7 bound to Zn(II) ion (*i.e.*, the active enzyme) together with DNA and therefore, it is challenging to understand the mechanism of the catalysis.

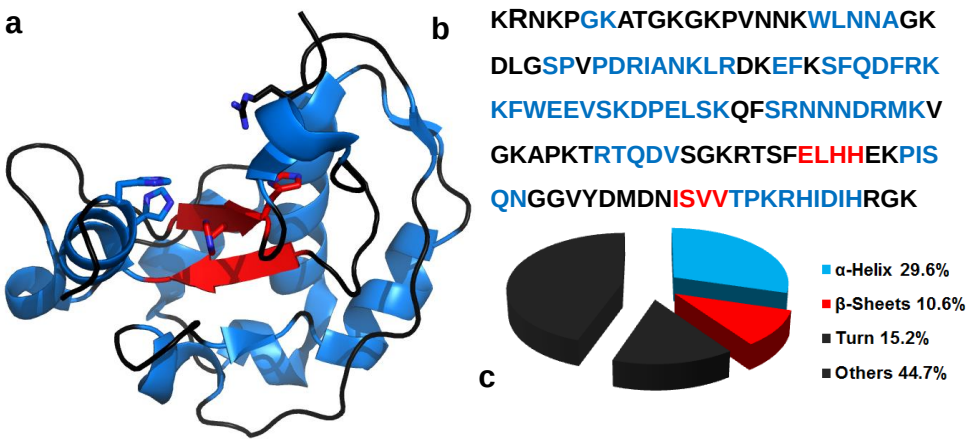

Figure 2.8. a) Crystal structure of NColE7 (PDB: 3FBD) **b**) Sequence of NColE7 (446-576), according to the original numbering of Colicin E7. **c)** The composition of the secondary structure elements of NColE7. The colors are related to the secondary structure elements in all panels: blue is for α-helices and red is for β-sheets, while black is for the turns and others.

Mutation studies approved residues, which are responsible for the nuclease activity and the DNA/metal ion binding. It was shown that the mutation of the Arg447 to Gly residue (R447G) in NColE7 did not significantly affect the overall structure or DNA and metal ion binding properties of the enzyme [131]. However, the Arg447 residue of NColE7 promotes the catalytic activity. The NColE7-R447G has decreased nuclease activity, which is ~ 10% in comparison with the wild type enzyme [140;141]. For this reason, it is easier to study its catalytic activity than that of the extremely active NColE7 enzyme [131]. The Trp464 (W464) residue of NColE7 has a significant

role in the stabilization of the enzyme structure. The NColE7-W464A mutation causes the collapse of the enzyme structure in solution as revealed by the circular dichroism spectra. This form also has less affinity towards the Zn(II) ion than the wild type enzyme [142]. However, the NColE7-W464A structure and Zn(II) ion affinity were restored upon binding to Im7 or DNA [143]. It is important to mention, that there is no crystal structure available for the wild-type or mutant apo-NColE7 in the absence of metal ion, Im7 and DNA. The reason for this may be the higher flexibility of the NColE7 structure in the absence of these interacting agents.

2.2.3. Metal ion binding of NColE7

The metal ion binding site of the NColE7 is similar to the metal binding sites of the carbonic anhydrase, metallo-β-lactamase, and carboxypeptidase enzymes [133]. NColE7 contains three His side-chains in the HNH motif: His544, His569, and His573 (this numbering is the original numbering related to the full-size colicin E7 protein). These sites bind only one divalent metal ion in tetrahedral geometry that is supposed to be a Zn(II) ion [127]. The Zn(II) ion is the most common metal ion required for the DNase colicins and generally for HNH endonucleases. The crystal structure of NColE7 (PBD ID: 7CEI) shows that the fourth coordination site of Zn(II) ion can be occupied by a water molecule [133;134] that can be replaced by the oxygen donor-atom of the phosphodiester group of DNA [127;139], or a phosphate or sulfate ion in the absence of DNA [125;126;134;144]. A mutation study has shown that the NColE7 active site is pre-organized to form the optimal tetrahedral cavity for Zn(II) ion binding [131].

NColE7 is suggested to require a Zn(II)-ion for hydrolytic activity but the metal ion is not required for DNA-binding [132]. The crystal structures of NColE7 (**Fig. 2.7**) show that the metal binding sites are almost identical in the absence and presence of metal ions, with the only difference being the His573 conformation. It is proven that the metal binding site of NColE7 has a high affinity for Zn(II) ions, which were purified together with NColE7 from the bacterial cells [125-127;133;140].

However, NColE7 could interact with other metal ions, such as Ni(II), Mn(II), and Mg(II) ions. The enzyme is active in the presence of these metal ions, but the nuclease activity measured against a supercoiled plasmid DNA decreased in the order Ni(II) > Mn(II) ~ Mg(II) > Zn(II) ions [127]. There is a debate about the identity of the functional metal ion, since for NColE9 Ni(II) ion was suggested to bind in the active site, and activate the coordinated water molecules for the catalysis [145;146]. A crystal structure in the presence of Im7 proved that NColE7 could bind

Ni(II)-ion, forming trigonal bipyramidal geometry (PDB ID: 1ZNV) (127). The addition of the Mg(II) ion to NColE7 promoted the catalytic reaction. However, the nuclease activity in the presence of Mg(II) ions is still uncertain because the enzyme has no Mg(II) ion-binding site [125].

2.2.4. NColE7 interaction with DNA

NColE7 is a nuclease that cleaves the chromosomal DNA randomly, with a slight preference for thymine-rich regions of the DNA because the A-T interaction is weaker than that of G-C, and it is easier to deform the DNA double strand at A-T base pairs [145]. NColE7 prefers cleavage at the 3'O-site of the DNA sequence in the following order: T 41.2%, A 29.5%, C 17.1%, G 12.2%. The shortest DNA, which can be cleaved by NColE7 is an 8 base pairs (bp) sequence [130]. This is probably due to the fact that the DNA-binding site is relatively far from the catalytic center, allowing also the Im7 protein to inhibit the catalysis by preventing the DNA binding [139]. Some other nucleases, such as DNaseI can cleave even dinucleotides.

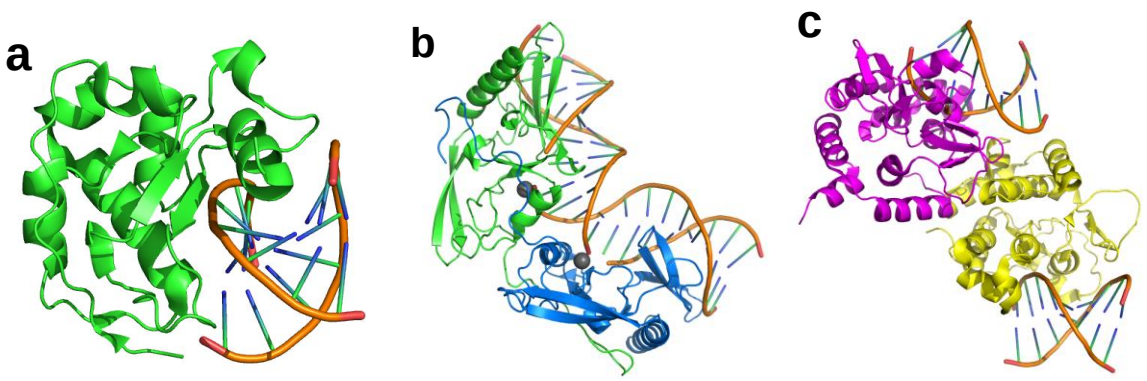

Figure 2.9. a) Crystal structure of the complex NColE7/DNA (PDB ID: 1PT3), NColE7 in green and DNA in orange color, **b**) Crystal structure of the complex dimer Vvn/short DNA (PDB ID:1OUP), the monomers of Vvn dimer are in pink and yellow colors, **c**) The crystal structure of the complex dimer I-PpoI/short DNA (PDB ID: 1IPP), the monomers of I-PpoI dimer are in green and blue colors.

The crystal structure with DNA (PDB code: 1ZNS) shows that the scissile phosphodiester bond is close to the metal ion with a Zn-O distance of 3.18 Å [127], while in another structure with PDB code: 2IVH this distance is 3.72 Å. [139] NColE7 binding to both the major and minor grooves at the same time leads to DNA bending with an angle that depends on the length of the substrate. The bending angle was 7° for 8 bp DNA, [130] 19° for 12 bp DNA, [127], and 54° for 18 bp DNA [139]. Sequence-specific cleavage performing restriction endonucleases induce even more extensive bending of the substrate. The crystal structures of NColE7, *V. vulnificus* nuclease

(Vvn) and an intron-encoded endonuclease from *Ph. polycephalum* (I-PpoI) in complex with DNA are similar with only minor differences in the orientation of the DNA minor groove and the ββα-type active center (**Fig. 2.9**). This suggested that these enzymes may cleave DNA with a similar mechanism [130].

2.2.5. Catalytic mechanism of NColE7

Generally, nucleases cleave phosphodiester bond at one of the two bridging P-O bonds (3′ or 5′) in a nucleic acid polymer by acid-base catalysis: a base generates the attacking nucleophile by deprotonation and an acid facilitates the product formation by protonating the leaving group (**Scheme 2.5**). The cleavage reaction is a bimolecular nucleophylic substitution (S_N2) [147]. The three main steps of the mechanism of the nuclease catalysis are the nucleophilic attack, formation of the intermediate, and the scissile bond cleavage. The nucleophile (usually an OH^- ion) attacks the phosphorous atom and a highly negatively charged penta-covalent intermediate (with bipyramidal geometry) forms. This intermediate takes two pathways, either the bond of O 5′ moves causing the bond cleavage to produce O 5′ nucleoside and P-O 3′ of nucleoside or the bond of O 3′ moves causing the bond cleavage to produce O 3′ nucleoside and P-O 5′ of nucleoside.

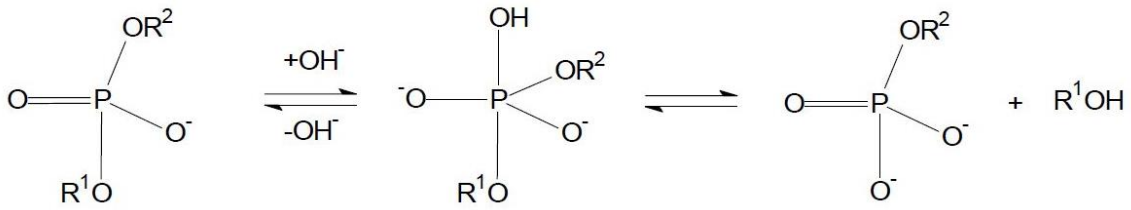

Scheme 2.5. Mechanism of phosphodiester cleavage, R^1 and R^2 can be substituted ribose or deoxyribose molecules in RNA or DNA, respectively. In RNA and DNA, adjacent nucleotides are connected by phosphodiester bonds. Nucleases break one of these two P-O-R bonds by the help of a nucleophile.

While NColE7 is a metalloenzyme, the His545 side-chain in the HNH active site is suggested to participate in generation of the OH^- ion nucleophile by promoting the deprotonation of the catalytic water molecule [126;148]. The catalytic mechanism of NColE7 involves the following steps (**Fig. 2.10**). (i) Zn(II) ion binds to the oxygen donor atom of the scissile phophodiester bond of DNA, that replaces the water molecule at the fourth coordination site. The crystal structures of NColE7 show that the Zn(II)-ion does not coordinate water molecule in the presence of the substrate. By binding, the role the Zn(II) ion also extends to increase the partial

positive charge at the phosphorous atom. (ii) His545 forming a hydrogen bond with the carbonyl group of Val555 residue acts as a general base to activate a water molecule to form the nucleophile to attack the phosphorous atom involved in the scissile P-O bond of the DNA. [125] (iii) The penta-covalent intermediate involving the phosphorous central atom bound to five oxygen atoms is highly negatively charged, and may be stabilized by the coordinated positively charged Zn(II)ion. (iv) This intermediate is then decomposed by the cleavage of the P-O3′ bond resulting a 5′-phosphate and the 3′-OH termini of the cleaved DNA strand. The initially formed 3′ alcoholate, as a very strong base, needs to be protonated to leave the catalytic site. The proton might be transferred from the protonated His545 residue by the participation of Arg447, which would explain the importance of this residue in the catalytic efficiency [149]. Otherwise, the proton may arise from His569, but it is a less likely pathway [133]. There are several proton transfer pathways suggested in the literature to protonate the leaving group. Accordingly, Arg538, Gln542, and His569 could also provide the proton for the leaving group [133;150]. Mechanistic studies on NColE9 suggested that the leaving group is protonated by the hydrogen ion that is originated from the same water molecule that initiated the nucleophilic attack [146]. In other nucleases the proton may also be provided by a metal ion bound water molecule, such as in I-PpoI or Serratia nucleases accommodating a Mg(II) ion in their active center.

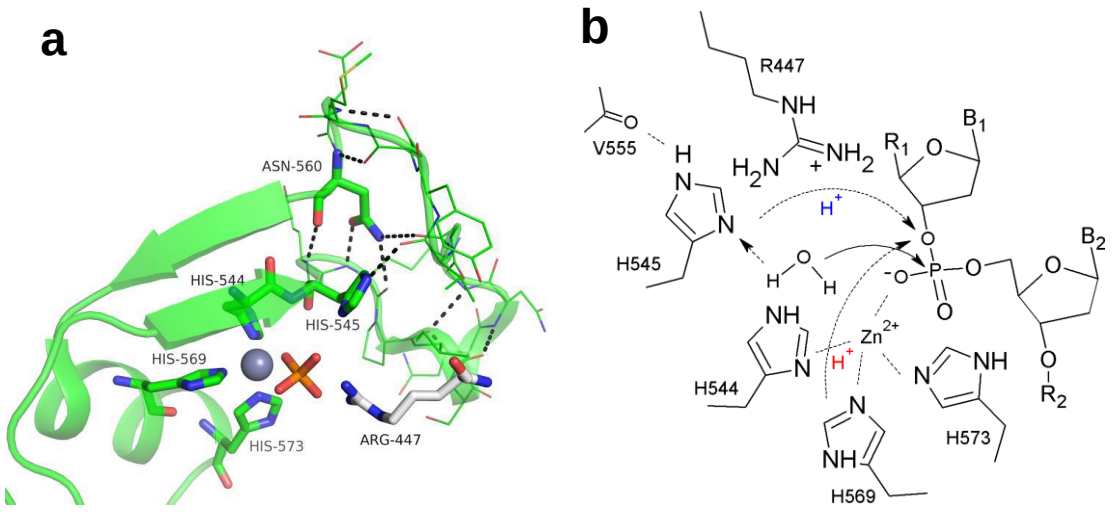

Figure 2.10 a) This figure is taken from [151]. The structure of the HNH-motif in NColE7 (1M08) is displayed, with the Arg447 residue, the conserved HNH residues (His545, Asn560, His573), and the metal-binding residues (His544, His569, His573) coordinated to the Zn(II) ion. **b**) Suggested schematic mechanism of DNA hydrolysis by NColE7. The leaving group's protonation can be explained using the red [133] and blue [149] protonation pathways.

The Asn560 residue has a structural role to stabilize the HNH structure and to orient the side chain of the His545 residue. Asn560 is located in the loop between the β-sheets of the HNH motif. The catalytic role of His545, His573 and Ans560 was studied by point mutations [134]. Accordingly, a nuclease activity decreased to 11% for His545Gln in comparison with the wild-type enzyme and complete cancellation was observed for His545Ala, and His545Glu mutants (**Table 2.3**). His573Ala and His573Glu mutants decreased the catalytic activity to 31% and 83% respectively of the wild-type enzyme [134]. The nuclease activity decreased to 7% for Asn560Asp, 24% for Asn560Ala, and 27% for Asn560His mutants. The $N_{\delta 1}$ atom of His545 is in appropriate position for the catalysis because the distance between H545-$N_{\delta 1}$ atom and the phosphodiester oxygen of DNA is ~2.4 Å, while it is ~2.9 Å for Asn560Ala, and ~3.7 Å for Asn560Asp mutants [125;134]. In conclusion, the decrease of the nuclease activity is related to the displacement of DNA. It is worth mentioning that NMR results of NColE9 bound Ni(II) ion showed that two of the His residues are coordinated through their$N_{\varepsilon 2}$ atoms and one His via its $N_{\delta 1}$ [152].

Table 2.3. The nuclease activities of the wild-type and mutants ColE7 that were measured by FRET methods [134].

	K_M (nM)	k_{cat}(s^{-1})	k_{cat}/K_M (M^{-1} s^{-1})
WT	74.9 ± 3.2	0.0045 ± 0.0010	60,600 (100%)
His545Ala	-	-	0 (0%)
His545Glu	-	-	0 (0%)
His545Gln	53.3 ± 2.2	0.0003 ± 0.0001	6,200 (11.38%)
Asn560Ala	52.3 ± 6.0	0.0008 ± 0.0002	14,400 (23.76%)
Asn560Asp	95.3 ± 4.8	0.0004 ± 0.002	4,200 (6.93%)
Asn560His	20.7 ± 8.2	0.0003 ± 0.0000	16,400 (27.08%)
His573Ala	62.4 ± 4.4	0.0012 ± 0.0001	18,700 (30.92%)
His573Glu	24.8 ± 5.0	0.0013 ± 0.0001	50,400 (83.24%)

The above data demonstrate the importance of various amino acid residues, as well as the role of metal ions in NColE7 providing a good opportunity to regulate the function of the enzyme, and therefore, it can be a promising building block of an artificial metallonuclease.

3. AIMS AND OBJECTIVES

Bacteria, antibiotics as well as metal ions are released into the environment through many ways leading to severe contamination. As a consequence, bacteria protect themselves by various defense mechanisms. Some of them are resistant or become resistant towards antibiotics. Others release antibacterial enzymes in case of environmental stress to kill the other bacteria. Most of these processes are related to the catalytic hydrolysis of a substrate molecule, such as the β-lactam antibiotics hydrolysis by e.g., TEM-1 β-lactamase, or genomic DNA cleavage by nuclease colicins. The presence of metal ions, as Lewis acids may interfere with these enzymes and processes. The interaction of bacterial enzymes with metal ions may lead to the development of highly aggressive bacteria in the environment or highly resistant bacteria may evolve towards the antibiotic drugs.

The aim of my PhD work was to investigate and understand the effect of the non-endogenous/non-native metal ions on two types of bacterial hydrolytic enzymes: (i) TEM-1 β-lactamase being responsible for the resistance of the bacteria against β-lactam antibiotics, and (ii) the nuclease domain of colicin E7 (NColE7), a metalloenzyme that targets the phosphodiester bonds of the DNA and thereby promotes non-specific hydrolytic digestion of DNA, through its two mutants: KGNK and KGNK-His. The workflow of the planned experiments is depicted in **Scheme 3**. During my PhD work I focused on the following objectives.

1. Synthesis and purification of the proteins

TEM-1 β-lactamases were extensively studied in the literature. They were purified by different techniques as recombinant proteins, but the purification method most commonly applied denaturing conditions and/or affinity purification tags. While the selected TEM-1 β-lactamase is not a metalloprotein, its amino acid sequence offers numerous metal binding sites, such as the side-chains of the His residues. The imidazole nitrogen donor atom in His residues is a borderline ligand that can be coordinated by borderline metal ions such as Ni(II), Cu(II), Zn(II) ions. So TEM-1 β-lactamase can be purified in its native fold with Ni(II)-loaded immobilized metal ion affinity chromatography (IMAC) resin. The questions addressed at this point included: (**i**) Is it possible to overexpress the protein, although its DNA gene is located outside of the multi-cloning site? (**ii**) What are the purification conditions of the protein based on its metal binding sites on immobilized

metal ion affinity chromatography? (**iii**) How much of the pure protein can we obtain in comparison with other published methods?

Previously, KGNK protein was purified by GST affinity chromatography supplied with HPLC, while KGNK-His was purified by a batch-type immobilized metal ion affinity method. We planned to express and purify KGNK-His by IMAC supplied with HPLC and to express and purify new batches of the KGNK protein by GST-HPLC.

2. Characterization of the proteins by mass spectrometry, UV-absorption and CD spectroscopy, and gel electrophoresis to identify and check the quality and quantity of the purified proteins

The next goal was to characterize the purified proteins (TEM-1 β-lactamase, KGNK, and KGNK-His). We planned to investigate the purified proteins running along the following points: (**i**) purity, (**ii**) yield/concentration, (**iii**) identification/molecular mass, and (**iv**) folding/secondary structure composition. The purity of the obtained proteins is primarily monitored by SDS-PAGE. While this method provides information on the concentration of the protein solution, we also planned to apply UV-absorption spectroscopy for this purpose. For determination of solution structural properties, CD spectroscopic measurements were foreseen, followed by the evaluation of the spectra to calculate the secondary structure compositions and comparison of the results with the published crystal structures of these proteins. The advantage of the planned mass spectrometric measurements (MS) is that they can identify the expressed protein in fragmentation experiments, and they provide information on the molecular mass and in some cases on the folding of the proteins.

3. Determination of the kinetic parameters of TEM-1 β-lactamase promoted ampicillin hydrolysis process

We observed fluctuations of the molar absorbance (ε) values of the hydrolysis product of ampicillin in the catalytic experiments published in the literature. As a consequence, various values of k_{cat}, and K_M were determined for TEM-1 β-lactamase promoted ampicillin hydrolysis, while the comparison is further complicated by mutations in the enzyme amino acid sequence. Therefore, we aim to find reasons for the fluctuation of the values of kinetic parameters by studying the kinetic activity of TEM-1 β-lactamase in the hydrolysis of ampicillin substrate under commonly used conditions. We planned to reevaluate the kinetic parameters using multi-wavelength monitoring of

the kinetic progress curves and their evaluation without preconceptions applied in classical Michaelis-Menten formalism. Tracking the hydrolysis product by mass spectrometry was expected to support the evaluation.

4. Unravelling the non-endogenous/non-native metal ion binding and their structural effects

TEM-1 β-lactamase possesses 7 His residues to bind borderline transition metal ions, 3 Cys and 10 Met residues with sulfur donor groups for soft metal ion binding, and further oxygen donor groups for interaction with hard metal ions. While KGNK and KGNK-His proteins were previously shown to purify together with Zn(II) ions supposed to be their native cofactor, they can bind other divalent metal ions, as well. Furthermore, KGNK-His contains a C-terminal 6×His affinity tag, which may affect the metal ion binding properties and thereby, the structure and function of the protein. Based on this, we aim to study the effect of the non-endogeneous metal ions, such as Ni(II), Cd(II), and Hg(II) on non-metalloenzyme TEM-1 β-lactamase, and the non-native Ni(II), Cu(II), and Cd(II) on the NColE7 mutants. The structural effects of metal ions on the proteins will be investigated by CD spectroscopy, mass spectrometry, and ^{199m}Hg(II) PAC spectroscopy in solution. These experiments were expected to clarify the following points: (**i**) changes in the secondary structure elements; (**ii**) the identity and number of metal ions bound to a protein; (**iii**) the relative affinity of the proteins toward the metal ions.

5. Determining the influence of metal ions on the catalytic activity of the proteins

The interaction of TEM-1 β-lactamase with metal ions can lead to modification of the catalytic activity of the protein in ampicillin hydrolysis. We planned to study the effect of Ni(II), Cd(II), and Hg(II) ions on the kinetics of ampicillin hydrolysis catalyzed by TEM-1 β-lactamase in solution, as well as in cells in a bacterial culture. The study includes the investigation of the following effects on the hydrolysis rate: (**i**) the quality and quantity of the metal ion; (**ii**) the interaction with ampicillin; and (**iii**) the effect of the applied conditions.

KGNK has only one strong metal binding site in the active center, while KGNK-His protein has two main metal binding sites: the active center and the His-tag. Furthermore, the His-tag has previously been shown to bind to the free coordination site of the Zn(II) ion coordinated in the active center, thereby inhibiting the catalytic activity. In this work, we aimed at studying the catalytic activity of KGNK and KGNK-His proteins with pUC119 DNA as substrate in the

presence of Ni(II), Cd(II), and Cu(II) ions. Ni(II) ions can occur as a contamination originated from the purification procedure by immobilized metal ion chromatography. Cu(II) ion is a strong Lewis acid and has high affinity to the His residues. Cd(II) ion was selected as the d^{10} analogue of the Zn(II) ion. We planned to investigate the following effects on the hydrolysis rate: (**i**) the role of a non-native metal ion; (**ii**) the effect of an excess amount of non-native metal ion; (**iii**) the regulation of the catalytic behavior with EDTA as a strong chelator; (**iv**) the effect of the competition between non-native and native metal ions.

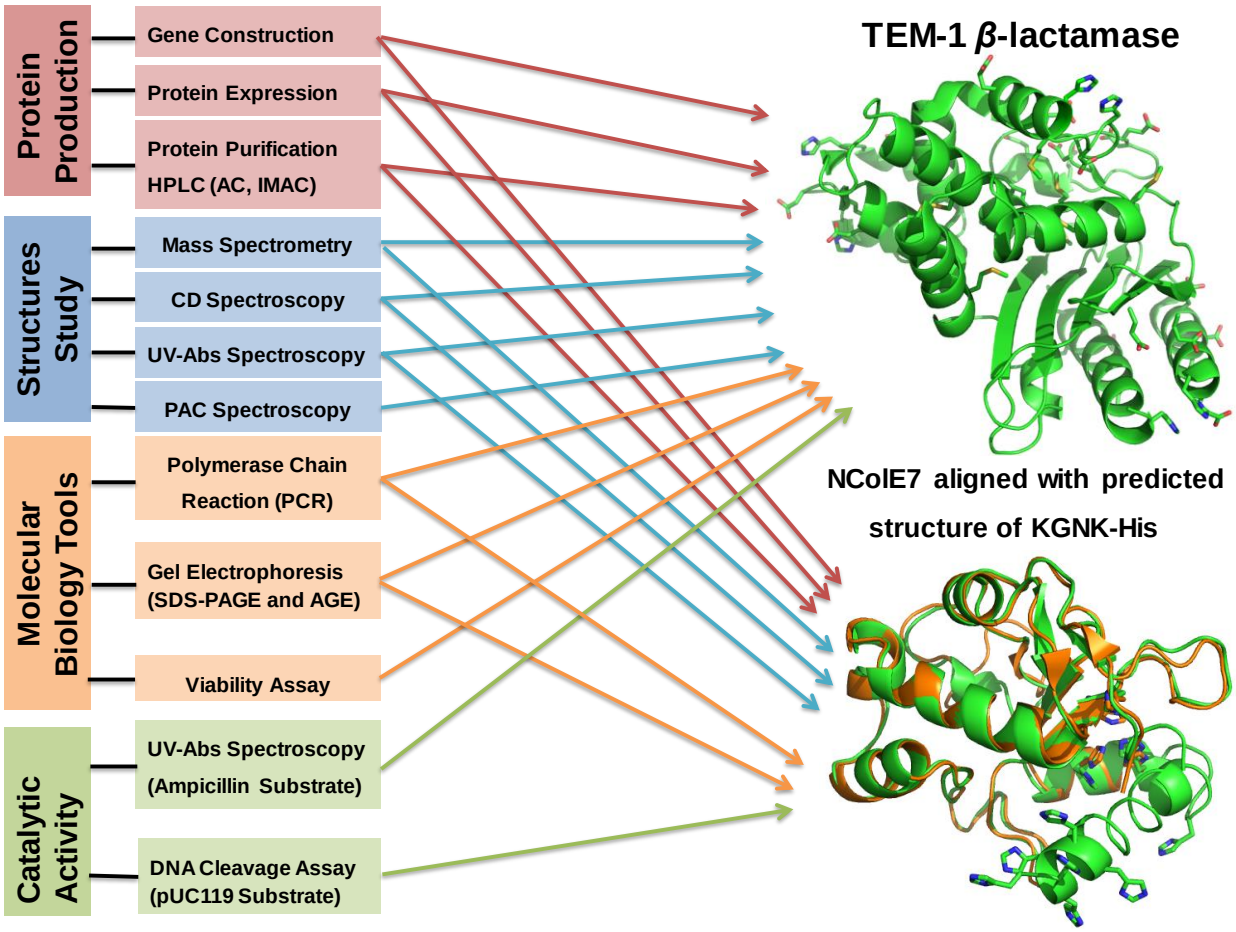

Scheme 3: The workflow of this research project including the two research lines: TEM-1 β-lactamase and mutants of NColE7.

4. REAGENTS AND METHODS

4.1. Reagents

All commercial reagents were used as purchased without further purification. IMAC Sepharose 6 Fast Flow (FF) resin, GSTPrep FF16/10 column, XK 16/20 packing column, and HiPrep Sepharose Q FF anion-exchanger were from GE Healthcare/Bio-Science AB products. Seakem LE agarose was obtained from Lonza, Rockland, ME. LB medium, $ZnCl_2$, $NiCl_2$, $CdCl_2$, $CuCl_2$ Na_2HPO_4, NaH_2PO_4, NH_4Cl, and glucose were obtained from Reanal Kft, Budapest. NaCl (Szkarabeusz Laboratóriumi, Vegyipari és Kereskedelmi kft), Acrylamide/bis-acrylamide (29/1) as a 30% (w/v) solution was from SERVA Electrophoresis GmbH. Bisacrylamide 2K standard grade, extra pure was bought from AppliChem Panreac; tris (hydroxymethyl) aminomethane and KCl from Molar Chemicals; isopropyl β-D-1-thiogalactopyranoside (IPTG, dioxane free) from Thermo Scientific; ampicillin sodium salt from Sigma-Aldrich. Imidazole, N-2-hydroxyethylpiperazine-N-2-ethane sulfonic acid (HEPES), and ammonium bicarbonate were from Sigma-Aldrich, tricine was from VWR Life Science. Kanamycin was a SERVA Electrophoresis GmbH, Heidelberg product. The pET-21a(+) vector was a Novagen product, while pGEX-6P-1 vector was GE Healthcare Bio-Sci. product. The *E. coli* DH10B bacterial strain was applied for DNA cloning [153], while *E. coli* BL21 (DE3) strain for protein expression [154]. The pQE70 plasmid containing the NColE7 and Im7 immunity protein genes was a generous gift from Prof. K.-F. Chak, Institute of Biochemistry and Molecular Biology, National Yang Ming University, Taipei, Taiwan.

4.2. Production of proteins

Generally, the first step of the synthesis of a protein is the construction of the functional gene of the protein of interest by recombinant DNA technology. Since the use of the biological tools in chemistry research field is less familiar, a brief introduction is presented below. This technology involves two or more DNA molecules from different organisms being recombined together and then introduced into a host organism – usually a bacterial cell [155]. This procedure also allows to change the genetic material to introduce mutations and thereby change desired amino acids in a protein. The new gene is ligated with a carrier DNA (vector, plasmid), cloned in bacteria and used for protein expression. (**Fig. 4.1**)

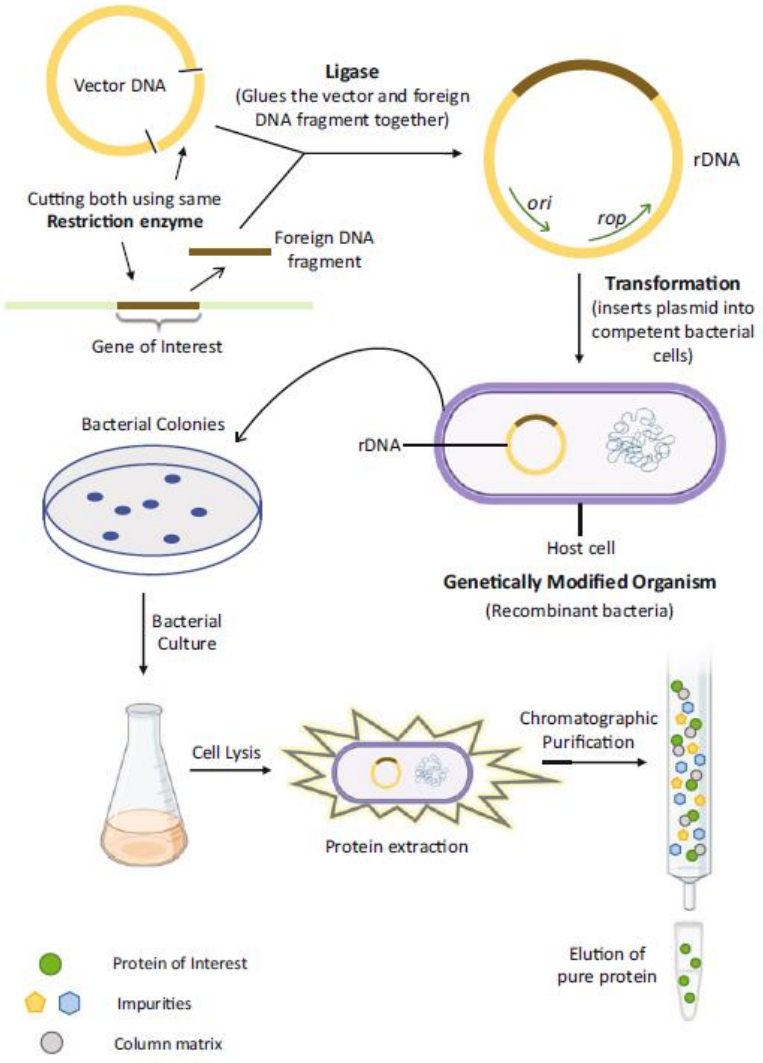

Figure 4.1. A simplified presentation of recombinant DNA technology up to the protein purification. Taken from [155].

4.2.1. Gene amplification and mutation by PCR

Polymerase chain reaction (PCR) is primarily utilized to amplify the gene of the target protein from a natural DNA source. The PCR reaction mixture contains the template DNA molecule, heat-stable polymerase enzyme (Taq polymerase), buffer containing Mg(II) ions (Taq buffer), deoxynucleoside triphosphates (dNTPs) as building blocks and two short oligonucleotides (forward and reverse primers) [156]. The primers are crucial elements of the reaction designed by the researcher. These molecules hybridize with the single-strands of the template DNA (after melting the dsDNA template) and assist the polymerase to start building up the complementary DNA strands. Primers thus, designate the start and end point of the amplified sequence and

introduce *e.g.*, restriction endonuclease enzyme cleavage sites at the termini of the target gene or mutations within the gene.

PCR is driven by a temperature control device in repeated cycles, each of which includes three steps. The first step is the melting of the template dsDNA to dissociate into single strands upon heating the mixture to > 90 °C. The second step is annealing, when the temperature of the mixture decreases to ~50–65°C (close to the melting point of the primers), so that primers can hybridize with their complementary sequences within the single-strand templates. The third step is elongation of the complementary strand at ~68-72°C (polymerase enzyme function temperature). Primers are prolonged in this step, resulting in the new ds DNA (**Fig. 4.2**).

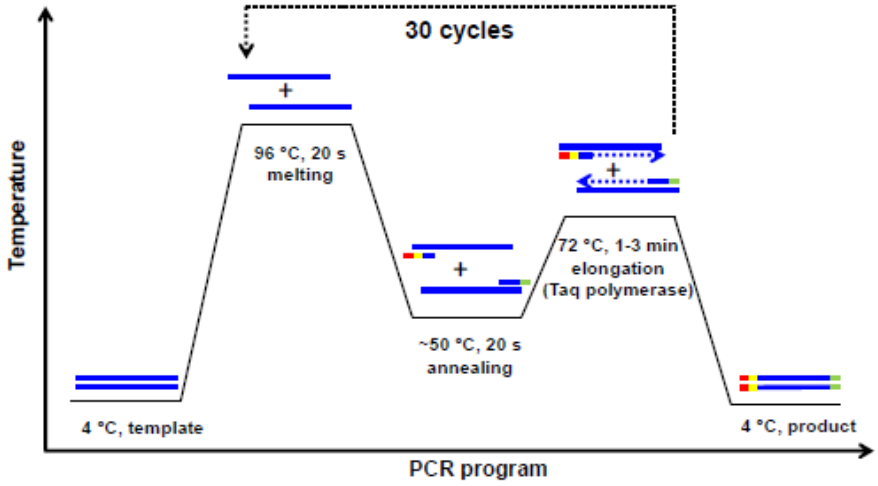

Figure 4.2. Program of a PCR. DNA template is indicated by blue line. Restriction enzyme cleavage sites carried by the primer molecules are indicated by red and green. The mutation by primers is indicated by yellow. The efficiency of the PCR would decrease after about 30 cycles (from Németh Eszter's PhD thesis).

Since the new dsDNAs formed in the elongation step serve as templates in the subsequent cycles, the amount of DNA is exponentially increasing (~2^n, where n is the number of cycles). It is recommended to use a small amount of template to avoid it as an impurity.

In this work, the nuclear factor I DNA binding domain (NFI-BD) gene (720 bp) was mutated from Gln164 to His164 (denoted as Q164H mutation) to get NFI-BDH. The NdeI and XhoI restriction endonuclease cleavage sites were introduced by the applied primer pair in PCR at the two termini of the gene. The NColE7-R447G (KGNK) gene was prepared earlier by PCR from the wild-type NColE7 gene, terminated by EcoRI and BamHI cleavage sites for insertion into the pGEX-6P-1 carrier DNA similarly to the NColE7-R447G (KGNK) gene constructed with NdeI

and XhoI cleavage sites in order to be inserted into the pET-21a(+) vector (AMP^R), in order to obtain KGNK-His protein.

4.2.2. Cleavage of the gene and carrier DNA and their ligation

The PCR product encodes the protein of interest, which can be expressed after gene insertion into a suitable carrier DNA. A vector is a relatively small (few thousands of base-pairs) circular, double-strand, extrachromosomal DNA within archaea, eukaryotic organism and in bacteria, which can be replicated independently within the cell. The gene of interest is inserted into the multi-cloning site (MCS) of the plasmid that is recognized and cleaved by several restriction endonucleases to promote the insertion. The termini of the genes and a plasmid cut by the same enzyme match specifically. In this work, the NFI-BDH gene and pET-21a(+) were cut by NdeI and XhoI enzymes. The ligase enzyme catalyzes the formation of covalent bonds at matched DNA termini, the process called ligation. As a result a new circular plasmid DNA is formed (**Fig. 4.3**).

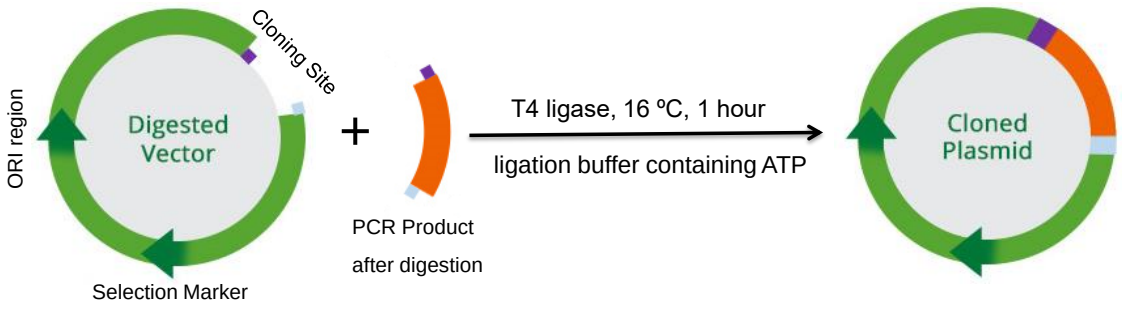

Figure 4.3. A simplified presentation of the ligation reaction in solution. A modified figure from Origene (https://www.origene.com).

During the ligation, several side reactions may occur, such as e.g., the formation of linear DNA molecules upon ligation at one side only, two or more insert molecules being ligated to each other, or the plasmids being recircularized. The DNA/ligase as well as the plasmid DNA/insert DNA ratios are important optimization parameters. The cleaved NFI-BDH gene was ligated with the cleaved pET-21a(+) vector using T4 ligase. As a result of this ligation a C-terminal 6×His-tag (an oligopeptide sequence encoded by the carrier DNA) will be fused to the protein in the expression procedure to promote its purification by immobilized metal ion affinity chromatography (IMAC). The ligation was carried out in ligase buffer at 16 ºC for one hour of incubation.

4.2.3. Transformation of the bacterial cells for DNA cloning

The successfully ligated gene in a plasmid is used for chemical or physical transformation of the host bacterial cells for multiplication of identical copies (cloning). In chemical transformation, the ligation mixture is added to a suspension of competent bacterial cells. *E. coli* DH10B and MachI cells are suitable to copy plasmids. The cells are subjected to a heat-shock treatment (0 °C → 37 °C) promoting the uptake of the ligated plasmid DNA. The plasmid also carries the gene of a protein providing resistance towards a specific antibiotic for selection against this drug molecule, In the suspension spread on a nutrition plate supplemented with a specific antibiotic, only those bacteria are viable, which carry the plasmid DNA providing the resistance (selection marker). After cultivation, a single bacterial colony is transferred into liquid LB medium to obtain high amounts of the new plasmid. The plasmid DNA can be then extracted by alkali lysis of the bacteria, followed by purification on a specific column and precipitation by ethanol.

In this work, the target gene ligated with a pET-21a(+) DNA vector was used to transform the *E. coli* DH10B cells. After the cloning, the sequence of the gene was verified by automated DNA sequencing using the commercial T7 promoter primer.

4.2.4. Expression of proteins

Protein expression involves a series of biological processes, in which the genetic code is translated into a functional protein. Transformed bacteria can be considered as factories for protein production. Several factors influence the recombinant protein expression: properties of the gene and the vector (plasmid), host cells, inducer, medium, and incubation temperature and period [155]. The most frequently used hosts are the modified *E. coli* strains BL21(DE3), BL21(DE3)pLysS and Rosetta. BL21(DE3) bacteria contain the phage T7 RNA polymerase gene linked to the isopropyl β-D-1-thiogalactopyranoside (IPTG)-inducible promoter, for use with any expression plasmid containing the T7 promoter (recognized by the T7 RNA polymerase), such as the pET-21a(+).

An increasing number of modified plasmids are available for recombinant protein expression. Examples used in our work are pGEX-6P-1, pETM11, and pET-21a(+), the map of which is shown in **Fig. A3** in Appendix. The expression vector also carries an antibiotic resistance gene (selection marker) towards particular antibiotics (ampicillin and kanamycin are familiar), a specific sequence as the origin of replication (ORI), and the multi-cloning site (MCS) between the promoter and terminator DNA sequences (initiating and terminating the transcription process). Protein expression is regulated by IPTG in pGEX-6P-1 or pET-21a(+) vectors. IPTG is usually

added to the bacterial culture in the log phase when the optical density (OD_{600}) value is ~ 0.4 – 0.6. Since the synthetic IPTG cannot be easily degraded, the expression will occur continuously. This allows for the "overexpression" of the target protein.

Some expression plasmids were re-designed to offer an affinity tag coding sequence that is fused to the gene of the target protein. As affinity tags, proteins or short peptides are generally applied. These facilitate the protein purification, and are cleaved with a specific protease from the purified protein. The pGEX-6P-1 vector carries the glutathione-S-transferase (GST) gene between the promoter region and the MCS. The protein expression therefore, results in an N-terminal GST-fused target protein. The GST-tag usually does not interfere with the folding and function of the target protein; it allows for affinity based purification, resulting in a high purity product; increases the solubility of some proteins; it can be cleaved or removed after the purification with a specific protease (Human rhinovirus C3 protease) [157] pET-21a(+) offers a non-cleavable C-terminal His-tag (6×His) for the genes without a stop codon. The detailed protocols of the expression of TEM-1 β-lactamase and NColE7 mutants are described in **Protocols A1** and **A2** in Appendix.

4.3. Methods of protein purification

The most common method for protein purification involves various kinds of preparative chromatography (**Table 4.1**). The purification strategy depends on the properties of the target protein to be separated from thousands of other proteins in the cell extract [155]. Affinity chromatography (AC) requires fusion of the target protein to a specific affinity tag. In an optimal case it allows for a single step protein purification, because of its high selectivity. It separates the proteins on the basis of the interaction between the affinity tagged protein and a specific ligand attached to the chromatographic matrix.

Table 4.1: Protein properties and the corresponding chromatographic methods used for purification

Protein property	**Chromatographic method**
Specific ligand recognition	Affinity chromatography (AC)
Metal ion binding	Immobilized metal ion affinity chromatography (IMAC)
Charge	Ion exchange chromatography (IEX)
Size	Gel filtration (GF) or size exclusion chromatography
Hydrophobicity	Hydrophobic interaction chromatography (HIC) Reverse phase chromatography (RPC)
Isoelectric point	Chromatofocusing

The interaction can be biospecific, such as the antibody binding to a protein as an antigene, or a receptor binding hormone, or substrate binding enzyme, as well as non-biospecific, such as a protein binding to a dye or a histidine containing protein binding to metal ions. Fast protein liquid chromatography (FPLC) or high performance liquid chromatography (HPLC) was developed for the efficient purification [158] providing high loading capacity, biocompatible aqueous buffers, fast flow rates and wide range of stationary phases, such as affinity, gel filtration, ion exchange and size exclusion columns [159]. The chromatographic system can be automatized including autosampler, gradient program control, peak collection. ÄKTA FPLC explorer system (**Fig. A4** in Appendix) is recently frequently used for protein purification. In the following, the chromatographic methods applied in this work will be briefly introduced. The detailed protocols for the purification of each protein are found in **Protocols A3-A5** in Appendix.

4.3.1. Affinity chromatography

GST affinity purification method is based on the biospecific interaction between glutathione S-transferase (GST) and glutathione bound to a chromatographic matrix (**Fig. 4.4a**), allowing for specific, reversible interactions. After equilibration of the column and loading the sample, the GST-fused target protein binds to the immobilized glutathione, while all other impurities of the cell extract flow through the column usually resulting in a broad band with high absorbance values on the chromatogram (**Fig. 4.5**).

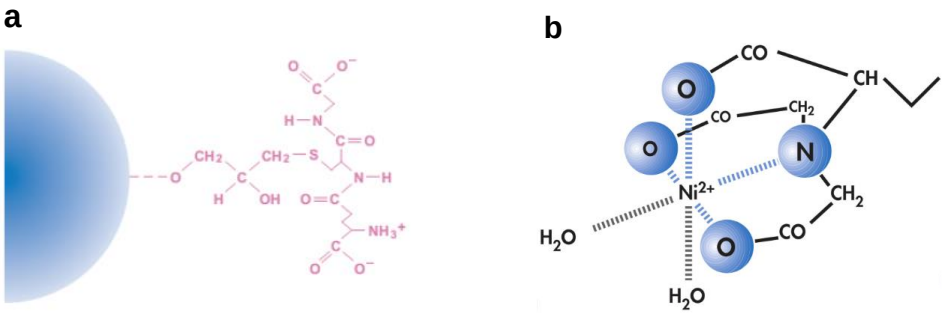

Figure 4.4. a) Glutathione linked to the sepharose matrix (from Amersham Biosciences Handbooks), **b**) Ni(II) bound NTA-resin (from Qiagen.com).

After washing the column for further 2-5 column volumes (CV) of the applied buffer, the GST-fused target protein can be eluted with a competing agent (such as reduced glutathione solution) that has comparable or higher affinity to the protein than the immobilized ligand.

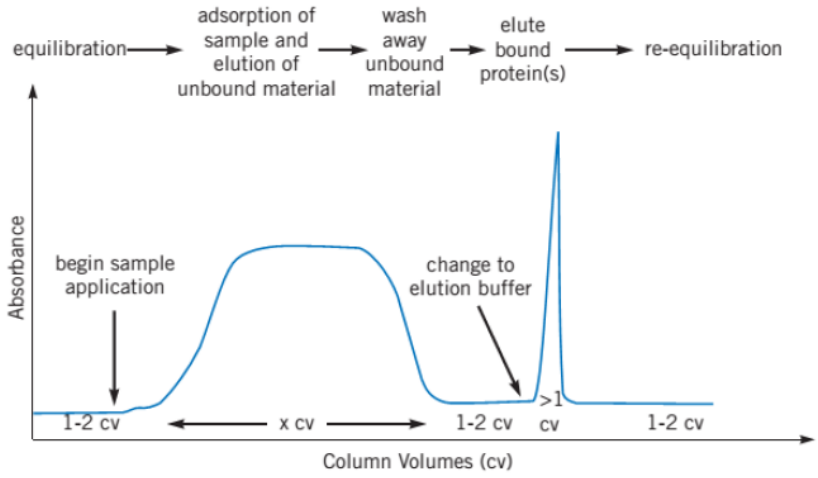

Figure 4.5. Chromatogram of affinity purification (from Amersham Biosciences Handbooks).

Immobilized metal ion affinity chromatography (IMAC) is a less stringently specific member of ACs. It is suitable for separation of metal binding proteins, and oligohistidine-tagged recombinant proteins with 6-10 His residues at either their N- or C-termini. The interaction with the resin is based on coordinative binding of histidine residues (as well as other amino acids with coordinating side-chains, such as Tyr, Cys, Glu or Asp) of protein with divalent transition metal ions, like Ni(II), Cu(II), Zn(II) and Co(II). The elution of the target protein may be carried out by decreasing the pH, increasing the ionic strength of the buffer or by adding a competitive molecule, such as imidazole, EDTA, or eventually metal ions. Stationary phase is a chelating sepharose with attached iminodiacetic acid, or nitrilotriacetic acid coordinated to the metal cations (**Fig. 4.4b**) leaving free coordination sites for the target protein.

The equilibration of the Ni(II) bound NTA column followed by sample loading, allows the His-tagged target protein and the other proteins with coordinating residues to bind to the column, while all other components of the cell extract flow through (**Fig. 4.5**). Washing the column with 2-5 column volumes (CV) of the washing buffer in presence of salt, or eventually a small concentration of imidazole as a competing agent, results in removal of the untargeted proteins. The His-tagged target protein can be eluted with an increasing concentration of imidazole, and the competitor is then removed by buffer exchange or size-exclusion chromatography.

4.3.2. Anion exchange chromatography

Anion exchange chromatography uses a positively charged resin with an affinity for molecules having net negative surface charges. The net surface charge of the proteins, as the basis of separation, depends on the surrounding pH. When pH is above the isoelectric point (pI) of the protein, it will bind to a positively charged resin (anion exchanger), when it is below pI a protein will bind to a negatively charged resin (cation exchanger). Strong ion exchangers maintain their binding capacity at both high and low pH levels, remain fully charged across a wide pH range.

Table 4.2. The types and functional groups of the ion exchangers **[**155**]**

Anion exchangers	**Type**	**Functional group**
Quaternary ammonium (Q)	strong	$-O-CH_2N^+(CH_3)_3$
Diethylaminoethyl (DEAE)	weak	$-O-CH_2CH_2N^+H(CH_2CH_3)_3$
Diethylaminopropyl (ANX)	weak	$-O-CH_2CHOHCH_2N^+H(CH_2CH_3)_3$
Cation exchangers		**Functional group**
Sulfopropyl (SP)	strong	$-O-CH_2CHOHCH_2OCH_2CH_2CH_2SO_3^-$
Methyl sulfonate (S)	strong	$-O-CH_2CHOHCH_2OCH_2CHOHCH_2SO_3^-$
Carboxymethyl (CM)	weak	$-O-CH_2COO-$

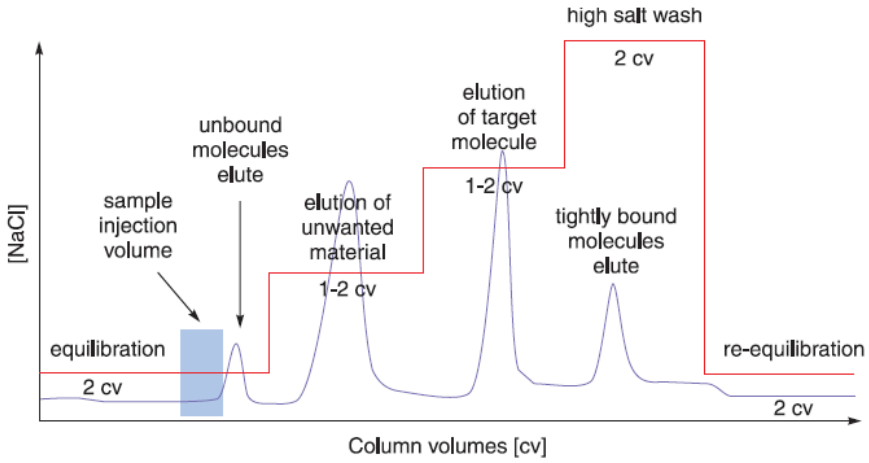

Figure 4.6. Example of an ion exchange chromatogram (from Amersham Biosciences Handbooks).

Weak ion exchangers, on the other hand, exhibit variability in their IEX capability in response to pH variations and gain or lose protons as a result. Examples of ion exchangers are included in **Table 4.2.** In the purification process, the system is equilibrated with a buffer, and then the sample is applied to the ion exchange column. After washing, an increasing ion concentration gradient or

pH-change is applied in order to elute the proteins depending on the strength of their interaction with the column (**Fig. 4.6**.). In the ion exchange chromatography, a peak of the chromatogram can still contain the mixture of proteins. It is important to optimize the gradient elution in order to get a high resolution.

In this work, a Sepharose Q Fast Flow column was used to purify TEM-1 β-lactamase. In this Fast Flow ion exchanger column 90 μm agarose beads serve as a matrix that is crosslinked (6%). The detailed protocol of the chromatographic protein purification procedures are provided in **Protocols A3-A5** in Appendix.

4.4. Detection of proteins by SDS-PAGE

Gel electrophoresis is a useful separation technique of macromolecules in an electric field. Polyacrylamide gel electrophoresis (PAGE) with sodium dodecyl sulfate (SDS) is commonly applied for the separation of proteins. SDS eliminates the effect of the protein structure and charge by binding to the protein backbone. As a consequence, proteins unfold into linear chains with negative charge, that is proportional to the polypeptide chain length within a wide pH range (**Fig. 4.7**). For the proteins containing cysteines, which can easily be oxidized to form disulfide bridges, the addition of a reducing agent is also needed. The proteins are then separated solely based on polypeptide chain length (molecular mass), strongly attracted toward an anode (positively-charged electrode). Unfolded small proteins migrate faster through a gel matrix than the large ones.

SDS-PAGE is used for estimation of relative molecular mass of the separated proteins, determination of the relative abundance of major proteins in a sample, determination of the proteins distribution among fractions, *i.e.*, purity of protein samples; monitoring the progress of a fractionation or purification procedure.

Polyacrylamide gel is prepared through the radical polymerization of acrylamide, by addition of N,N-methylene bis-acrylamide as a crosslinking agent. The reaction is initiated with ammonium-persulfate (APS) and controlled with N,N,N',N'-tetramethylethylenediamine (TEMED). The electrophoresis is carried out in a vertical direction. The gel has two layers: a short stacking gel (5-7% (*w/v*) acrylamide, pH = 6.8) and a long resolving gel (12-16 % (*w/v*) acrylamide, pH = 8.8). The protein sample is prepared with the addition of cracking buffer that includes the 0.01 M Tris-HCl buffer, pH ~ 8.5, ~1 % (*w/v*) SDS solution; 10 % (*w/v*) glycerol; 0.06 mg/mL Coomassie Brilliant Blue dye (CBB), and 0.05-0.1% (*w/v*) mercaptoethanol (for reduction of disulfide bridges). The mixture of protein samples with cracking buffer is incubated at ~ 95 °C for

5-10 min. The protein sample is loaded into the wells of the gel in parallel with an unstained protein mixture (marker with known size), used to compare with the investigated protein. In a careful experiment the protein concentration can also be estimated.

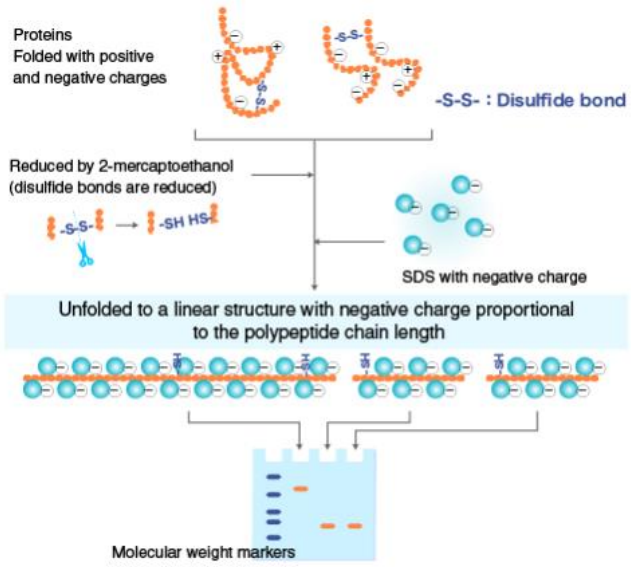

Figure 4.7. Preparation of the protein samples for SDS PAGE, from Medical and biological laboratories CO (https://ruo.mbl.co.jp/)

During the SDS PAGE experiment, the proteins run through the stacking gel under low voltage condition to form highly concentrated narrow bands. After that the voltage is increased to ~ 120 V. After the electrophoretic run, the protein bands in the gel are stained with the Comassie Brilliant Blue dye, an anionic triphenylemethane dye that nonspecifically binds proteins.

In this work, the purification steps of the targeted proteins (TEM-1 β-lactamase, KGNK, and KGNK-His) were monitored by 12.5-15% (*w/v*) (acrylamide:N,N-methylene bis-acrylamide 19:1) SDS PAGE in order to examine the final product and approve the identity, purity and to determine the concentration of the target proteins in comparison with a mixture of seven unstained proteins (116, 66.2, 45, 35, 25, 18.4, and 14.4 kDa) as a molecular marker. The experiment was carried out at room temperature at 70 V for 30 min, then 120 V for 150-180 min, using 0.1 M Tris-HCl, 0.1 M tricine, and 0.1% (*w/v*) SDS, pH 8.3 as the cathode buffer and 0.2 M Tris-HCl, pH 8.9 as the anode buffer.

4.5. Detection of DNA by agarose gel electrophoresis

Agarose gel electrophoresis (AGE) is a separation technique for macromolecules such as DNA, RNA, and detecting their interactions with proteins. Different molecular size and structure causes different electrophoretic mobility in a gel matrix in an electric field. In agarose gel electrophoresis, the gel is in horizontal direction. In most of the cases the protein/DNA complexes migrate more slowly in the gel than the free DNA due to altered shape and charge. It is also possible to distinguish between specific and nonspecific binding, the former resulting in a sharp band, while a smear can be observed for non-specific interactions.

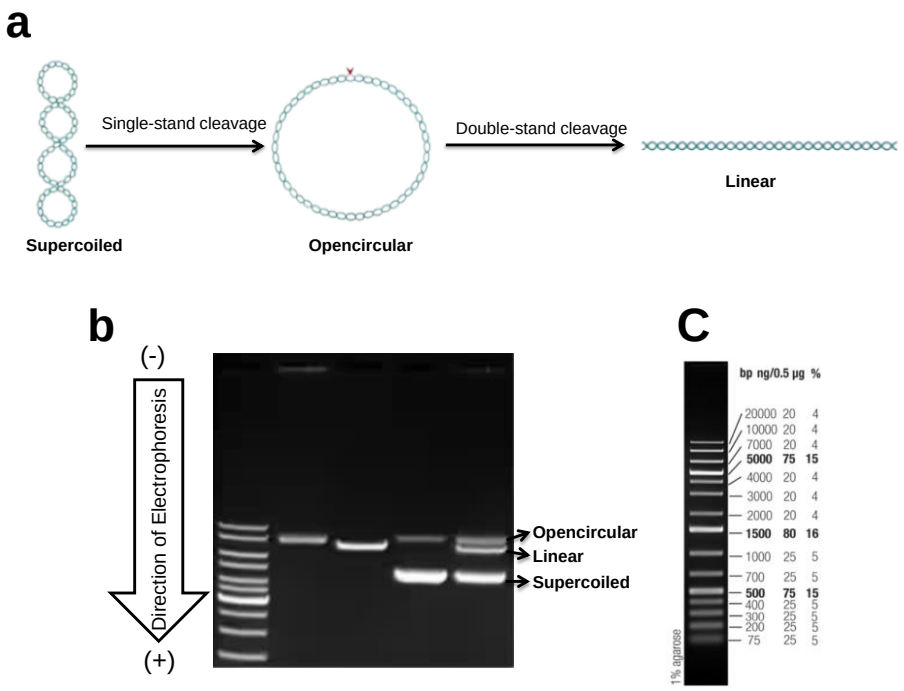

Figure 4.8. a) Various forms of the plasmid DNA. **b)** Agarose gel electrophoresis of a plasmid DNA sample **c)** Gene Ruler 1 kb DNA Ladder (Marker), from Thermofisher (https://www.thermofisher.com/).

The method is simple, robust and suitable for DNA between 100-10000 bp size, while for very low quantity or short DNA, native PAGE is more appropriate. Bacterial plasmids (cyclic DNA) are naturally in their superhelical (supercoiled) form. A single strand cut (nick) turns the DNA molecule into a relaxed open circular form. A double strand cleavage results in a linear DNA form of the same molecular size (**Fig. 4.8a**). Electrophoretic mobility shift assay (EMSA) is a common choice to differentiate among these forms and thus, the cleavage of DNA by nucleases can also be tracked (**Fig. 4.8b**).

The detection of the DNA band is usually based on the significant change of the light emission intensity of a fluorescent molecule upon DNA binding. Ethidium-bromide is a frequently used example that intercalates between the neighboring base pairs of the DNA molecule followed by increased fluorescence intensity. A more sensitive detection of DNA molecules includes radiolabelling by γ-^{32}P, but is requires a special treatment. The size of the DNA is estimated by a comparison with a DNA mixture containing molecules with known size – marker (**Fig. 4.8c**)

4.6. Study of proteins by mass spectrometry

Mass spectrometry (MS) is a powerful and sensitive analytical technique that can be used for identification and partially for quantification of the compounds in a mixture. It is precisely identifying molecules based on their intact molecular mass, as well as the molecular masses of fragments formed from the molecules [160]. First, the molecules are ionized and transferred to a gas phase, and then the charged molecules are accelerated in the mass analyzer under vacuum. The molecular ions fly with a velocity and/or track that depend on their m/z value, and finally they are detected.

Several types of ionization methods in MS were developed, [160] *e.g.*, electron impact (EI), fast atom bombardment (FAB), atmospheric pressure chemical ionization (APCI), electrospray ionization (ESI), matrix assisted laser desorption ionization (MALDI), and electrospray ionization (ESI) is a soft ionization technique that is frequently applied for macromolecules. The molecular ions are established by applying a high voltage on a flow of liquid through a capillary at a rate of a few μL/min. Evolving nano-ESI decreased the necessary sample amount [161]. The sample droplets are desolvated and directed to an opening in the vacuum system of the mass spectrometer. The formed ions are ejected from the droplets and accelerated into the mass analyzer. Because of its success, ESI is being continuously developed. New variants are nanospray, static nanospray or picospray and desorption electrospray ionization (DESI) methods. In static nanospray or picospray techniques, flow is created by the electrostatic spray or a small gas pressure. In desorption electrospray ionization (DESI) the spray extract ions from the surface into the mass spectrometer. Nanospray has the following properties: highly sensitive; capillary has a diameter of 1-10 μm and coated with a conducting material e.g. gold; 1-5 μL is required of sample for loading; the capillary is placed 0.5-2 mm from the electrode orifice under camera control; flow is 20-50 nL/min; applied voltage is 500-1500 V; 0.1-10 μM is required concentration for proteins. The droplets diameter is

around 150 nm, while the droplets diameter in ESI is around 1.5 μm, therefore there is less possibility to get fission and shrinkage process; salt-tolerance is about 10^{-2} M NaCl without interference with the measurement [161].

Examples of common mass analyzers include the magnetic sector, ion trap and time-of-flight (TOF), and orbitrap mass analyzers. The Orbitrap mass analyzer was introduced in 2005 by Thermo Fisher Scientific. It is composed of an outer barrel-shaped electrode which is kept neutral with a radius r2 and a central spindle electrode along the axis of radius r1 and with a fixed direct current (**Fig. 4.9**). The ions are confined around a central electrode with harmonic oscillations using only direct current and without utilizing radiofrequency (RF) or magnetic field. The image current generated by the oscillating ions is detected and analyzed [162].

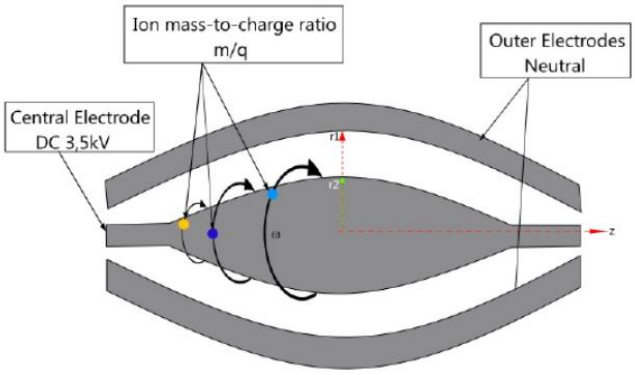

Figure 4.9. Schematic of an orbitrap mass analyzer from [163]

The m/z spectra of proteins typically represent multiple charge states. In the most frequently used positive mode of measurements, the basic sites of the proteins get protonated. The neighboring peaks in a simplified mass spectrum shown in **Fig. 4.10**, correspond to protein molecules differing in one H^+. The three equations shown in (**Fig. 4.10**) contain three unknowns (z_1, z_2, M), where m_1 and m_2 are the values read from the peaks of the mass spectrum, z_1 and z_2 are the corresponding charges, and M_H is the mass of the proton, thus the molecular mass of the protein (M) can be determined. This can be repeated for all peaks and the averaged results provide a precise solution for the molecular weight.

The deconvolution of an m/z spectrum into a mass spectrum is carried out by the help of computer programs. The obtained data are compared with the expected molecular mass of the sample. However, if there are metal ion cofactors, disulfide bridges or other modifications in the

protein, the expected mass will differ from the calculated one. In the presence of a bound metal ion the expected molecular mass is calculated by the formula:

Expected Mass = Calculated Mass + Metal ion Mass – metal ion charge (z).

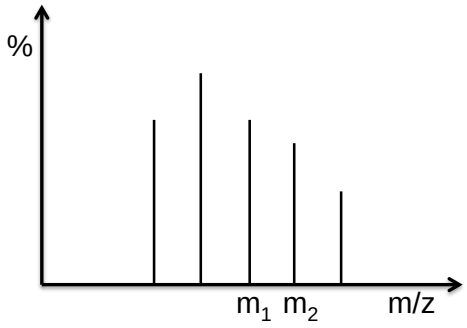

$$m_1 = \frac{M + z_1 M_H}{z_1}$$

$$m_2 = \frac{M + z_2 M_H}{z_2}$$

$$z_2 = z_1 + 1$$

Figure 4.10. **a**) A hypothetical multiply charged m/z spectrum. **b**) Equations describing the calculation of the molecular mass from the two neighboring peaks in the theoretical spectrum shown in panel **a**.

The m/z spectra can provide further structural details. In the m/z spectra the folded protein molecules usually a narrow, low charge state range is observed, because only certain groups on their surface can be protonated. As in opposite, unfolded proteins appear at low m/z values due to higher charge states and in a wide range depending on the completeness of protonation. Therefore, this technique can be applied to study the metal-ion dependent structural features of the proteins. [164;165]

In our experiments, a TriVersa Nanomate (Advion) chip-based nanoelectrospray ion source coupled to a linear trap quadrupole LTQ-Orbitrap Elite (Thermo Scientific) high resolution mass spectrometer was utilized for intact protein analysis. Measurements were carried out in positive mode at 120,000 resolution (R=120,000 at 400 m/z) in ammonium hydrogen carbonate buffer (pH ~7.8). The protein analysis based on tryptic fragments was performed on an Orbitrap Fusion Lumos mass spectrometer. The deconvolution of the spectra to yield the masses of $M+H^+$ ions and spectrometric pattern simulations were performed using the Freestyle 1.6 or Xcalibur 2.2 softwares (Thermo Scientific). Deconvolution of 10×10 consecutive scans provided a standard deviation of the peak positions being less than 0.02 mass units.

2.0 μM TEM-1 β-lactamase was used in each individual sample containing 0, 1, 2, 5, and 10 equivalents of $NiCl_2$, and $HgCl_2$ in 50 mM ammonium bicarbonate/NH_3(aq), ~ pH 7.8 buffer. For the SDS-PAGE band analysis, TEM-1 β-lactamase was analyzed by cutting the protein band

from the SDS PAGE (expression SDS PAGE) then sliced it into small pieces and subjected to in-gel digestion. After that the sample was reduced with dithiothreitol, alkylated with iodoacetamide, and digested with trypsin for 4 h at 37 °C. Tryptic peptides were extracted, dried in a vacuum concentrator and reconstructed in 20 µl of 0.1% (*v/v*) formic acid. An aliquot of these (5 µL) was loaded to Evosep One tips and subjected to liquid chromatography-tandem MS analysis. NColE7 mutants (KGNK, and KGNK-His) concentrations were 3.0 µM in each individual sample containing different molar ratios with individual and mixed equivalents of $NiCl_2$, $CdCl_2$, $CuCl_2$, and $ZnCl_2$ in 2.5 mM ammonium hydrogen carbonate buffer, pH ~7.8.

4.7. Study of proteins by circular dichroism spectroscopy

There are three types of polarized lights (PL), which are linearly (LPL), circularly (CPL), and elliptically (EPL) polarized lights. In linearly polarized light, the electromagnetic wave oscillates along a single plane; in elliptically polarized light, two perpendicular waves have unequal amplitude and differ in phase by 90°, while in circularly polarized light, the two perpendicular waves are equal in amplitude with a 90° difference in phase as the light beam propagates. In a circular dichroism spectrophotometer, the linearly polarized light is converted into circularly polarized light by a photo-elastic modulator (PEM).

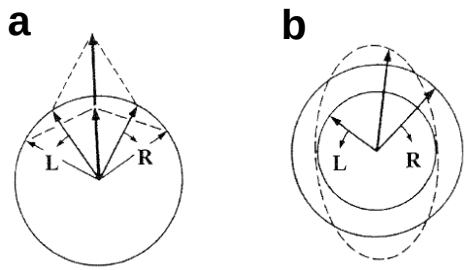

Figure 4.11. a) Combination of the left and right circularly polarized light beams of the same intensity results in a linearly polarized light in the original plane. **b**) Elliptical polarization results from the combination of the left and right circularly polarized light beams being absorbed to a different extent by a chiral molecule. This figure is from [166].

Circular dichroism (CD) spectroscopy is based on the differential absorption of left and right circularly polarized light by an optically active (chiral) substance resulting in elliptically polarized light (**Fig. 4.11**). It is an essential analytical technique for the determination of conformation and structural changes upon interactions and thereby, determination of equilibrium dissociation constants (K_d) of chiral molecules, such as proteins, nucleic acids (DNA and RNA),

carbohydrates, amino acids, etc. Most CD experiments require a small amount of sample compared to other structural techniques.

The far-UV region (180-250 nm) of the CD spectrum is related to the peptide backbone of the protein described by the three dihedral angles at each amino acid residue that change depending on the protein conformation and it is characteristic for the ordered secondary structure elements. There are two absorption bands related to the CD spectrum in this range, which can be deconvoluted to estimate the composition of the secondary structure (α-helices, β-sheets, turns, and unordered) elements of the protein under different conditions. These are attributed to the strong $\pi \rightarrow \pi^*$ transition centered around 190 nm and a weaker but broader $n \rightarrow \pi^*$ transition between 210-220 nm (**Fig. 4.12**). The aromatic side chains and disulfide bridges also contribute to the far-UV spectrum. In analysis and evaluation of the secondary structure components, the experimental CD spectrum is fitted using a set of reference spectra recorded for proteins of known secondary structure compositions [167]. The near-UV CD spectrum (250-320 nm) is related to the protein tertiary structure. The aromatic side chains of Phe, Tyr, and Trp residues show peaks between 255-270 nm, 275-285 nm, and 290-305 nm, respectively.

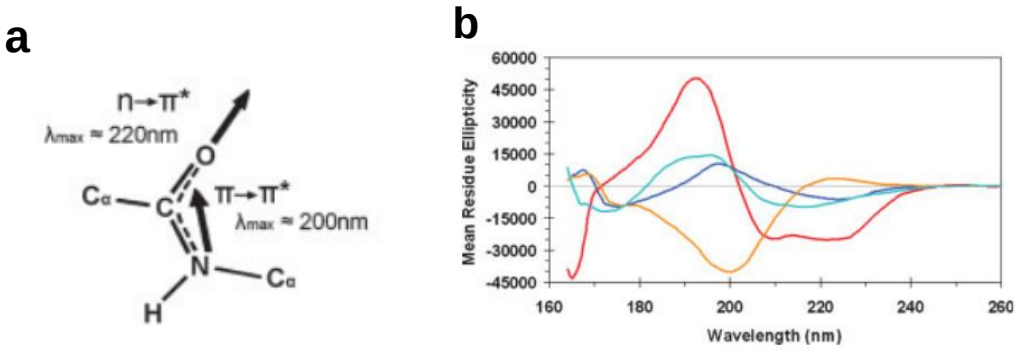

Figure 4.12. a) Electronic transitions of peptide bonds, **b**) Typical CD spectra of the different protein secondary structure compositions, a mostly helical protein in myoglobin (in red), mostly β-sheet proteins in concanavalin A (blue) and β-lactoglobulin (cyan), and a polyproline-rich protein in collagen (orange). This figure is from [167].

In a CD spectrometer, the absorbance difference $\Delta A = A_L - A_R$ is measured, where A_L and A_R is the absorbance of the left and right circularly polarized light, respectively. Beer's Law is also applied for CD measurements according to: $\Delta A = A_L - A_R = \varepsilon_L \, l \, c - \varepsilon_R \, l \, c = \Delta\varepsilon \, l \, c$, where A is the absorbance, ε is the molar absorption, l is the cell path length in cm, and c is the sample concentration. The difference in absorbance results in an elliptically polarized light, characterized

by the ellipticity (θ), in millidegrees. Ellipticity is defined by the equation $\tan\theta$ = b/a where b and a are the minor and major axes of the resulted ellipse (**Fig. 4.11**). The relationship between the ellipticity (mdeg) and the absorbance difference can be written as: $\Delta A = \theta$(mdeg)/32980 [166]. The mean residue molar ellipticity [θ] is given in deg cm^2 dmol^{-1} units. The molar ellipticity can be formulated as: $[\theta]_{\text{molar},\lambda} = (100\ \theta_\lambda)/(c\ l)$, where λ is the wavelength, c the molar concentration and l the path length in cm. For data in absorption units, the molar molar absorbance ($\Delta\varepsilon$) is usually calculated. If the observed difference in absorbance at a certain wavelength of a solution of concentration (c) in a cell of pathlength (l) is ΔA, then $\Delta\varepsilon = \Delta A/c\ l$. The unit of the molar absorbance is M^{-1} cm^{-1}. The relationship between $[\theta]_{\text{molar},\lambda}$ and Δε is given by: $[\theta]_{\text{molar},\lambda} = 3298\ \Delta\varepsilon$. For proteins the molar CD used for the secondary structure calculations is related to a mean residual value.

It is not possible to record CD spectra below ~180 nm using conventional CD instruments because the intensity of the xenon light source decreases at ~180 nm, as well as water, salts, and several buffers drastically increase the absorption at low wavelengths. N_2 gas is used to purge the optical units to protect the optics from ozone and exclude oxygen that absorbs in the range 180–200 nm. However, in the synchroton radiation CD-spectroscopy (SRCD), it is possible to measure down to ~160 nm [168], due to high intensity of the beam and the vacuum system [169].

In our study, the CD spectra were recorded at room temperature on a Jasco J-1500 CD spectrometer. The parameters were adjusted as described in the following. Wavelength range: 300 – 180 nm in case of TEM-1 β-lactamase and 180 – 280 nm for NColE7 mutants; path length: 0.2 mm (Hellma quartz cuvette); D.I.T.: 2 sec; bandwidth: 1.0 nm; scanning speed: 50 nm/min (continuous scanning mode). Each spectrum was the average of three accumulated measurements. Water and the buffer solution spectra were recorded for baseline correction and the spectra were plotted without smoothing. The concentration of TEM-1 β-lactamase was 8.6 μM in 20 mM Tris-HCl (pH 7.5). TEM-1 β-lactamase was titrated with $NiCl_2$, $CdCl_2$, and $HgCl_2$ to adjust protein: M(II) molar ratios to 1:0, 1:1, 1:2, 1:5, and 1:10. The concentrations of the NColE7 mutants (KGNK, KGNK-His) were 18.0 μM in 3-10 mM HEPES, pH 7.7. The measurements were carried out with apo enzyme, and in the presence of EDTA, phosphate, chloride ions and/or various metal ions ($ZnCl_2$, $CuCl_2$, $NiCl_2$ and $CdCl_2$) at 1:0, 1:1, 1:2, 1:3, and 1:5 protein:M(II) molar ratios.

4.8. Determination of protein concentration

Several procedures, used to determine the concentration of a protein by UV-Vis absorbance spectroscopic method (comassie blue staining, Biuret, Lowry, and Bradford methods) apply a

reference protein to determine the target protein concentration. Direct UV-Vis absorbance spectroscopy of a protein includes measurement of the absorbance of the protein sample at 280 nm and apply the Lambert-Beer law based on the estimated molar absorbance. The estimation is carried out by the Expasy online tool [170].

Comassie blue staining is also applied in the electrophoresis of the protein at different sample volumes, in parallel with a standard protein as a control (with known concentration). After the SDS PAGE experiment, the gel is stained, and then the band intensities are analyzed [171-173] and compared to a control band.

In this work the molar absorbance of the proteins ε_{280} for TEM-1 β-lactamase was estimated to be 28,085 $M^{-1}cm^{-1}$, for NColE7 mutants (KGNK, and KGNK-His) 12,490 $M^{-1}cm^{-1}$. A UV absorbance spectrum of pure TEM-1 β-lactamase was recorded in 20 mM Tris-HCl, pH 7.5, while NColE7 mutants were in 20 mM HEPES pH ~7.7. In addition, the quantity of purified targeted proteins (TEM-1 β-lactamase, and NColE7 mutants) was estimated by ImageJ analysis of the SDS PAGE band intensities of the loaded target protein and the marker.

4.9. Study of TEM-1 β-lactamase by PAC spectroscopy

The perturbed angular correlation (PAC) spectroscopy detects the hyperfine interaction between the external electromagnetic field and the electromagnetic moments of the nuclear state [174].

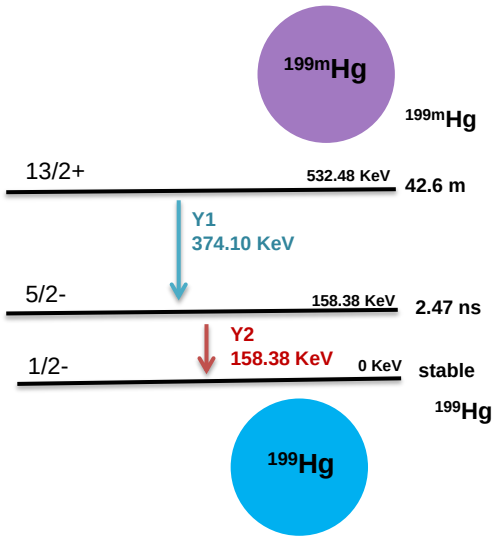

Figure 4.13. The nuclear PAC levels of Hg(II) split through hyperfine interactions between nuclear moments and electronic field.

The idea behind perturbed angular correlation is to create a radioactive nucleus, bring it into the host material under study, and let it decay across a γγ-cascade in the ground state of the daughter nucleus (**Fig. 4.13**), while an angular correlation between the two emitted γ-rays is observed. The interaction of the radioactive nucleus with the surrounding, *i.e.*, with the protein, perturbs the angular correlation of the γ-rays. The measured nuclear quadrupole interaction (NQI) is mainly determined by two parameters, the quadrupole frequency, ν_Q, and the asymmetry parameter, η [174]. In addition, the parameter δ reflects the so-called static line broadening due to static (on the PAC time scale) variations in structure from one molecule to the next, λ reflects the effect of dynamics (local and global rotational diffusion), and the signal amplitude is denoted A [175]. These parameters are affected by the chemical surroundings, thus they provide information about the coordination mode of Hg(II) in our experiments. ^{199m}Hg PAC measurements were carried out by the PAC group of Lars Hemmingsen (University of Copenhagen) in an international collaboration at the ISOLDE laboratories at CERN [176]. The details of the measurements are described in detail in **Protocol A6** in Appendix.

4.10. Catalytic activity of enzymes

4.10.1. Catalytic activity of NColE7 mutants

The catalytic activity of the NColE7 mutants (KGNK and KGNK-His) was monitored against plasmid DNA (pUC119) as a substrate. In a few experiments, the proteins were treated with EDTA. The concentrations of KGNK and KGNK-His were 1.0 μM and 2.8 μM, respectively, while the DNA concentration was 74 μM for base pairs in 10-20 mM HEPES, pH 7.7. DNA cleavage was performed in the absence and presence of different metal salts: $ZnCl_2$, $CuCl_2$, $CdCl_2$ and $NiCl_2$, at different molar ratios of the enzyme to metal ion. The reaction mixtures were prepared by mixing all of the components, except for the plasmid DNA, which was added to the mixture last. At least three replicates were carried out for each experiment. The mixtures were incubated at 37°C for 120 min. Aliquots of 5 μL of the reaction mixture were taken 3-4 times and the reaction was stopped by adding 5 μL of 2% (*w/v*) SDS solution (1% final concentration) for enzyme denaturation. The products of the DNA cleavage assays were checked by 1.0 % (*w/v*) agarose gel electrophoresis containing 0.5 g/mL ethidium bromide for the visualization of the DNA. Electrophoresis was performed in the TAE buffer (40 mM tris(hydroxymethyl) aminomethane, 20 mM acetic acid and 1 mM ethylenediaminetetraacetic acid, pH 8.0) using Bio-Rad wide mini sub cell VR GT, applying

7 V/cm potential gradients (100 V for 40 min). Gene ruler 1 kb plus DNA ladder as reference and non-cleaved pUC119 as a negative control was applied for comparison.

4.10.2. Kinetic investigation of TEM-1 β-lactamase

The kinetic parameters for the hydrolysis of various concentrations of ampicillin solutions (230 μM – 930 μM) catalyzed by the purified TEM-1 β-lactamase or metallized TEM-1 β-lactamase were determined in two buffers (20 mM Tris-HCl, pH 7.5; and 50 mM phosphate buffer, pH 7.0) in our experiments. The final concentration of purified enzyme was between 0.24 - 2.4 nM with and without metal ions ($HgCl_2$, $Hg(ClO_4)_2$, $NiCl_2$, $CdCl_2$) at various protein:metal ion molar ratios. The kinetic reactions were monitored using a Cary 3500 UV-Vis double beam multi-cell and controlled temperature spectrophotometer at two temperatures (25 ºC and 30 ºC) at multiple wavelengths between 210 – 235 nm, with 1.0 cm path length quartz cuvette (Hellma).

The kinetic calculations were performed using ChemMech program [177]. This program was developed specifically to fit more experimental curves simultaneously in a single run. The concentration versus time curves were applied to calculate rate constant values and initial concentrations. The absorbance versus time curves can be calculated by the Beer-Lambert equation with an appropriate set of molar absorbance values. After that, the fitting process involved automatic adjusting the molar absorbance values and rate constants, as well as recalculating the A(t) curves, until the minimal difference between the calculated and observed curves was obtained. During the calculations, the number of time points was reduced to 120 for each curve. The points were distributed along the arc of the curves as proportionally as possible, so the calculations included the whole monitored time range to obtain reliable information. The fitting procedure was carried out in several ways, such as changing the fitted and fixed parameters.

4.11. Bacterial viability assays

We used cell culture-based bacterial viability assays depending on the conditions adjusted within the M9 minimal medium (0.0442 M Na_2HPO_4; 0.0211 M KH_2PO_4; 0.0086 M NaCl; 0.0185 M NH_4Cl; 0.002 M $MgSO_4$; 2.0 g/L glucose; 0.0001M $CaCl_2$; and distilled H_2O) [178] in the presence of various concentrations of metal ions, such as Hg(II), Cd(II) or Ni(II) ions. The number of the cells in a bacterial culture is reflected by its McFarland, or optical density (OD_{600}) value. A McFarland densitometer was used to monitor the growth of the bacterial cells.

The *E. coli* BL21(DE3) cells were transformed with a modified pET-21a-NFI-BDH vector providing ampicillin resistance or with the pET-M11-SUMO3-GFP DNA vector providing

kanamycin resistance [179], and grown in 50 mL lysogeny broth (LB) media containing ampicillin at 37 ºC. When the bacterial culture reached McFarland value ~2.6, these bacterial cultures were centrifuged at 4000×g for 15 min at 4 ºC, and then the bacterial pellets were washed twice with cold M9 minimal medium and resuspended in cold M9 minimal medium. These bacterial cells were distributed into 5 mL aliquots and incubated with shaking at 37 ºC. When the McFarland values reached ~1.0 or ~2.3, the chemicals (ampicillin, kanamycin, IPTG, and metal ions) were supplemented at various concentrations (**Table A1** in Appendix), and then the samples were incubated at 24 °C for up to 17 h, while monitoring the McFarland values.

5. RESULTS AND DISCUSSION

5.1. TEM-1 β-lactamase

5.1.1. TEM-1 β-lactamase expression

The 861 base pair (bp) gene of TEM-1 β-lactamase is designed in several pET DNA vector series, and it is located between deoxy-nucleotides 3985-4845 in the pET-21a(+) in the same orientation as the gene of the protein of interest is inserted in the multi-cloning site (MCS). However, the TEM-1 β-lactamase gene is positioned outside of the MCS. This gene is transcribed and translated within the host bacterial cells to produce the 286 amino acid-long ampicillin resistance protein. While enough protein is synthesized to provide resistance against ampicillin antibiotics, this can be considered as a poor protein expression. Therefore, the overexpression of TEM-1 β-lactamase from pET-21a(+) in the presence of IPTG inducer is not a typical approach of its purification. Generally, in TEM-1 β-lactamase overexpression process, the gene of the enzyme itself is inserted in the MCS of an expression vector that carries the gene of an another antibiotic resistance protein for selection *e.g.*, the pET-24a-d(+) vectors providing kanamycin resistance to cells.

In this work, TEM-1 β-lactamase overexpression was achieved using a pET-21a(+) vector, often used in our laboratory, carrying the coding sequence of a foreign protein, the DNA binding domain of the His-tagged Nuclear Factor I protein [180] known as NFI-BD, or its mutant NFI-BDH. The 720 bp genes of NFI-BD and its mutant NFI-BDH were amplified by PCR to be terminated with NdeI and XhoI restriction enzyme recognition sites, as shown in **Scheme A1** in Appendix. The PCR products were ligated into pET-21a(+) DNA vector after digesting both the PCR fragments and the vector with NdeI and XhoI restriction enzymes. The deoxy-nucleotide sequences of the inserted genes (NFI-BD and NFI-BDH) were verified by automated DNA sequencing using the commercial T7 promoter primer. The proteins were expected to be overexpressed with a C-terminal 6×His residues (His-tag), with similar sizes to TEM-1 β-lactamase (the molecular mass of NFI-BD is 29,082.3 Da, NFI-BDH is 29,091.3 Da, while for TEM-1 β-lactamase is expected to be 31,515.2 Da according to the description of the supplier of the vector).

The proteins were expressed using high concentration of IPTG inducer (1mM) and by incubation of the *E. coli* BL21-DE3 host cell cultures at 24ºC for 17 hours. The SDS PAGE (experiment with NFI-BDH is shown as an example) revealed a protein band about 30 kDa with noticeably increased intensity compared to the control experiments carried out with the pET-21a(+) vector itself and also those without applying IPTG (**Fig. 5.1**). Previously, the expressed NFI-BDH

protein was highly insoluble, while TEM-1 β-lactamase is a well soluble protein [181]. The SDS PAGE band of the target protein was detected in the soluble fraction (**Fig. 5.1b**). Based on the size of the proteins, it is difficult to distinguish between the SDS-PAGE band of the TEM-1 β-lactamase and the NFI-BDH protein.

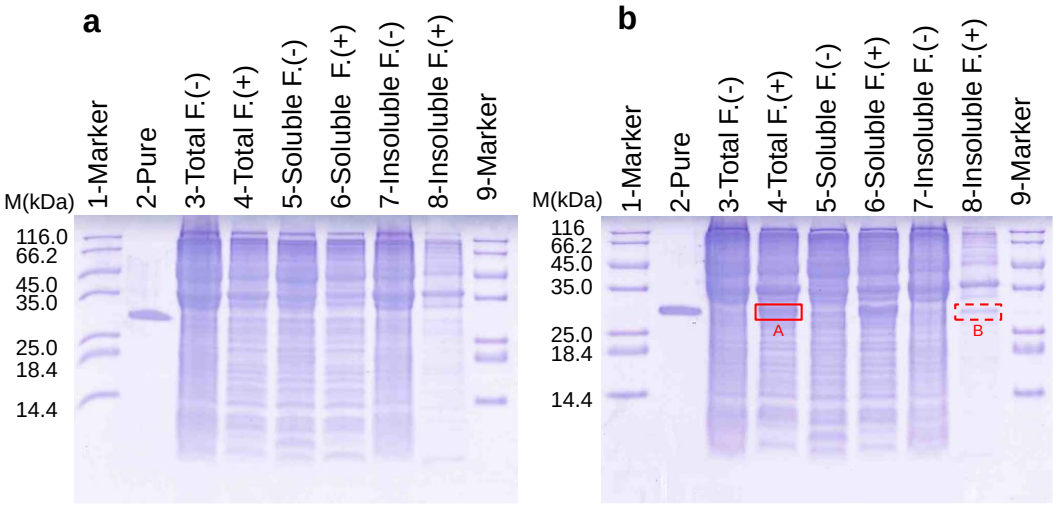

Figure 5.1. SDS PAGE monitoring of the protein expression in BL21(DE3) *E. coli* bacterial cells using pET-21a(+) **(a)** and pET-21a(+) with the inserted NFI-BDH gene **(b)** (–) without IPTG inducer, (+) in the presence of IPTG inducer at 1 mM concentration. **(**a) (1 and 9) marker, (2) pure protein, (3, 5, and 7) total, soluble, and insoluble protein fractions (lysates), respectively, without inducing by IPTG, while (4, 6, and 8) were the total, soluble, insoluble protein fractions (lysates), respectively, with 1 mM IPTG. **(**b) (1, and 9) marker, (2) pure protein, (3, 5, and 7) total, soluble, and insoluble protein fractions (lysates), respectively, without adding IPTG to the culture, while (4, 6, and 8) total, soluble, insoluble protein fractions (lysates), respectively, using 1 mM IPTG inducing agent [P1].

Therefore, the band of the target protein (**Fig. 5.1b**, lanes no. 4 and 8) was cut from the gel, and analyzed by mass spectrometry using trypsin-digested peptide fragments (see the results in **Table A2** in Appendix). The subsequent database search revealed the dominant component to be the *E. coli* TEM-1 β-lactamase (UniProtKB-P62593 (BLAT_ECOLX); EC: 3.5.2.6). Thus, the observed band was related to the TEM-1 β-lactamase instead of the expected NFI-BDH protein. Only traces of NFI-BDH could be identified based on a few detected peptide fragments. This result is surprising because the TEM-1 β-lactamase gene is located outside of the MCS. According to the pET System Manual, TEM-1 β-lactamase can be accumulated in the presence of IPTG when the T7 transcription terminator is removed. However, this is not the case in our system, and thus other reasons (not investigated here, because this was out of the frame of our studies) may have

contributed to the obtained result. This fortunate chance prompted us to study TEM-1 β-lactamase as a fascinating hydrolytic enzyme.

5.1.2. TEM-1 β-lactamase purification strategy

Previously, several studies reported the different types of β-lactamase purification using fused affinity tags such as His-tag [182-184]. The remained affinity purification tag can change the properties of the enzyme. For example, the tag bound to the targeted protein can interact with metal ions, thereby modifying the function of the protein. Therefore, an extra step in the purification process shall be invented to remove the affinity purification tags. This extra step consumes time and extra effort, increasing expenses, and can also cause modifications in the quantity and quality of the yielded proteins. In addition, purification of a protein under re-denaturation conditions can also change the properties or function of the purified protein. For example, Lawung [50] purified the TEM-1 β-lactamase in a denaturing condition, and the catalytic activity of the purified enzyme was 32-fold higher than that of the native enzyme. Purification of the enzyme by IMAC under denaturing condition, however, may allow for chelating by increasing number of His residue side chains.

As it was already mentioned in the literature review (**Section 2.1.2.3**), TEM-1 β-lactamase offers a large number of amino acids with side-chains being potentially able to coordinate metal ions. The crystal structure of TEM-1 β-lactamase shows several putative metal ion binding sites, such as His pairs that can be coordinated to borderline transition metal ions, such as Ni(II), Zn(II), Co(II), *etc*.

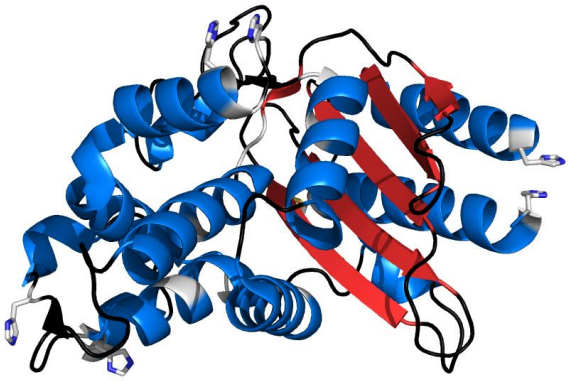

Figure 5.2. Cartoon representation of the crystal structure of TEM-1 β-lactamase (PDB ID: 1ZG4) with the putative surface metal ion binding sites shown by sticks.

A closer look at the available crystal structures revealed, that these sites are located on the protein surface (**Fig. 5.2**), and therefore, we decided to apply immobilized Ni(II)ion affinity chromatography for TEM-1 β-lactamase protein purification keeping the enzyme in its native structure, without denaturation or fusing affinity tags. The applied 3-step purification strategy is shown in **Scheme 5.1**. The purification steps were monitored by SDS PAGE, detecting the protein at ~30 kDa. In the first IMAC purification step, the gradient elution of the proteins was carried out by increasing imidazole concentration. TEM-1 β-lactamase was eluted at ~200 mM imidazole in the PBS solution (~40% (*v/v*) of a 500 mM imidazole solution) (**Fig. 5.3a**). However, the SDS PAGE image of the elution fraction peak showed that high amounts of other proteins were eluted together with the target protein (**Fig. 5.3b**). Thus, the purity of the obtained TEM-1 β-lactamase was unsatisfactory.

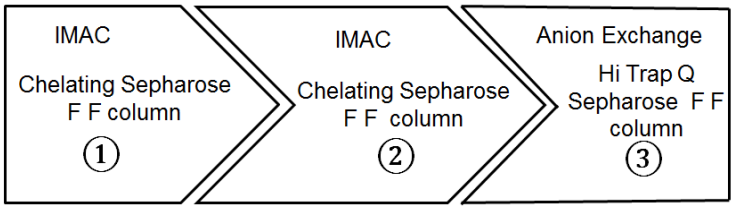

Scheme 5.1. The simplistic representation of the purification strategy using IMAC and anion exchange fast flow (FF) chromatographic columns [P1].

In a second IMAC purification step, 250 mM NaCl in the PBS solution was applied to increase the ionic strength. This shall facilitate the elution of the untargeted proteins bound weakly to the Ni(II)-loaded NTA resin prior to the elution of TEM-1 β-lactamase. In this step, the elution buffer (imidazole) of the E3-E6 elution fractions (as it is shown in **Fig. 5.3b**) of the first IMAC step was removed by ultrafiltration, then loaded on the IMAC column and the elution of the proteins was carried out by ~8–10% (*v/v*) of a 250 mM imidazole and 250 mM NaCl containing PBS solution. The SDS PAGE image of the elution fraction peak showed significantly lower amount of protein impurities than in the first IMAC purification step (**Fig. 5.3c,d)**. The elution buffer (imidazole) of the elution fractions of the second IMAC step was removed by ultrafiltration, then loaded on the FF Q-sepharose (anion exchange) column. The gradient elution was performed by increasing NaCl concentration. The target protein eluted at ~300 mM NaCl (~30% (*v/v*) of a 1.0 M NaCl solution) yielding highly pure enzyme **(Fig. 5.3e,f**). The elution buffer was finally exchanged to 20 mM Tris-HCl, pH 7.5 by ultrafiltration.

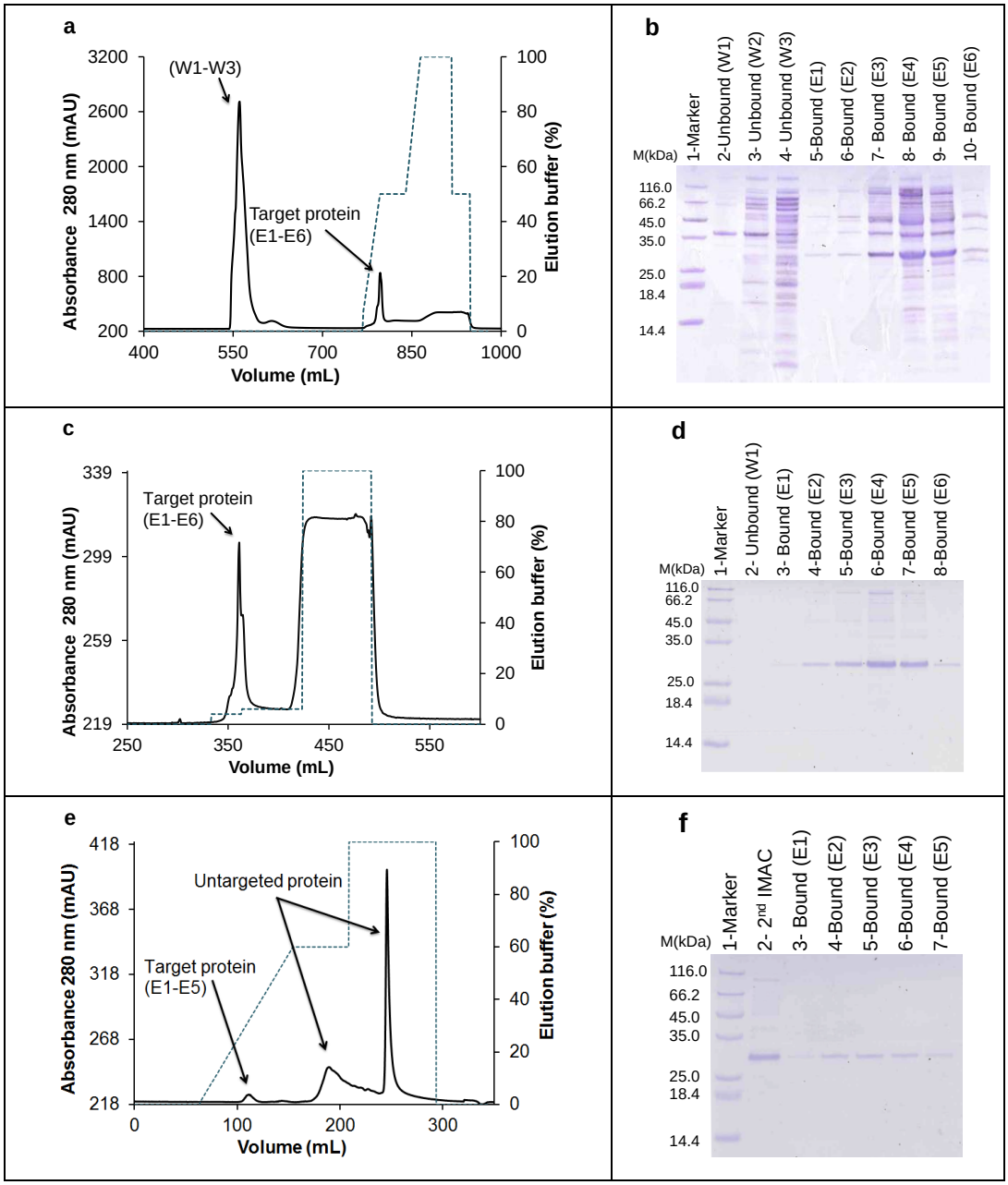

Figure 5.3. The HPLC purification steps of TEM-1 β-lactamase and their SDS-PAGE monitoring. **a** and **c** show the chromatograms of the 1st and 2nd steps of immobilized Ni(II) ion affinity purification, respectively. **e** is the chromatogram obtained during the anion exchange purification step. The dashed lines in panels **a, c** and **e** indicate the fraction of the elution buffers containing the appropriate competitor (imidazole for buffers B1and B2 and NaCl for buffer B3) during the gradient elution. **b**, **d** and **f** show the SDS-PAGE analysis of the **a, c** and **e** purification steps, respectively. **b**: 1 marker, 2-4 wash fractions (W1-W3), 5-10 elution fractions (E1-E6). E3-E6 fractions were collected and subjected to buffer exchange and further purification. **d:** 1 marker, 2 wash fraction, 3-8 elution fractions (E1-E6). E2-E6 fractions were pooled for subsequent anion exchange purification step. **f**: 1 marker, 2 eluted protein from 2nd purification step, 3-7 elution fractions (E1–E5). The **a, c** and **e** panels also show the changes in the composition of the eluent during the whole purification process. Abbreviations: E–elution fraction, and B–bound protein [P1].

The purity of TEM-1 β-lactamase was assessed in each chromatographic step by using the ImageJ tool [171-173] to analyze the SDS-PAGE band intensities, and the results are shown in **Table 5.1.** It represents the intensity ratio of the target protein band to the total intensity of all the protein bands in the same SDS-PAGE lane. The purity of the TEM-1 β-lactamase from the final purification step was determined to be >92.5%.

Table 5.1. Purity (%) of TEM-1 β-lactamase after consecutive purification steps estimated from the SDS-PAGE analysis by Image J [P1].

Purification Step	Purity %
Crude Extract	3.3
Chelating Sepharose FF	35.8
Chelating Sepharose FF	82.7
HiPrep Q Sepharose FF	>92.5

The yield of the purified TEM-1 β-lactamase was estimated by analyzing the SDS PAGE bands and UV absorbance spectra. The intensities of the bands of TEM-1 β-lactamase at increasing loaded volumes (**Fig. A5a** in Appendix), as well as the bands related to approximated amounts of the marker proteins were analyzed by ImageJ program. The yield of the purified protein in solution was estimated to be 0.17–0.34 mg/mL. In another unit it was estimated to be ~1.9 mg per gram of the bacterial pellet (wet weight), and this corresponds to ~10 mg protein per liter of bacterial culture. Previously, TEM-1 β-lactamase was purified from the liquid phase medium, not directly from the cell pellet because the protein is excreted by the bacterial cells into the liquid phase medium to hydrolyze the available β-lactam antibiotic. Thus, the obtained yield is hard to compare with yields from the literature. Pure protein obtained by J. Yang et al. was 2-20 mg per liter of the bacteria culture [51]. On the other hand, Sosa-Peinado and coworkers reported an extremely high yield of pure protein about 140 mg per liter bacterial culture, which was not observed elsewhere, by changing the translocation signal sequence [185]. Nevertheless, the obtained yield here is higher than that achieved earlier by IMAC purification of the protein using Zn(II) ions, this purification resulted ~1.1 mg pure protein/L bacterial culture, with the note that prior to the purification, 1 L of the culture produced ~8 g bacterial wet pellets [50].

5.1.3. Characterization of the purified TEM-1 β-lactamase

5.1.3.1. Mass spectrometric measurements

Electrospray ionization mass spectrometry was used to verify the identity and molecular mass of purified TEM-1 β-lactamase. According to the pET System Manual, the expected average and monoisotopic molecular masses of full-length *E. coli* TEM-1 β-lactamase are 31515.2 and 31495.2 Da, respectively. While the expected average and monoisotopic molar masses for the mature protein are 28907.0 and 28888.8 Da, respectively. The detected mass for monoprotonated $[MH]^+$ species was 28901.9 Da (**Fig. 5.4**), so the monoisotopic intact molecular mass of the purified mature TEM-1 β-lactamase was 28900.9 Da being close to the expected value, but not identical.

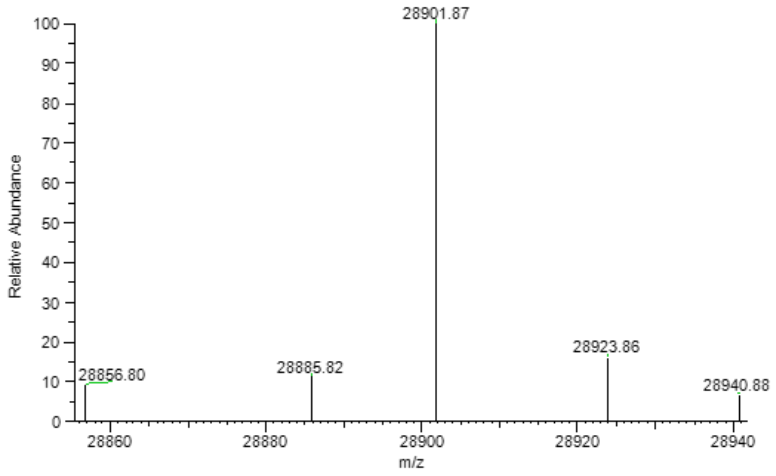

Figure 5.4. The ESI mass spectrum of intact TEM-1 β-lactamase [P1].

However, checking the DNA coding sequence of TEM-1 β-lactamase within the pET-21a(+) vector revealed that its enzyme product differs from the *E. coli* enzyme [186] by a single amino acid (**Scheme 5.2**). There was an isoleucine in position 82 (according to the full-length numbering of our enzyme: 1-286, or in position 84 according to standard numbering of amino acids by [25]) in the purified protein, instead of the valine in the *E. coli* TEM-1 β-lactamase identified by MS in trypsin digestion experiments.

It is interesting to note that the peptide sequence in the close vicinity of the Val84Ile mutation (according to standard numbering of amino acids by [25]) was missing among the identified trypsin-digestion fragments, similarly to those amino acids constructing the N-terminal signaling sequence (**Scheme 5.2**). These observations also support both the cleavage of the

signaling sequence and the Val84Ile mutation. The Val84Ile exchange would account for the difference in the measured and expected molar masses.

a

HPETLVKVKDAEDQLGARVGYIELDLNSGKILESFRPEERFPMMSTFKVLLCGAVLSRIDAGQEQLGRRIHYSQNDLV
EYSPVTEKHLTDGMTVRELCSAAITMSDNTAANLLLTTIGGPKELTAFLHNMGDHVTRLDRWEPELNEAIPNDERDTT
MPAAMATTLRKLLTGELLTLASRQQLIDWMEADKVAGPLLRSALPAGWFIADKSGAGERGSRGIIAALGPDGKPSRIV
VIYTTGSQATMDERNRQIAEIGASLIKHW

b

***MSIQHFRVALIPFFAAFCLPVFA*HPETLVKVKDAEDQLGARVGYIELDLNSGKILESFRPEERFPMMSTFKVLLCGAV**
LSRVDAGQEQLGRRIHYSQNDLVEYSPVTEKHLTDGMTVRELCSAAITMSDNTAANLLLTTIGGPKELTAFLHNMGDH
VTRLDRWEPELNEAIPNDERDTTMPAAMATTLRKLLTGELLTLASRQQLIDWMEADKVAGPLLRSALPAGWFIADKSG
AGERGSRGIIAALGPDGKPSRIVVIYTTGSQATMDERNRQIAEIGASLIKHW

Scheme 5.2. a) The sequence of the mature pET-21a(+) TEM-1 β-lactamase. **b**) The sequence of *E. coli* β-lactamase identified by MS after the digestion of the protein by trypsin. The signal peptide is in italic. The red colored sequence was covered by the detected protein fragments, while the black colored sequences were not detected by MS. The Val84Ile mutation compared to the *E. coli* enzyme sequence is marked by blue color in both sequences, while the Val184Ala mutation (A as a green character) is an amino acid exchange in comparison with the protein shown in PDB ID: 1ZG4 structure in **Fig. 5.2** (Numbering is based on the full-length enzyme: 3-288, according to [25])

The expected monoisotopic and average molar masses of the mutated protein from pET-21a(+) are 28902.8 and 28921.0 Da respectively, while the measured monoisotopic mass for the purified protein was 28900.9 Da. This clearly proved that the two Cys residues (Cys77 and Cys123) of the mature enzyme form a disulfide bridge, being also demonstrated by the crystal structure with PDB ID: 1ZG4. The distance between two Cys residues of 2 Å is related to oxidized thiol groups of Cys residues by formation of a disulfide bridge. [187]

A protein sequence similarity search by BLAST program showed that the sequence of our purified protein is identical to A0A369I059_9BACT (*Runella aurantiaca*), A0A4R6AER2_9RHOB (*Fluviibacterium aquatile*), and A0A4Q0MMF1_9DELT (*Desulfovibrio sp. DS-1*) β-lactamases. TEM-1 β-lactamase in the crystal structure with PDB ID: 1ZG4 was designated as an *E. coli* enzyme [186]. Nevertheless, the sequence of the protein included in 1ZG4 crystal structure differs from the *E. coli* enzyme (UniProtKB - P62593 (BLAT_ECOLX)) by Val84Ile and Ala184Val mutations. We have found that it is rather identical to the protein isolated from *Haemophilus ducreyi* [50]. The reason of the diversity in TEM-1 β-lactamase sequences in literature is most likely due to the high transmissibility of the plasmids carrying the genes of various

TEM-1 β-lactamases. Therefore, it is recommended to determine the exact molar mass and sequence of the purified protein in each research study.

Based on the precise protein sequence we were able to predict the molar absorbance value of the purified TEM-1 β-lactamase by ExPaSy on-line tool [170], to be 28085 $M^{-1}cm^{-1}$ at 280 nm. The protein concentration was then determined from UV absorption spectrum to be ~8.0 μM (**Fig. A5b** in Appendix).

5.1.3.2. Circular dichroism spectroscopic measurements

CD spectroscopy is a recommended method for characterization of the purified proteins [188]. Investigating the purified TEM-1 β-lactamase in solution, the secondary structure composition of protein can also be estimated by analysing the CD spectrum.

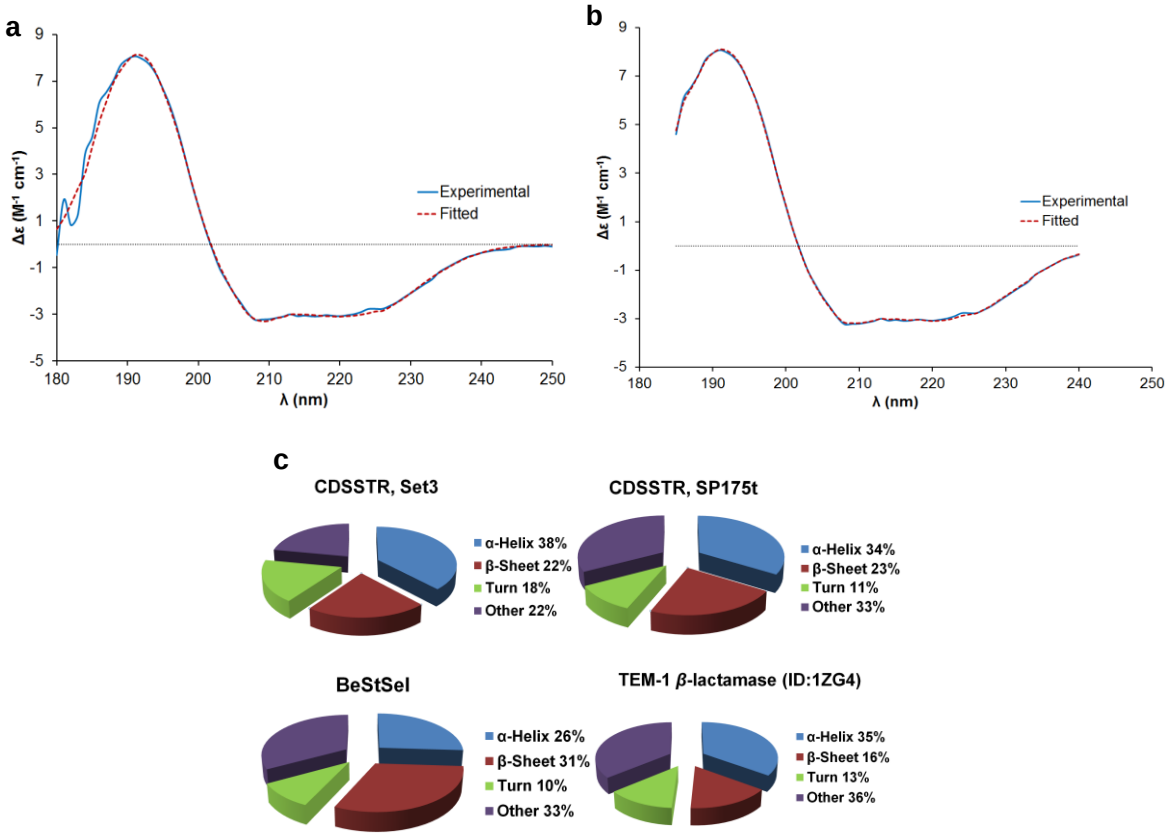

Figure 5.5. Fitting of the measured CD spectrum of TEM-1 β-lactamase by (**a**) BestSel and (**b**), by CDSSTR program. The region of the experimental spectrum below 185 nm was not considered during the secondary structure analysis because of the high absorbance of the measured solution. (**c**)**,** Comparison of the secondary structure contents of the purified TEM-1 β-lactamase estimated from the CD spectrum by CDSSTR and BeStSel programs with that obtained by analyzing the crystallized protein (PDB ID:1ZG4) [P1].

The obtained CD spectrum of TEM-1 β-lactamase (**Fig. 5.5**) displays two negative peaks at ~208 and ~223 nm, and a single positive peak at ~190 nm. These peaks are characteristic of proteins containing a significant fraction of α-helices. The CD spectrum of purified TEM-1 β-lactamase was analyzed by BeStSel program [40;41] and the CDPro program suite at the Dichroweb website [167;189]. The best fitted spectra achieved using BeStSel and CDSSTR were in good agreement with the experimental CD spectrum in the wavelength range 185-250 and 185-240 nm, respectively (**Fig. 5.5a,b**). However, the fitted CD spectrum using SP175 reference dataset revealed an acceptable agreement with the experimental CD spectrum only between 190 and 240 nm [190]. The obtained secondary structure composition (percentage of α-helices, β-sheets, turns, and other conformations) by CDSSTR (**Fig. 5.5c**), is close to that calculated from the published crystal structure (PDB ID: 1ZG4). The evaluation of the measured CD spectrum thus, supports folding of the protein in its functional structure.

It is worth mentioning that the protein sequence found in the published crystal structure (PDB ID: 1ZG4) is different from the investigated protein by single amino acid (V184A mutation, Scheme **5.2**), but this shall not be the reason for a substantial difference in their structures, as revealed by the comparison of the crystal structures of various TEM-1 β-lactamases with slightly different amino acid sequences shown in **Fig. 2.4**. Previously, it was shown that BeStSel often provides a lower percentage of α-helices than CDSSTR, while overestimates the 'other' fractions of the secondary elements [143;191]. The reason for this is that BeStSel was optimized for proteins being rich in β-sheets, and it classifies any distorted helices into the 'other' fraction.

5.1.3.3 Catalytic activity of TEM-1 β-lactamase

Previously, the kinetic parameters related to the hydrolysis of β-lactam antibiotics catalyzed by TEM-1 β-lactamase were determined at various conditions (buffer, pH, temperature) and with various substrates. The TEM-1 β-lactamase sequence deviations posed further difficulty to compare the available data appropriately.

To follow the hydrolysis of ampicillin via collection of the absorbance values, the generally accepted wavelength is 235 nm in the literature. Previously published data showed alterations in the determined molar absorbance values of both the substrate and the product, causing ambiguities in the determined catalytic parameters. Molar absorbance values of the product were determined to be between 1040 and 1260 $M^{-1}cm^{-1}$, while the molar absorbance values of the substrate scattered between 1710 and 2160 $M^{-1}cm^{-1}$ (**Table 5.2**). Initially, the molar absorbance of ampicillin was

obtained experimentally in our laboratory to be 1921 $M^{-1}cm^{-1}$, and for the hydrolysis product it was 1041 $M^{-1}cm^{-1}$ falling in the range of the literature data. The average specific activity was 596 ± 25 μmol of ampicillin hydrolyzed by 1 mg of TEM-1 β-lactamase within 1 min at 25 °C in 20 mM Tris-HCl (pH 7.5).

Table 5.2 The molar absorbance values at 235 nm (ε_{235nm}) for ampicillin and the hydrolysis product, as well as their differences collected from the literature [P2].

ε_{235nm} (Amp) (M^{-1} cm^{-1})	$\Delta\varepsilon(A\text{-}P)_{235nm}$ (M^{-1} cm^{-1})	$\Delta\varepsilon(P)_{235nm}$ (M^{-1} cm^{-1})	Reference
1710	670	1040 (calc.)	[85]
-	820	-	[86;192]
-	900	-	[87]
2160	900	1260 (calc.)	[88]
-	820	-	[193]

The Michaelis-Menten formalism is a common procedure for data analysis of enzymatic reactions [1;94;95]. Large number of publications in the literature characterizing the catalytic experiments with TEM-1 β-lactamase using V_{max}, or k_{cat} and $K_{M,}$ as well as k_{cat}/k_M obtained from the initial rates. The kinetic parameters determined for TEM-1 β-lactamase under similar conditions were collected in **Table 2.1** in the literature review. These values cannot be considered fully independent because the majority of the data was determined by the same study group. [23; 96-98;100]. However, still there are large deviations in kinetic parameters for different batches of the TEM-1 β-lactamases, due to the various sources of TEM-1 β-lactamases, different DNA plasmids (slightly different TEM-1 β-lactamase sequences), and partially different applied conditions.

We investigated the catalytic activity of the purified TEM-1 β-lactamase quantitatively by UV-absorbance spectrometry using ampicillin as a substrate at two different conditions: measurements of **series 1** were carried out in 20 mM Tris-HCl buffer, pH 7.5 at temperature 25 ºC, while those of **series 2** in 50 mM phosphate buffer, pH 7.0 at temperature 30 ºC. In the measurements of **series1**, the used substrate concentration was either 230 or 930 μM, the enzyme concentration ranged between 0.2 and 1.2 nM as final concentration. The hydrolytic reaction of the substrate was monitored by UV absorbance in the wavelength range of 210 – 235 nm instead of using a single wavelength (235 nm). This provided us with a set of informative data. The relationship between the concentrations and the measured absorbance values was linear and strictly

valid in the absorbance range 0 – 2.5, so only the measured data above the value of A = 2.5 were ignored during the evaluations. A typical hydrolysis curve revealed fast conversion of the substrate (**Fig. 5.6**). However, a slow but continuous decrease was observed while recording the absorbance values for an extended time period. This suggested a further transformation of the primary hydrolysis product, which may affect the data analysis, such as the kinetic model.

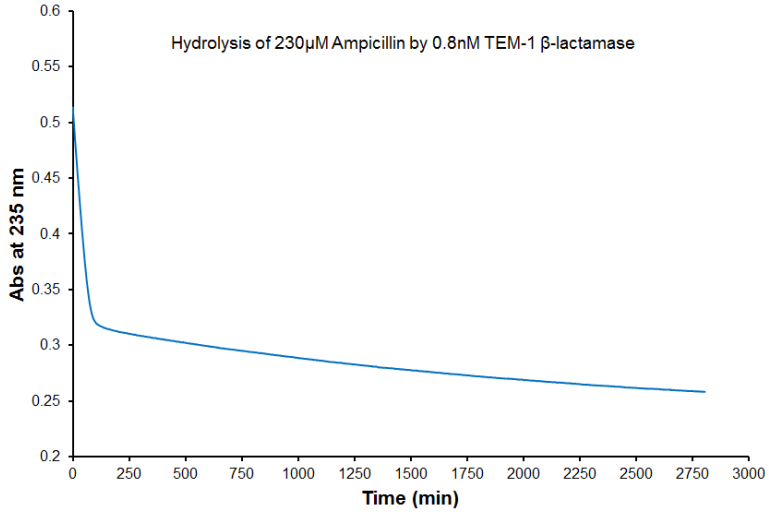

Figure 5.6. TEM-1 β-lactamase activity monitored by spectrophotometry via the hydrolysis of ampicillin as a substrate in an extended time scale **series 1** experiment.

Slow conversion of the hydrolysis product may account for the scattered molar absorbance values of the hydrolysis product in the literature (**Table 5.2**), because the measured absorbance is continuously decreasing. This phenomenon prompted us to apply matrix rank analysis to the recorded absorbance dataset [194] to conclude the required minimal number of independent absorbing species (NIAS) for describing the catalytic system. NIAS determined by this method is independent of both the specific chemical model and any concentration uncertainties. The special feature of the program is that it also allows for the calculation of the residual absorbance curves related to the unexplained absorbance values upon increasing the number of putative colored species. The inspection of these curves clearly showed that even after including two species, such as the substrate and the primary hydrolysis product, there is a clear systematic and considerable deviation from the noise level (several milli-absorbance values) of the spectrophotometric experiment (**Fig. 5.7**). Considering the third colored species, these systematic biases disappeared. These results justify the inclusion of a secondary product in the data analysis process.

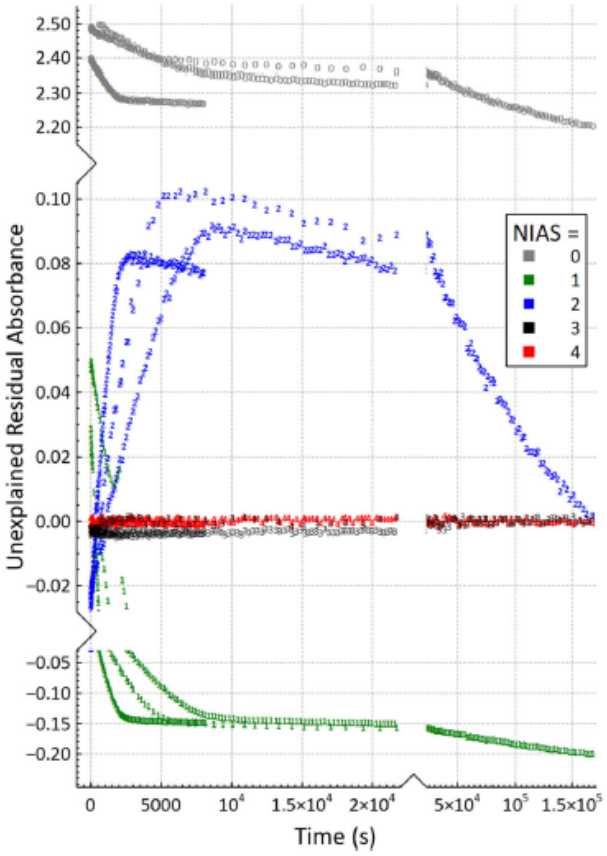

Figure 5.7. The residual absorbance curves calculated during the matrix rank analysis to determine the minimal number of spectrally independent absorbing species (NIAS). The data used for this calculation were all recorded absorbances at the lower initial substrate concentration (230 μM) in the 235 – 214 nm range of the **series 1** kinetic experiments. The systematic deviation of the residual absorbances from the noise level upon sequential inclusion of new colored species suggested the presence of at least three absorbing species [P2].

Previous studies, focusing on the degradation of ampicillin but without a detailed kinetic analysis, revealed that the primary hydrolysis product of ampicillin and similar antibiotics may be converted into different molecules depending on the pH and temperature [195-199]. Nevertheless, the formation of a secondary product has not been accounted for in studies of ampicillin hydrolysis catalyzed by TEM-1 β-lactamase to date. Therefore, the collected data in **series 1** experiments were analyzed here using the kinetic formalism assuming the presence of a secondary product. Instead of the Michaelis-Menten model we used the following stoichiometric and rate equations for the calculations (equation set no. 1):

$$S+E \underset{k_2}{\overset{k_1}{\rightleftharpoons}} (ES) \quad , r_1=k_1\cdot[S]\cdot[E] \text{ and } r_2=k_2\cdot[(ES)]$$

$$(ES) \xrightarrow{k_3} P_1 \quad , r_3=k_3\cdot[(ES)]$$

$$P_1 \xrightarrow{k_4} P_2 \quad , r_4=k_4\cdot[P_1]$$

S represents the substrate, E is the enzyme, and (ES) is the enzyme-substrate complex as a macroscopic species including all possible microscopic species. **P_1** and **P_2** are the first and second products, respectively, and r_i is the reaction rate of the i^{th} reaction step. During the calculations, the following sets of equations were applied (equation set no. 2):

$$\frac{d[S]}{dt} = -k_1 \,.\, [S].\,[E] + k_2 \,.\, [(ES)]$$

$$\frac{d[E]}{dt} = -k_1 \,.\, [S].\,[E] + (k_2 + k_3) \,.\, [(ES)]$$

$$\frac{d[(ES)]}{dt} = k_1 \,.\, [S].\,[E] - (k_2 + k_3) \,.\, [(ES)]$$

$$\frac{d[P_1]}{dt} = k_3 \,.\, [(ES)] - k_4 \,.\, [P_1]$$

$$\frac{d[P_2]}{dt} = k_4 \,.\, [P_1]$$

The result of the fitting is shown in **Fig. 5.8**. The experimental curves could fit with this model satisfactorily; unlike with the simple Michaelis-Menten-like model that did not include the secondary product **P_2**. As expected, the latter model cannot appropriately describe those parts of the experimental curves, where the conversion of **P_1** into **P_2** dominates.

The kinetic experiments executed with different starting concentrations of the substrate and the enzyme, clearly revealed that the partial adjustment of the initial enzyme concentrations was necessary for the proper fit of the curves. The explanation of this is that the enzyme is very sensitive to any change of the conditions during its preparation, such as the freeze/thaw procedure, storage buffer, extreme dilution and temperature change. The experiments also include errors, such as the pipetting of the small volumes (in the few microliter range), material of the pipette tips and sample containers which can cause eventual adsorption of the enzyme. On the other hand, no any analytical method is suitable to determine such low concentrations (~1 nM) of protein precisely. Simultaneous evaluation of all catalytic experimental data (under the same buffer and temperature

conditions) revealed a single set of parameters with good agreement between the fitted and experimental data.

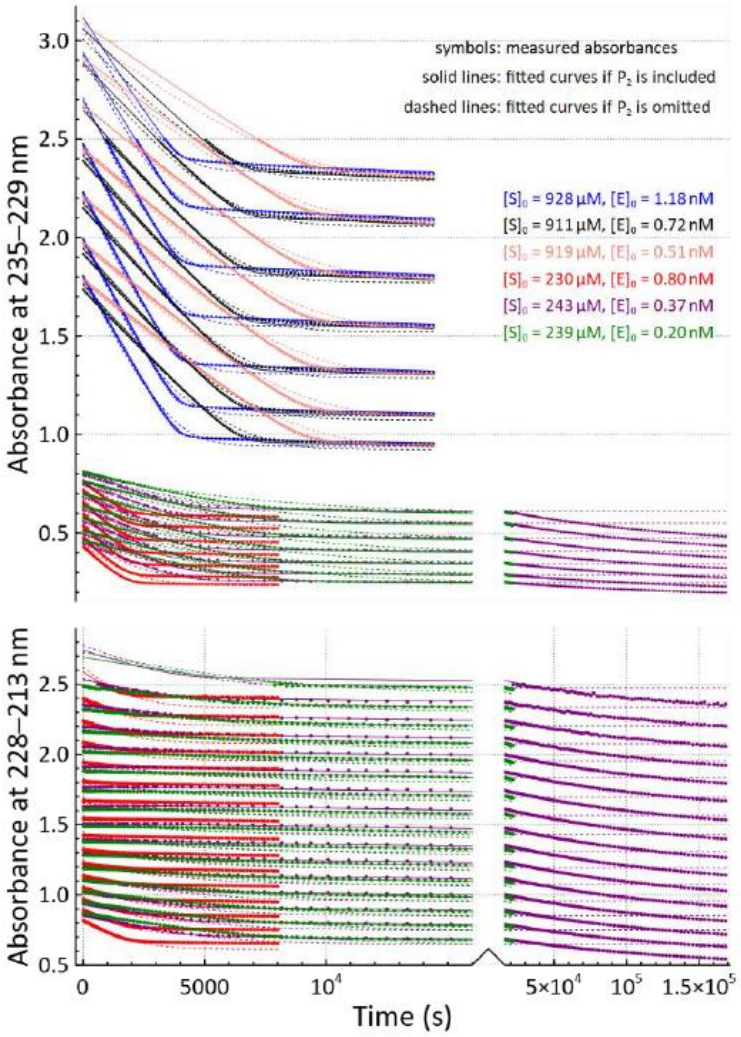

Figure 5.8. Fitting of the spectrophotometric data at different wavelengths, showing the initial enzyme and substrate concentrations. The dotted lines show the fit based on the traditional Michaelis-Menten model when the second product **P₂** is ignored. The full lines show the fit of the experimental data, by the extended model including the reaction steps in equation set no. 1 [P2].

This also made it possible to clearly characterize the activity of enzyme in catalytic processes. The kinetic data and parameters of the species obtained from this data evaluation procedure are collected in **Table 5.3**. The relatively low k_3 value obtained may be due to the applied measurement conditions. In the **series 2** experiments, the catalytic reaction conditions of 50 mM phosphate (pH 7.0) buffer at 30 °C are the most frequently applied conditions reported in the

literature. The evaluation of the data in the **series 2** experiments yielded parameters, which are comparable to those previously published (**Tables 2.1** and **5.3**) but by supplementing the results with information about the second hydrolysis product.

Table 5.3. Kinetic parameters for the hydrolysis of ampicillin including the processes catalyzed by TEM-1 β-lactamase and the further conversion of the primary product **P₁** into the secondary product **P₂** and their standard deviations as obtained from the kinetic calculations [P2]. [a]Derived data.

Parameter	Series 1	Series 2
$k_1(M^{-1}s^{-1})$	$(4.34\pm0.12) \times 10^6$	$(4.81\pm0.30) \times 10^6$
$k_2(s^{-1})$	$<1.4 \times 10^{-2}$	$<1.7 \times 10^{-2}$
$k_3(s^{-1})$	$(2.24\pm0.03) \times 10^2$	$(3.44\pm0.01) \times 10^2$
$k_4(s^{-1})$	$(7.50\pm0.18) \times 10^{-6}$	$(1.76\pm0.04) \times 10^{-5}$
ε_{235nm} of Amp $(M^{-1}cm^{-1})$	1931±2	1920±1
ε_{235nm} of P_1 $(M^{-1}cm^{-1})$	1064±1.4	1081±1
ε_{235nm} of P_2 $(M^{-1}cm^{-1})$	709±13	791±5
$K_M(\mu M)$[a]	51.6±1.4	71.6±4.4
$k_{cat}/K_M(\mu M^{-1}s^{-1})$[a]	4.34±0.12	4.81±0.30

Series 2 experiments revealed a significant increase of the **P₂** yield in comparison with **series 1**, due to increase of the temperature in the **series2** experiments by just 5 °C. This indicated that the conversion of the primary product **P₁** to second product **P₂** clearly requires to be taken into account in the characterization of the ampicillin hydrolysis. The k_4 constant characteristic for the conversion of **P₁** into **P₂** is a relatively small value. However, the **P₁** concentration is higher than the enzyme concentration by several orders of magnitude, so **P₂** is formed in significant quantities as shown in the species distribution during the hydrolysis (**Fig. 5.9**).

The chemical reactions take place on practically three different time scales. In few milli-seconds, the enzyme-substrate complex is completely formed. However, not all enzyme molecules are transformed to enzyme-substrate complex because the rate of the first reaction step (r_1) is continuously decreasing, while the rate of **P₁** formation (r_3) is increasing. Approximately after three milliseconds the proportion of the rates of these two steps become such that the decomposition of the product-enzyme complex is continuously recovering the free enzyme.

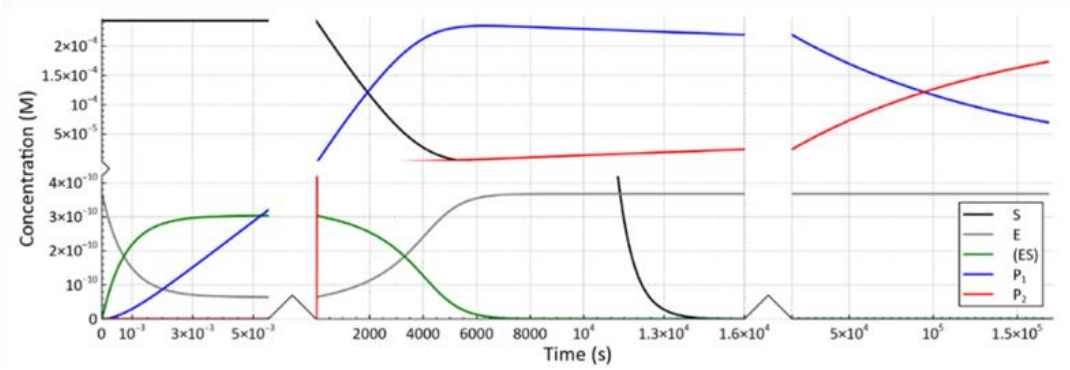

Figure 5.9. Distribution of species in the time course of the ampicillin hydrolysis, catalyzed by TEM-1 β-lactamase with $[S]_0$ = 243 μM and $[E]_0$ = 0.37 nM in 20 mM Tris-HCl (pH 7.5) buffer at 25ºC followed for almost 2 days [P2].

We will note that this initial portion of the curves in **Fig. 5.9** is extrapolated because there are no data from our tests in this very short time frame. The ES complex is a macroscopic species that undergoes multiple transformations prior to product formation, as evidenced by recent time-resolved X-ray diffraction data that showed changes in the millisecond interval of the hydrolytic reaction catalyzed by a metallo-β-lactamase [200]. This phenomenon may lead to complex branched catalytic pathways of β-lactam hydrolysis. However, fast kinetic techniques like flow and relaxation approaches are needed to identify additional rate constants [101;103], or single turnover kinetic conditions shall be adjusted [104;105]. Such experiments could reveal valuable insights into the fine details of the mechanism of action, but such investigations were out of scope of our studies. In the second timescale (up to ~4 hours), almost the full amount of the substrate disappears, and the main reaction of the last stage is the formation of $\mathbf{P_2}$ from $\mathbf{P_1}$. The significant difference in molar absorbances at wavelength 235 nm obtained for $\mathbf{P_2}$ from the two series (**Table 5.3**) can also be understood based on **Figure 5.9**: in **series 1** experiments, one set of the kinetic data was recorded for ~48 hours resulting in high concentration of $\mathbf{P_2}$, and reliable molar absorbance value.

The hydrolysis process of ampicillin promoted by TEM-1 β-lactamase was studied by mass spectrometry that identified $\mathbf{P_1}$ and $\mathbf{P_2}$ products (**Fig. 5.10**). The expected molar mass of $\mathbf{P_1}$ (ampicilloic acid) was in good agreement with measured molar mass, so the m/z value of the measured monoprotonated species 368.1 is higher than the m/z value of the ampicillin by 18.0 Da. This reveals that ampicillin (m/z = 350) is indeed hydrolyzed by uptake a water molecule during the first reaction step.

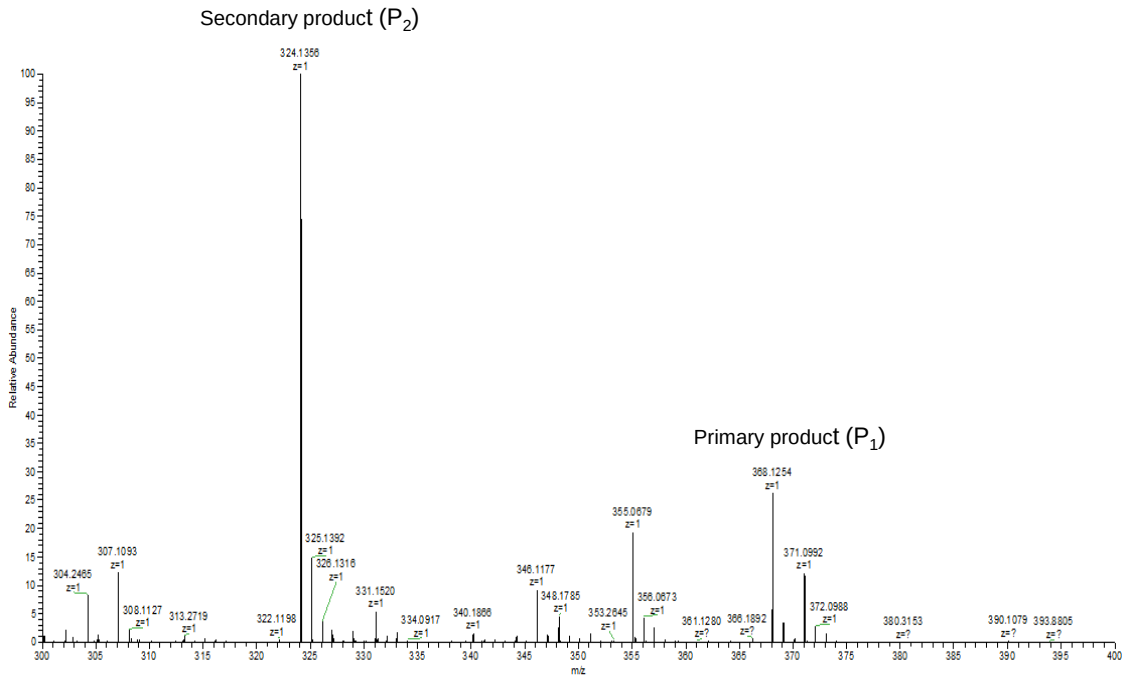

Figure 5.10. The ESI mass spectrum of intact hydrolysis products of 930 μM ampicillin sodium that was hydrolyzed by 0.8 nM TEM-1 β-lactamase at 30°C in 50 mM phosphate buffer pH 7.0.

The sample was incubated for an elongated time to convert **P1** to **P2**. The m/z value of the new species was found to be 324.1 which is the molar mass of **P2**. This reveals that ampicilloic acid was decarboxylated by release carbon dioxide molecule (decrease of the m/z value by 44.0) during the last reaction step. **Scheme 5.3** shows the suggested processes in our experiments. Similar products of ampicillin were identified previously in the non-enzymatic ampicillin degradation studies [195-198].

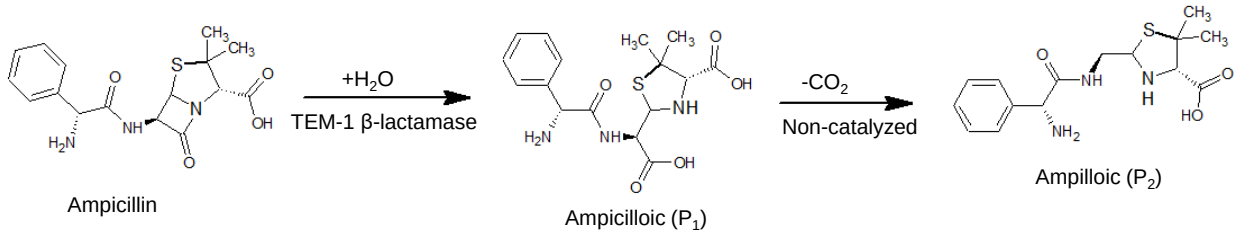

Scheme 5.3. Hydrolysis of ampicillin by TEM-1 β-lactamase in **series 1** and **2** conditions.

At the beginning of the reaction, the amount of **P2** is relatively low in comparison with amount of the **P1**, so the effect of **P2** is negligible in this short initial time interval. Thus, **P2** will

not significantly influence initial rates. Therefore, we tried to evaluate the experiment by the conventional method for comparison. However, determination of the Michealis-Menten constant (K_M) value using the usual Lineweaver-Burk plot requires a constant final absorbance (A_∞) value of the product, being and invalid precondition for the TEM-1 β-lactamase/ampicillin system. Therefore, this evaluation revealed K_M values which were extremely sensitive to the slightly variable A_∞ values, as shown in **Fig. 5.11**.

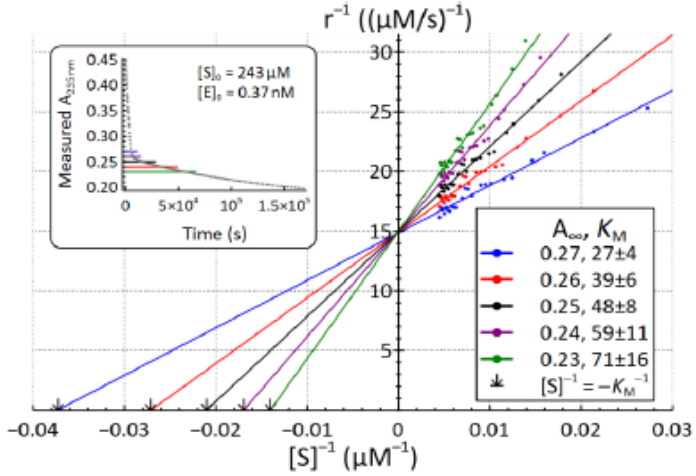

Figure 5.11. Lineweaver-Burk plots for one kinetic curve at a single wavelength by choosing different A_∞ values (denoted by different colors). The inset figure in the left top rounded box shows the experimental curve used and the horizontal lines indicate the positions of the applied A_∞ values. The main figure shows the lines fitted to the linear part of the r^{-1} vs. $[S]^{-1}$ curves. The right bottom box includes the calculated K_M values [P2].

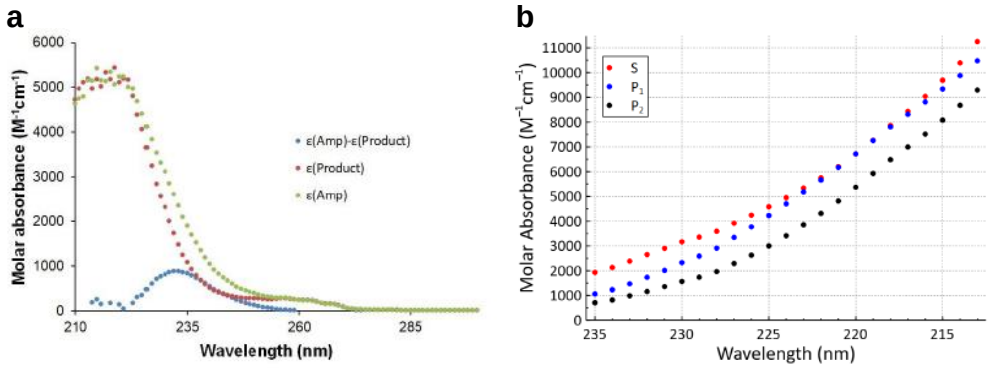

Figure 5.12. Determination of molar absorbances. (**a**) The molar absorption spectra of ampicillin and the hydrolyzed product (mixture) determined from serial dilutions and the difference spectrum displaying its maximum around 235 nm. (**b**) The molar absorption spectra of ampicillin and the two hydrolyzed products obtained from the fitting of the catalytic curves [P2].

In our example, 180 % increase in the calculated K_M values was resulted from 15 % decrease in the A_∞ values. It is worth mentioning that the Lineweaver-Burk plot is applied for the evaluation of a single kinetic experiment at a single wavelength, while our kinetic evaluation procedure included all kinetic experimental curves at all wavelengths in a single calculation procedure. This kind of data treatment also provides the precise molar absorbance values at multiple wavelengths (**Fig. 5.12**).

5.1.4. Catalytic activity of metallized TEM-1 β-lactamase

While TEM-1 β-lactamase is not a metalloenzyme, we have already discussed that it offers a large number of amino acids that can coordinate metal ions. The success of the purification procedure by immobilized Ni(II) ion affinity chromatography proved that it can bind *e.g.*, Ni(II) in its native form. In other words, the three pairs of His residues on the TEM-1 β-lactamase surface allowed for binding to the borderline transition metal ion such as Ni(II). As discussed above, the two Cys residues of the mature TEM-1 β-lactamases close to the active center are involved in a structural disulfide bridge [187] that is rarely bound to metal ions. Nevertheless, soft Lewis metal ion such as Hg(II) were shown to interact with a disulfide bridge [201]. In addition, the mature TEM-1 β-lactamase has 9 further sulfur donor atoms in the thioether groups of Met residues that can bind Hg(II) ion and more weakly Cd(II) and Ni(II) as it is reported for various amino acids, peptides and proteins [53-56]. Beside the mentioned metal binding sites, there are other negatively charged side chains of TEM-1 β-lactamase a.a. residues, such as Asp, Glu that can support and stabilize the interaction with the metal ion.

Complexation of TEM-1 β-lactamase by a metal ion may cause changes in the catalytic efficiency of the enzyme in the hydrolysis of β-lactam molecules. It is intriguing to study the effects of metal ions, in light of the fact that β-lactams can also be hydrolyzed by metallo-β-lactamases [95;202], and metal ions play important roles in enzyme catalyzed hydrolytic reactions [203]. Therefore, first we have mixed the aqueous ampicillin solution with Hg(II), Ni(II) or Cd(II) ions at identical concentrations and conditions to those applied in the kinetic assays in presence of the enzyme. No significant changes were observed in the ampicillin absorbance at 235 nm in comparison with the ampicillin solution in the absence of metal ions. A slow decrease, being less than 0.01 absorbance unit within three hours incubation was found (**Fig. 5.13**), indicating that even the first step of the ampicillin hydrolysis occurred to a negligible extent as compared to the enzyme catalyzed system.

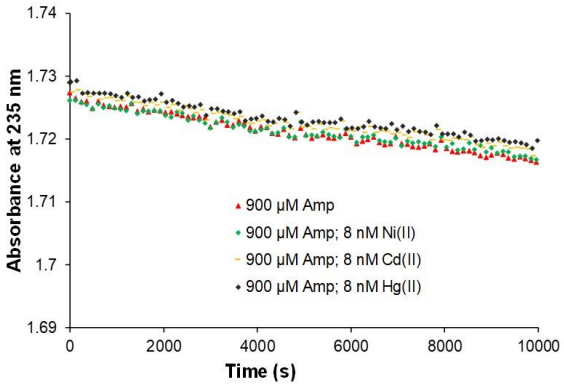

Figure 5.13. The effect of metal ions on the absorbance of the ampicillin solution. The absorbance change was less than 0.01 unit within a 10000 s measurement period [P2].

The catalytic experiments were performed with the same enzyme batches and substrate solutions under the same reaction conditions in the absence and in the presence of Ni(II), Hg(II) and Cd(II) metal ions at various molar ratios to demonstrate the effect of metal ions on the hydrolytic process.

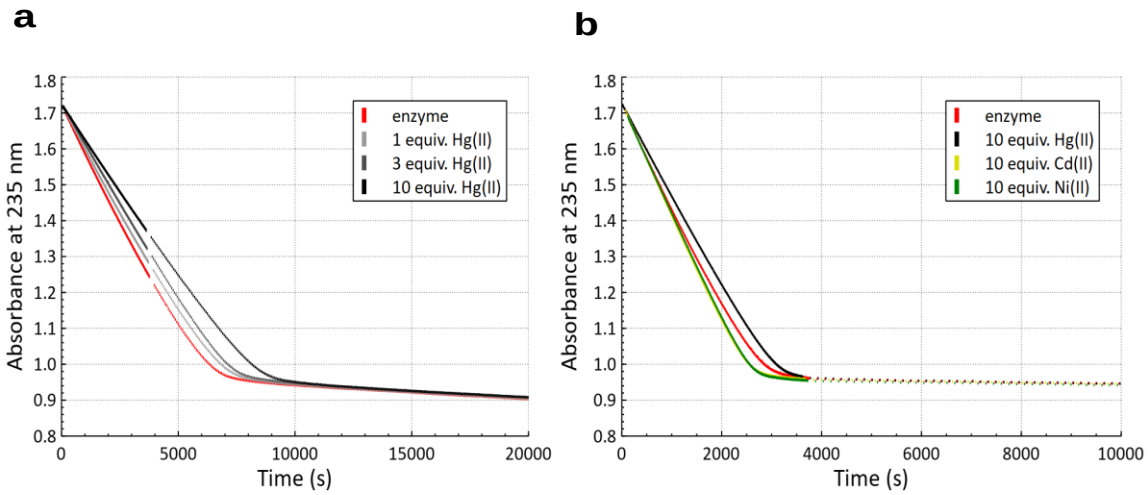

Figure 5.14. The effect of metal ions on the hydrolytic process of ampicillin catalyzed by TEM-1 β-lactamase in 50 mM phosphate buffer (pH 7.0) at 30ºC. **a**) The time dependence of the absorbance values in parallel experiments hydrolyzing 900 µM ampicillin by 0.8 nM enzyme in the presence of 1, 3 and 10 equivalents of Hg(II) ions referred to the enzyme concentration. **b**) The kinetic curves recorded concurrently in the systems of 900 µM ampicillin and 1.6 nM enzyme in the absence of metal ions, as well as with tenfold excess of Ni(II), Cd(II) and Hg(II) referred to the enzyme concentration [P2].

The experiments with Hg(II) ions were carried out in the presence of three different metal ion to enzyme molar ratios of 2:1, 5:1, and 10:1. The catalytic activity of TEM-1 β-lactamase was slightly reduced by the gradual increase the Hg(II) ion concentration as shown in **Fig. 5.14a**. The changes in the catalytic activity, as revealed by the kinetic curves could be fitted by decreasing the active enzyme concentration upon increasing metal ion concentration. In this way, the fitting procedure led to the same parameter values as in the absence of Hg(II) ion. This suggests that the V_{max} values decreased in correlation with the increased molar ratio of the Hg(II) ion and the enzyme, *i.e.*, that Hg(II) ions did not affect the substrate binding property of the enzyme in a competitive manner, but they rather influenced the concentration of the catalytically effective enzyme. Hg(II) ions of highly soft character may interact with the available sulfur donor atoms of Met residues [204], thereby blocking a fraction of the enzyme molecules.

A network of Met residues in TEM-1 β-lactamase is shown in **Fig. 5.15 a**. In panel **b** of the same figure, the putative metal ion binding amino acids around each Met residue sulfur atom within a ~5 Å distance are gathered, based on the crystal structure with PDB ID: 1ZG4. Some of these donor atoms, together with additional amino acids with putative coordinating donor groups can be found in a ~8 Å surroundings of the catalytic Ser70 sidechain. Among these, the two adjacent Met residues (Met68 and Met69) (numbering of amino acids according to [25]) may provide the most stable binding site. The published crystal structure (PDB ID: 1ZG4) places them within a 6 Å sphere surroundings of the active site [186]. The donor atom-rich 129–132 (MSDN) (numbering of amino acids according to [25]) segment, which includes Met129 and is located within 8 Å of the active center, may also be a good Hg(II) binding location. TEM-1 β-lactamase is sensitive towards Met68 and Met69 residues, and its activity is affected by mutation of these residues, while it was previously demonstrated that the 129-MSDN-132 sequence is an important main target for the researchers to mutate the enzyme [99;205;206].

Based on the above considerations, Hg(II) ions most probably interact with the enzyme more strongly than with ampicillin, *i.e.*, there was no or weak binding to ampicillin, although a sulfur donor group is also present in the antibiotic molecule. These findings would fit to the recently illustrated importance of Met residues at various levels in proteins [207].

In parallel, the experiment containing different metal ions at 10× excess as compared to the apo-enzyme itself, revealed that in contrast to the Hg(II) containing catalytic system, the presence of Ni(II) or Cd(II) ions slightly promoted the catalytic activity of TEM-1 β-lactamase (**Fig. 5.14b**).

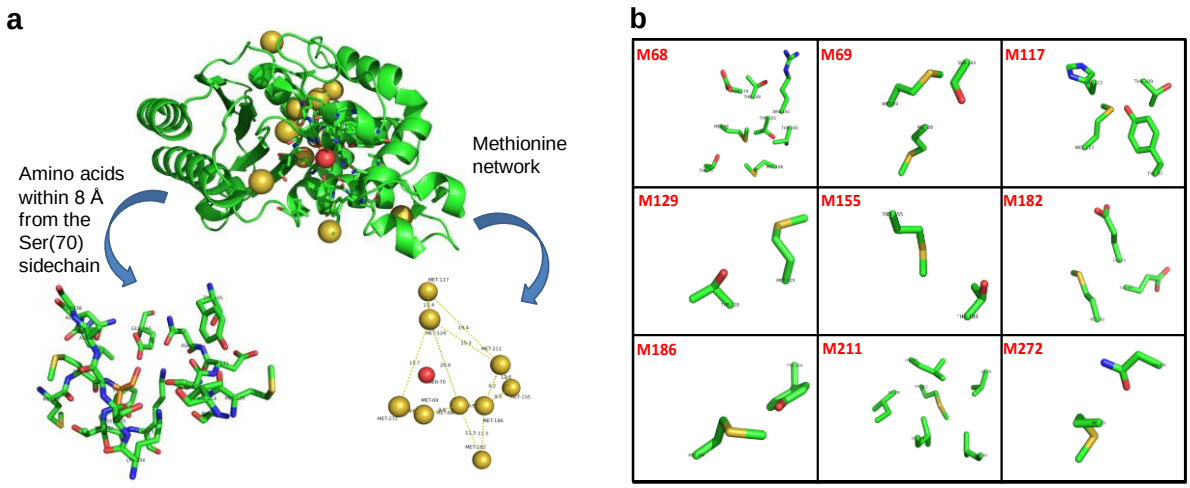

Figure 5.15. Structure of the TEM-1 β-lactamase (PDB ID: 1ZG4) highlighting the putative Hg(II) ion binding sites. **a**) Amino acids with potential donor groups for metal ion coordination within the 8 Å surroundings of the S70 sidechain and the network of methionine residues with distances between the sulfur donor atoms. **b**) Amino acids containing further putative coordinating donor atoms in the 5 Å surroundings of each methionine sulfur (numbering of amino acids according to ref [25]) [P2].

Ni(II), as a borderline transition metal ion, and Cd(II), which has a moderately soft character, probably could bind to the His residue pairs that are positioned on the surface of the enzyme. These His residue pairs are far away from the active center, so this could not account for a direct effect of Ni(II) and Cd(II) on substrate-enzyme complex in the active center.

On the other hand, these metal ions are also supposed to bind ampicillin close to the β-lactam ring via nitrogen and oxygen donor groups [204;208]. It is well known that the Lewis acid property of metal ions may promote the hydrolysis processes of the β-lactam ring by a different mechanistic pathway. Previously, it was revealed that metal ions can catalyze the hydrolysis of ampicillin, but mainly in strongly acidic or alkaline media, such as a reaction of ampicillin with Ni(II) for analytical purposes in alkaline medium [209;210]. Therefore, we propose that the hydrolytic mechanism may be influenced by the Ni(II) or Cd(II) ions, by binding to the antibiotics with a concomitant activation of the substrate for the nucleophilic attack by Ser70 residue of the enzyme [211;204]. Cd(II) ions were also shown to coordinate to the active center of a metallo-β-lactamase, which remained catalytically active, although with less activity than the native Zn(II) ion, supporting the ability of Cd(II) ion to promote the hydrolysis, while Hg(II) ion inhibited the same enzyme [212].

These observations could explain and support our hypothesis about the effect of different metal ions. It is an interesting outcome of this study that the metal ions of different properties show double selection against the TEM-1 β-lactamase/ampicillin system, by interaction with various components and donor groups. Ni(II) and Cd(II) would rather interact with N (and O) donor-atoms, promoting the nucleophilic attack of the enzyme on the activated substrate molecule, while Hg(II)ions interact with multiple sulphur donor atoms of the enzyme in the vicinity of the active center, inhibiting the catalytic process. Having such a high significance, the metal ion binding of TEM-1 β-lactamase was studied in detail as described in the following sections.

5.1.5. Interaction of TEM-1 β-lactamase with Ni(II)

5.1.5.1. CD spectroscopic measurements

Previously, TEM-1 β-lactamase was purified by IMAC under denaturing condition using Zn(II) ions [50]. Denaturing allows for chelation by His residue side-chains independently on the 3D structure of the protein. In contrast, in our purification process, the enzyme was in its native structure, so that each metal ion binding site provided two strong donor groups (imidazole side-chains of His residues) to coordinate a single metal ion. The binding affinity of Zn(II) ion to two His residue is expected to be in the range of logβ ~2.9 - 3.9 [213-217], while Ni(II) or Cu(II) ions bind two His residues side-chains with stability constants logβ ~3.4 - 4.5 and logβ ~5.2-6.5, respectively, so these metal ions may be more suitable for the protein purification. The TEM-1 β-lactamase interaction with Ni(II) ions was indeed proven by the success of the purification by chelating to a Ni(II)-loaded NTA resin on the column.

TEM-1 β-lactamase coordination to Ni(II) ions was investigated by CD spectroscopy to monitor the eventual secondary structure changes of the enzyme and also to estimate the number of bound Ni(II) ions. We used molar ratios 2:1, 5:1 and 10:1 of Ni(II) ions to the enzyme. The accumulated parallel CD measurements performed with a difference of 15 min in each solution were identical. Their averages are plotted in **Fig. 5.16**. There were slight but systematic changes in the CD spectra upon increasing the Ni(II) ion content in comparison to the apo-TEM-1 β-lactamase. According to the distance between side chain of His pairs, structures, purification processes, and CD results, this suggested that the enzyme could bind Ni(II) ions on the surface of the enzyme with low affinity, and without remarkable changes in the secondary structure composition of the enzyme.

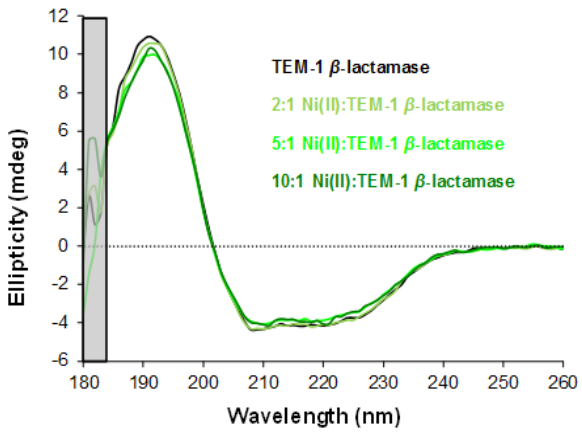

Figure 5.16. Circular dichroism spectra of TEM-1 β-lactamase in the presence of increasing Ni(II) ion concentrations. The molar ratio of Ni(II):TEM-1 β-lactamase was varied from 0:1 to 10:1. The shadowed region of the spectrum was not considered during the secondary structure analysis (shown above in **Fig. 5.5**) because of the high absorbance [P1].

According to several crystal structures of TEM-1 β-lactamases (PDB ID: 1ZG4, 1TEM, 1ERM, and 3DTM), the enzyme contains three putative metal ion binding sites, each site composed of two His residues for chelating borderline transition metal ions: His26 and His289; His96 and His112, as well as His153 and His158 pairs (**Fig. 5.2**) (numbering of amino acids according to [25]). The analysis of the structures (PDB ID: 1ZG4, 1TEM, 1ERM, and 3DTM) revealed that the distance between the imidazole side chains of the His26 and His289 pair is ~10 Å; for the His96 and His112 pair it is ~4.5Å; while for the His153 and His158 pair it is ~3.2 Å. The His residues in two of these putative metal ion binding sites are at more than 4 Å distance from each other, and they cannot coordinate to the same metal ion without a significant change in the folded protein.

5.1.5.2. Mass spectrometric measurements

The interaction of Ni(II) ion with TEM-1 β-lactamase was also monitored by mass spectrometry at 2:1, 5:1 and 10:1 Ni (II):enzyme molar ratios (**Fig. 5.17a**). At molar ratio 2:1 (Ni(II):enzyme) the main peak in the mass spectrum is assigned to the monometallated enzyme and minor peaks are assigned to apo-enzyme and dimetallated enzyme. At molar ratio 5:1 (Ni(II):enzyme) the main peak in the mass spectrum is still assigned to the monometallated enzyme and minor peaks are assigned to dimetallated enzyme, for which the peak intensity was slightly increased. Similarly, even at molar ratio 10:1 (Ni(II):enzyme) the main peak in the mass spectrum is assigned to the monometallated enzyme, and minor peaks are assigned to di- and tri-metallated enzyme. Only a slight increase of the intensity of the di-metallated enzyme was observed, and detection of traces of the protein bound to three Ni(II) ions became possible upon increasing the Ni(II):enzyme ratio.

This suggests that TEM-1 β-lactamase coordinates more than one Ni(II) ions with different affinities. The first binding site of the enzyme has the highest affinity to the Ni(II) ion, the next binding site is weaker, while the third site barely binds the Ni(II) ions. Upon closer inspection of the three putative binding sites comprised of His residue pairs (**Fig. 5.17b**), we could conclude the following in agreement with the CD spectroscopic results:

(i) the imidazole donor atoms of His153 and His158 are at ~3.5 Å distance, which is ideal for Ni(II) ion binding. Furthermore, there are two more amino acid residues (Asn154 and Asp157) in their close vicinity with O,N donor groups, which may strengthen the interaction with the metal ion. Such effect was observed for peptides, in which the side chain donor groups of Asn and Asp in the vicinity of the two coordinating His residues increased the stability of the metal ion-peptide complexes [63-66]. This suggests that the stability constant of the Ni(II) complex formed with the 153-HNMGDH-158 peptide sequence within TEM-1 β-lactamase shall be at higher end of the data interval of two His-imidazole coordination modes: $\log\beta \geq 4.5$ [66].

(ii) His26 and His289 residues are at the opposite termini of the enzyme sequence, but these residues become close to each other in the folded structure, with a distance between the imidazole donor groups about ~4.0 Å. This may allow for Ni(II) coordination with intermediate stability.

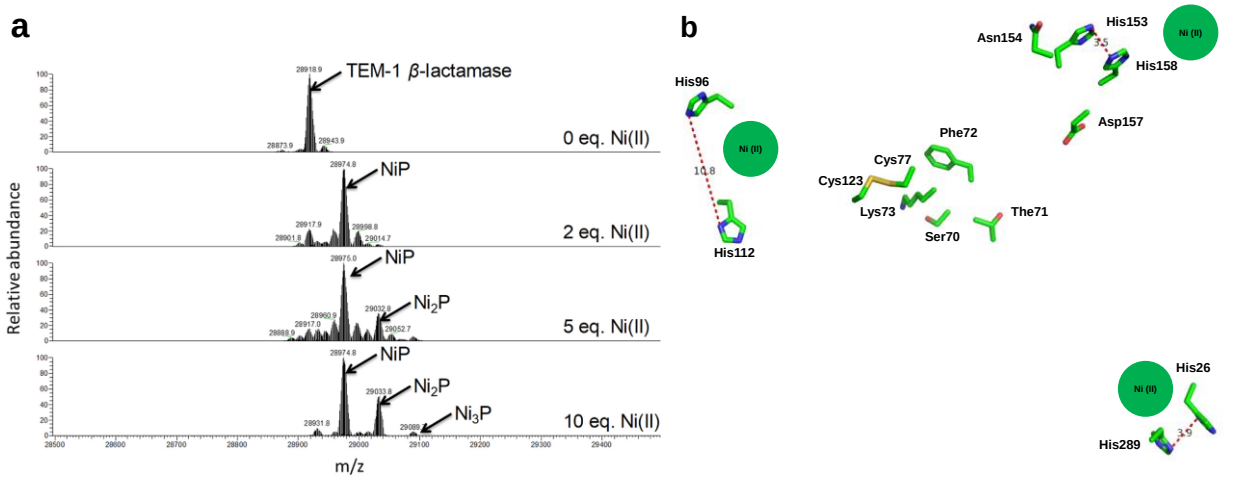

Figure 5.17. a) Deconvoluted electrospray ionization mass spectra of TEM-1 β-lactamase with increasing amounts of Ni(II). NiP, Ni_2P and Ni_3P denote the mono-, di- and trimetallated TEM-1 β-lactamase protein species, respectively. **b**) The relative positions and distance between the side-chains of the metal ion binding residues in the enzyme (PBD ID: 1ZG4) for the Ni(II) ion, disulfide bridge (Cys77 and Cys123) and the active center (SXXK motif) (numbering of amino acids according to [25]) [P1].

(iii) The distance between the donor atoms of the third His pair (His96 and His112 residues) is ~10 Å, which might be inappropriate for metal ion binding. These His side-chains could most probably coordinate independently to Ni(II)-NTA resin to form complex. The stability constants for the Ni(II) coordinated to one imidazole side-chain in peptides are in the range logβ ~2.3–3.1 [218-221].

Based on the above considerations, the low affinities can be attributed to the second and third Ni(II) ions weakly bound to TEM-1 β-lactamase, as it was revealed by the MS results (**Fig. 5.17**). The results of IMAC, CD and MS suggest that the metal binding site consisting of the His153 and His158 (amino acids numbering is according to [25]) residues may be the paramount metal ion binding site.

5.1.6. Interaction of TEM-1 β-lactamase with Cd(II) and Hg(II) ions

5.1.6.1. CD spectroscopic measurements

The mature TEM-1 β-lactamase contains the two Cys residues in a disulfide bridge, but there are further 9 sulfur donor groups which can also be involved in the coordination of the soft metal ions like Hg(II) and Cd(II). In the literature, Hg(II) was shown to bind to sulfur donor groups of methionine, and methionine residues of peptides with different affinities. [54;56]

The changes in the secondary structure of TEM-1 β-lactamase upon interaction with Hg(II) or Cd(II) ions were studied by circular dichroism spectroscopy. Cd(II) ion has most probably identical coordination mode to that of Ni(II) ion *i.e.*, it can be coordinated to His residues at the surface of the enzyme. The thioether-type metal binding sites in methionine residues are located inside the enzyme structure and are good candidates for binding of the soft metal ions such as Hg(II) and Cd(II) ions. Addition of Hg(II) or Cd(II) ion to TEM-1 β-lactamase solution at different molar ratios (M(II):enzyme = 2:1, 5:1, 10:1) of Hg(II) or Cd(II) resulted in slight gradual change of the CD spectra on increasing the excess of the metal ions (**Fig. 5.18a,b**). These changes in the CD spectra upon excess amounts of metal ion were, however, almost negligible, similarly to those changes observed for Ni(II) ions, in spite of the different chemical properties and affinities toward various binding sites. The secondary structure composition of the Hg(II)-TEM-1 β-lactamase was calculated from the CD spectra using different data analysis tools such as Dichroweb and BeStSel. These results demonstrated a gradual decrease of the α-helix content upon increase of the Hg(II) concentration (**Fig. 5.19**). Nevertheless, the CD spectra do not reflect remarkable secondary structure changes, even in the presence of an increased amount of Hg(II).

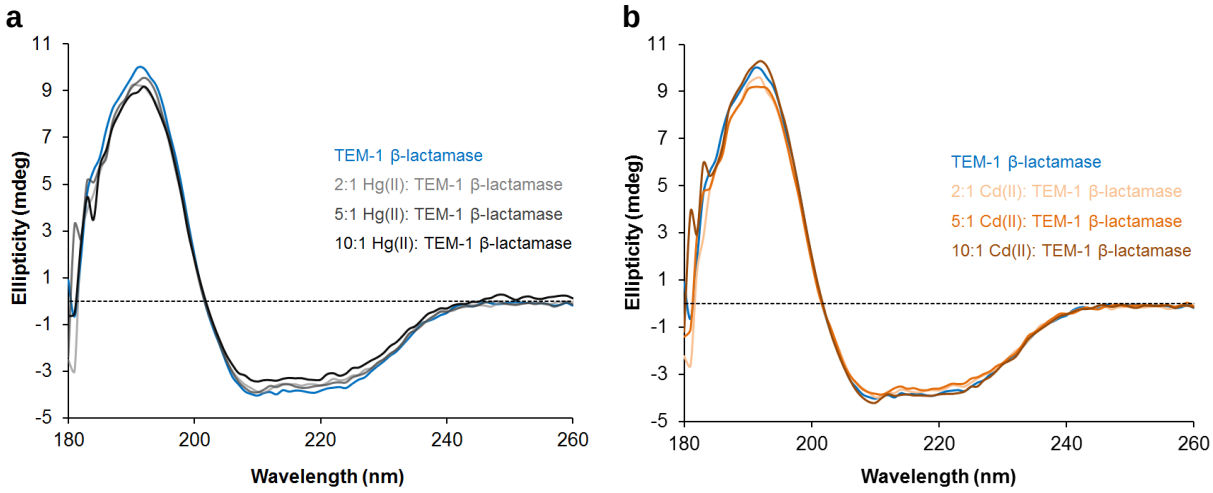

Figure 5.18. Circular dichroism spectra of TEM-1 β-lactamase in 20 mM Tris-HCl (pH 7.5) in the presence of **a**) Hg(II)ion and **b**) Cd(II) ion at different molar ratios, 2:1, 5:1, and 10:1 of metal ions (Hg(II) or Cd(II) ions) to TEM-1 β-lactamase [P2].

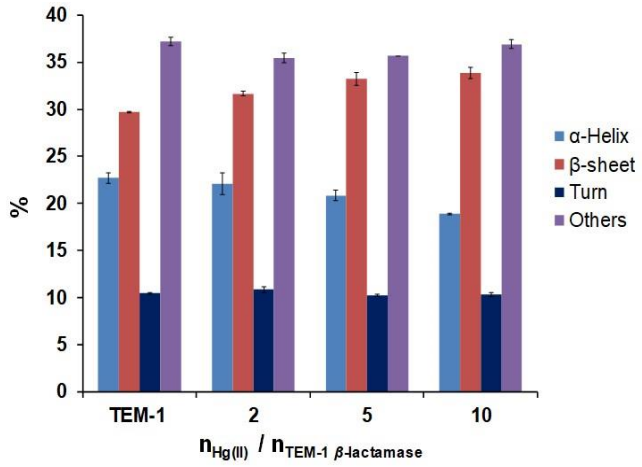

Figure 5.19. The fractions of the secondary structure elements of TEM-1 β-lactamase in presence of Hg(II) ion at molar ratios (0:1, 2:1, 5:1, 10:1 of Hg(II) ion to enzyme) calculated from the circular dichroism spectra with the BeStSel program [40-43] [P2].

5.1.6.2. Mass spectrometric measurements

Hg(II) ions exerted a significant effect on the catalytic activity of TEM-1 β-lactamase, which was suggested to be related to their interaction with the enzyme. Thus, we decided to investigate this metal ion in the following experiments. Mass spectrometry (ESI MS) revealed that Hg(II) ions interact weakly and non-specifically with TEM-1 β-lactamase. There are 9 Met residues as sulfur-containing amino

acids in the enzyme, few of them being close to the enzyme active center. In addition, a disulfide bridge is close the active center. The Met thioether groups and disulfide bridge offer several binding sites for the soft metal ion like Hg(II). The results of mass spectrometry support that the interaction of Hg(II) with the TEM-1 β-lactamase may occur at several weak binding sites in parallel at high molar ratios of Hg(II):enzyme about (10:1). However, the apo-enzyme could be still detected even at Hg(II) ion excess (**Fig. 5.20**).

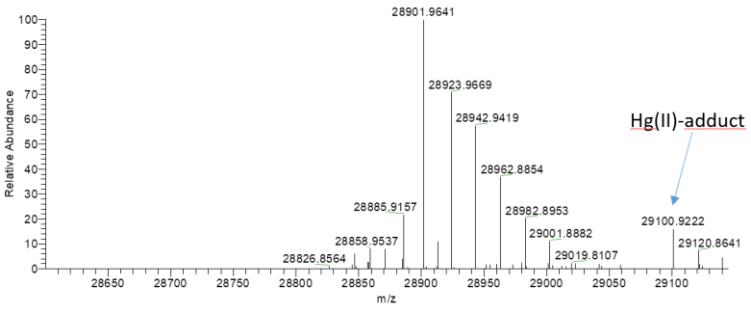

Figure 5.20. Deconvoluted electrospray ionization mass spectrum of TEM-1 β-lactamase in the presence of tenfold Hg(II).

5.1.6.3. PAC spectroscopic measurements

^{199m}Hg perturbed angular correlation of (PAC) spectroscopy of γ-rays is suitable for studying the interaction of Hg(II) with biomolecules [222]. PAC experiments were carried out in collaboration with Lars Hemmingsen (University of Copenhagen) and his PAC team upon addition of 0.9 eq. Hg(II) and 1.9 eq. Hg(II) with respect to TEM-1 β-lactamase. PAC spectroscopy may provide information on the coordination geometry of Hg(II) at the metal binding site. This information is related to the nuclear quadrupole interaction (NQI) parameters. The experimental data, together with those of the reference samples ($Hg(Cys)_2(s)$) and the Fourier transformed spectra are shown in **Fig. 5.21,** and the fitted PAC parameters are presented in **Table 5.4**. Two NQIs were needed for the successful fit.

The most important finding of these experiments were the following:

(i) the exponentially decaying signal, NQI1, is most probably related to multiple binding sites and/or rapid dynamics of the exchange of free Hg(II) with Hg(II) non-specifically bound to TEM-1 β-lactamase; **(ii)** NQI2 reflected a well-defined binding site (or several similar binding sites). Concerning the metal site structure, NQI2 suggests that the coordination number of Hg(II) may

vary between 2- and 3- coordinated Hg(II) [222], with coordinating methionine(s) and/or histidine(s). Finally, based on the results the Hg(II) binding site does not have high affinity for the metal ion, the apparent K_d is estimated to be in the order of μM.

Table 5.4. Parameters obtained for the ^{199m}Hg PAC data [P2].

Sample	$C_{Hg(II)}$ (μM)	ν_Q (GHz)	η	δ x 100	λ (μs^{-1})	A x 100	χ r^2
Hg(Cys)2(s)	-	1.460 (5)	0.10 (8)	0.0 (7)	7 (8)	18.4 (9)	0.70
Hg(Cys)2(s)	-	1.460[a]	0.10 (2)	0.0 (5)	3 (1)	14.4 (7)	0.70
TEM-1 β-lactamase	2.7	- 1.35 (2)	- 0.21 (5)	- 9 (3)	1.5 (6)[c] 0 (12)	8.9 (4)[b] 7.4 (2)[b]	0.68
TEM-1 β-lactamase	5.7	1.39 (2)	- 0.18 (5)	- 12 (3)	0.4 (2)[c] 0 (16)	4.0 (4)[b] 10 (1)[b]	0.70

[a]Calibrated for the analogue instrument to be the same as for the digital instrument.

[b]The amplitudes are sensitive to the value of λ for the "fast" component (1.5(6) μs1 and 0.4(2) μs1). The best fit is presented here but the amplitudes were not used for any quantitative conclusions.

[c]These rate parameters, λ, for the "fast" component, have a different physical meaning than the other values indicated in the same column, see [175] for details.

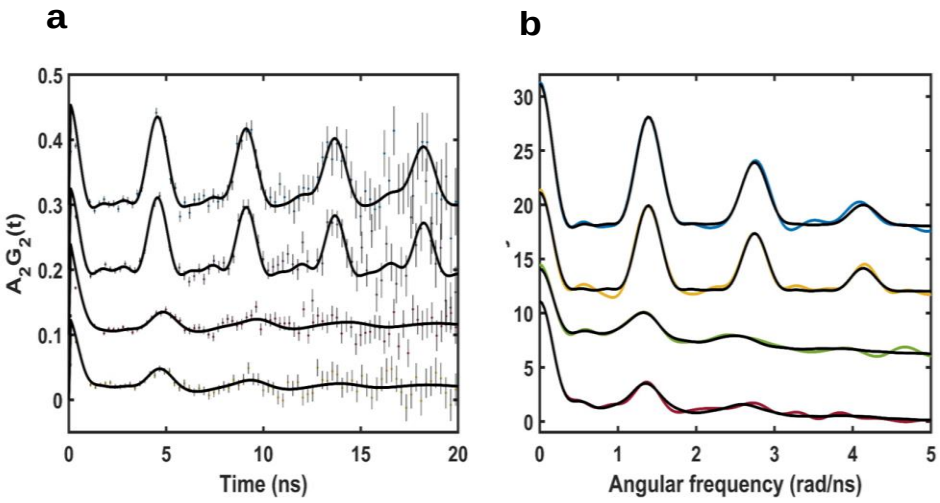

Figure 5.21. ^{199m}Hg PAC data, **a**) experimental data and fit. Data points with error bars as 5-point average of raw data and fit as full line. **b**) Fourier transformed data (colored thin lines) and fit (black lines). From top to bottom: $Hg(Cys)_2$(s) reference recorded on the digital PAC instrument; Hg(Cys)2(s) reference recorded on the analogue PAC instrument; 3.0 μM TEM-1 β-lactamase and 2.7 μM Hg(II); and 3.0 μM TEM-1 β-lactamase and 5.7 μM Hg(II); conditions for the latter two samples: 10 mM HEPES (pH 7.4), 50% (*w/w*) sucrose at 1°C [P2].

5.1.7. The effect of metal ions on bacterial cells expressing TEM-1 β-lactamase

A synergic relationship between heavy metal ions and β-lactam antibiotics in their action against bacteria [223;224], as well as experimental data on a parallel development of resistance against antibiotics and heavy metal ions [225-228] were reported in the literature. The behavior of bacteria in metal ion containing cultures is very complicated. The effect of metal ions is diverse and depend on many factors, such as the type of bacteria studied, the applied media and concentrations, *etc.* [229]. The degradation of β-lactam antibiotics by metal ions may participate in decrease of the antimicrobial effect [211;204]. Cd(II) ions were shown to catalyze the degradation of ampicillin in methanol [230] or in Luria-Bertani bacterial growth medium [231].

We applied M9 minimal medium to monitor the effect of Hg(II), Ni(II), and Cd(II) on the viability of *E. coli* BL21 (DE3) bacterial cells under well controlled conditions. The cells were transformed with a modified pET-21a(+) providing ampicillin resistance. 270 μM ampicillin, a concentration usually applied in our laboratory, was non-toxic for these bacteria. We observed that the growth of the bacteria in presence of chemical agents was dependent on the initial number of the bacterial cells.

Series 1 experiments were carried out in bacterial cultures with low starting McFarland value of 1.0 (1.0 McFarland unit corresponds to ~3×10^8 viable cells/1mL of the bacterial culture). Various concentrations of Hg(II), Ni(II), or Cd(II) ions and/or ampicillin and IPTG were added to the bacterial cultures. The McFarland units were plotted as the function of the incubation time (**Fig. 5.22**). Independently of the presence or absence of ampicillin, at 1.0 mM concentration Cd(II) ion was slightly toxic for bacteria, while at 1.0 and 0.5 mM concentrations, respectively, Ni(II) and Hg(II) ions did not allow the bacteria to proliferate at all (**Fig. 5.22a**).

As observed, the toxic effect of metal ions was dependent on the presence or absence of ampicillin at significantly decreased concentration (10 μM) of the metal ions. In the absence of ampicillin, Cd(II) ions at 10 μM did not affect the bacterial growth, while the 10 μM Ni(II) or Hg(II) ions still did not allow the bacteria to proliferate. Unexpectedly, a significant decrease of 10 μM Ni(II) or 10 μM Hg(II) ion toxicity was observed in presence of ampicillin in the solutions (**Fig. 5.22b**). 1.0 μM Ni(II) and Cd(II) ions were not toxic for bacteria even in the absence of ampicillin. Hg(II) ion was still toxic at this low concentration, but this effect was also cancelled by ampicillin (**Fig. 5.22b**). This observation can be explained by complex formation between metal ions and the antibiotic resulting in a compound with a lower toxicity than the metal ions. There are

only ambiguous stability data of the complexes of these metal ions with ampicillin in the literature. Generally, a weak binding is suggested (logK_1 ~2) [232-235]. We suggest that ampicillin-metal ion complexes may be formed in our systems under the applied conditions, because the ampicillin concentration was at about 27-fold excess as compared to that of the metal ions.

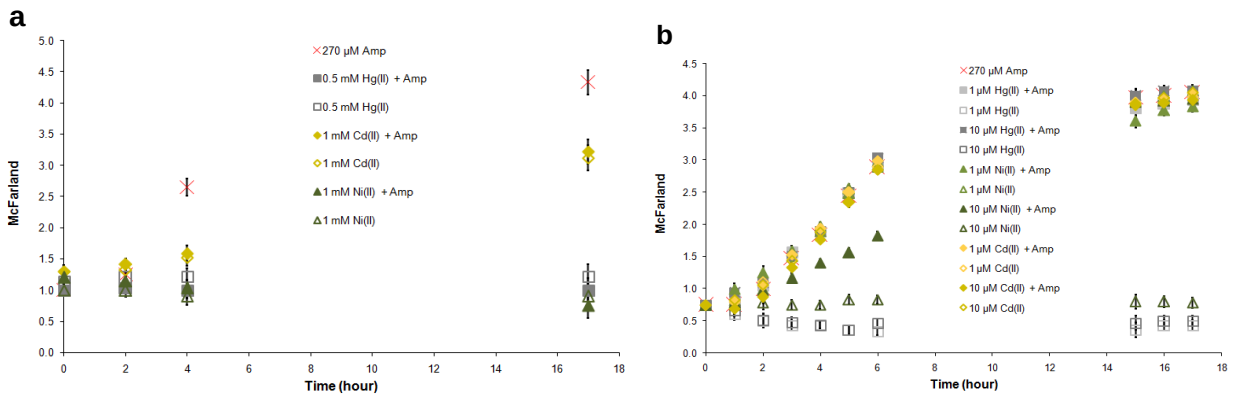

Figure 5.22. Viability of ampicillin resistant *E. coli* BL21(DE3) cells transformed with a modified pET-21a(+) DNA vector in bacterial cell cultures grown in M9 minimal medium – **Series 1**. The McFarland values of the cultures grown in the presence or absence of 270 mM ampicillin are compared with those obtained for the cultures containing (**a**) Hg(II) at 0.5 mM while Ni(II) and Cd(II) at 1 mM concentrations; (**b**) Hg(II), Ni(II) or Cd(II) at 1 or 10 µM concentrations [P2].

This suggested that the toxicity of Hg(II) and Ni(II) ions can be neutralized by ampicillin, although this neutralization was more pronounced for Hg(II) ions than for Ni(II) ions. This can probably be explained by the different coordination modes of the two metal ions with ampicillin molecules. The most likely scenario is that Ni(II)ion can coordinate with ampicillin through the β-lactam oxygen and nitrogen donor atoms [209;210], while Hg(II) ion may interact with the sulfur donor atoms of the β-lactam ring in ampicillin [204], and these complexes are less toxic, leading to reduced Ni(II) and Hg(II) toxicity.

Overexpressing TEM-1 β-lactamase from the modified pET-21a(+) DNA vector upon inducing by 1mM IPTG, did not significantly influence the above observations. The TEM-1 β-lactamase in the lysate of the collected bacterial pellets was analyzed by SDS PAGE (**Fig. A6** in Appendix). At range 1.0-10.0 µM concentrations of Cd(II) ion did not change the TEM-1 β-lactamase overexpression in samples. The overexpression of TEM-1 β-lactamase was reduced in the presence of 10.0 µM Hg(II) ion, and 10.0 µM Ni(II) ion in the presence of ampicillin, while the overexpression was completely inhibited at the same concentrations Hg(II) or Ni(II) in the absence

ampicillin, being related to the decreased bacterial viability caused a drastic decrease of the total protein amounts.

In the **series 2** experiments, the influencing chemicals (metal ions, IPTG, antibiotic) were supplemented at ~2.3 McFarland values of the bacterial cultures. In the experiments without ampicillin none of the metal ions exhibited any toxic effect at 1.0 μM concentrations on the bacterial growth (**Fig. 5.23**). Only Hg(II) ions at 10.0 μM inhibited the bacterial growth significantly, but this toxicity could be neutralized by the ampicillin.

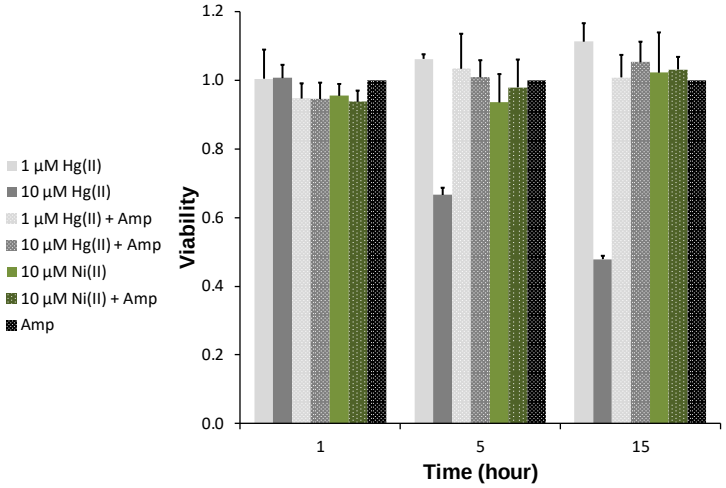

Figure 5.23. Viability of the ampicillin resistant *E. coli* BL21cells transformed with a modified pET-21a(+) DNA vector in bacterial cultures grown in M9 minimal medium. The McFarland values of the culture grown in the presence of 270 μM ampicillin are compared with those obtained for the cultures containing metal ions at various concentrations. At each measurement point the viability was normalized to that of the cell culture containing only ampicillin as an added reagent [P2].

It is worth mentioning that the replacement of ampicillin by another antibiotic, kanamycin in the similar type of experiment could not prevent the toxicity of metal ions. We have repeated the viability experiments with *E. coli* BL21 (DE3) bacteria transformed by the pET-M11-SUMO3-GFP DNA vector providing kanamycin resistance instead of ampicillin [179]. Hg(II) ion was toxic, while Ni(II) was slightly toxic at 10.0 μM concentrations and this effect was independent of the presence of kanamycin (**Fig. 5.24**). These results demonstrated that the presence of kanamycin could not protect the bacteria from the metal ion toxicity. This further proves that ampicillin can protect the cells from the metal ion toxicity through complexation reactions.

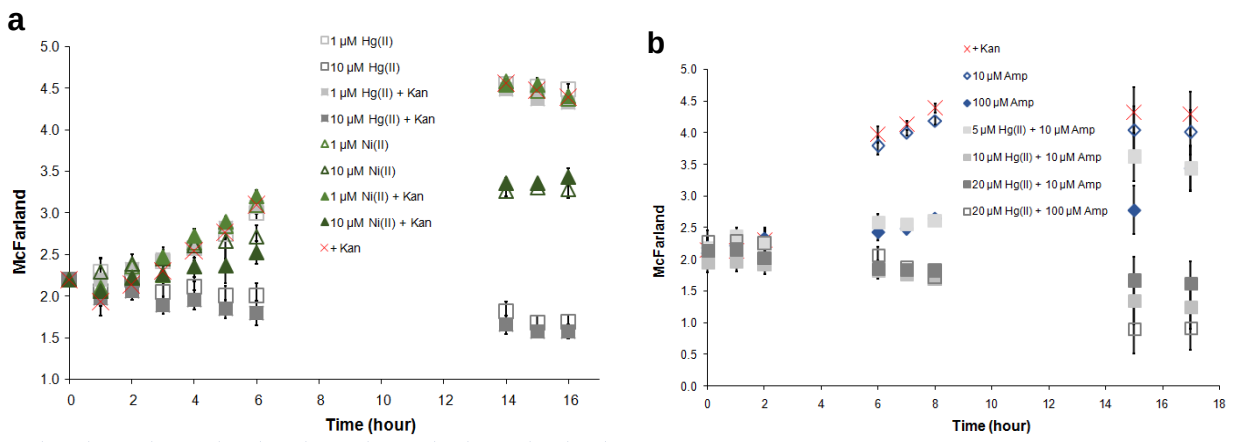

Figure 5.24. Viability of kanamycin resistant *E. coli* BL21 (DE3) cells transformed with a modified pET-M11-SUMO3-GFP DNA vector in bacterial cultures grown in M9 minimal medium – **Series 2**. The McFarland values of the culture grown in the presence of 100 mM kanamycin are compared with those obtained for the cultures containing (**a**) Hg(II) or Ni(II) at 1.0 or 10.0 mM concentrations (**b**) in the presence of Hg(II) and ampicillin at various molar ratios [P2].

With the same cells, the effect of ampicillin could also be monitored. 10.0 μM ampicillin proved to be nontoxic to these bacterial cultures; but 100 μM ampicillin had a slight toxic effect. However, 10.0 and 100.0 μM concentrations ampicillin seemed to be too small to compensate for the effect the metal ion toxicity (**Fig. 5.24b**). Thus, the addition of the antibiotic at high excess is required to decrease the metal ion toxicity. This is in agreement with the literature data about the low stability of the ampicillin-metal ion complexes [234].

5.2. NColE7 nuclease and its mutants

During my PhD work, we studied two mutants of the nuclease domain of colicin E7 protein (NColE7): NColE7-R447G and His-tagged NColE7-R447G (**Fig. 5.25**). Previously, both of these mutants were prepared, purified, and characterized in our laboratory. As well as, our research group proved that the mutation of Arg447 to Gly447 (R447G) led to a significantly less active mutant enzyme than the wild type, that is advantageous to monitor the catalytic activity of this mutant instead of the extremely active wild type enzyme [131]. NColE7-R447G is abbreviated as KGNK according to the amino acid sequence at the N-terminus of the native sequence (446-KRNK-449) showing the R447G mutation. I have purified the KGNK protein according to the previously published HPLC method [131] using a GST-affinity column via GST-tag, which was then cleaved by a specific protease (*vide infra*). The His-tagged NColE7-R447G protein is abbreviated as KGNK-His. This mutant contains a linker sequence and a 6×His oligopeptide (His-tag) at the C-

terminus of the protein. The KNGK-His was previously purified by immobilized metal ion affinity method via His-tag and Ni(II)-NTA resin using batch method [236]. The properties of both of these mutants were studied in the presence of only Zn(II) ions, supposed to be the native metal ion for NColE7 [131;236]. Our aim was to investigate, whether non-native metal ions can interact with the enzyme, or compete with Zn(II), and to study the consequences related to the structure and catalytic activity.

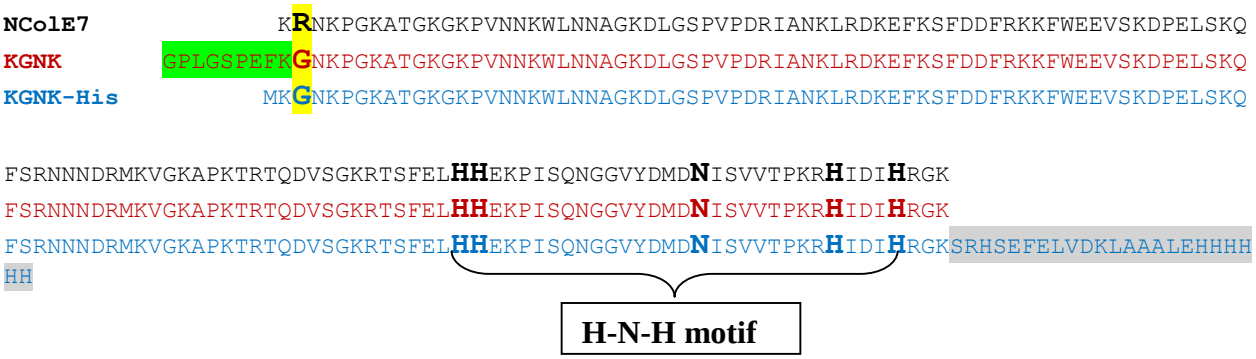

Figure 5.25. Comparison of the amino acid sequences of the studied His-tagged NColE7-KGNK (mutant) and NColE7-KGNK (mutant) with that of the wild-type NColE7 protein. The R447 position is highlighted by a yellow background. The N-terminal sequence of NColE7-KGNK, remained after the GST cleavage is highlighted by green background. The C-terminal sequence of His-tagged NColE7-KGNK mutant that allows for IMAC purification is highlighted by gray background.

5.2.1. Expression and purification of NColE7 mutants

For the purpose of further studies, we have purified new batches of the proteins. KGNK with a fusion affinity tag was co-expressed with the immunity protein7 (Im7) to protect the DNA of the *E. coli* BL21 (DE3) host cells from the nuclease activity of this enzyme. The GST-fused KGNK enzyme was purified via its glutathione-S-transferase (GST) fused form together with the immunity protein Im7, as described earlier [131]. Briefly, some important facts are mentioned here. The Im7 protein has high binding affinity to KGNK with K_d being in the nM range, and the KGNK/Im7 protein complex cannot be separated by increasing the ionic strength. Therefore, the Im7 protein was removed by decreasing the pH to 3.0, while under these conditions the Zn(II) ion is also removed from the KGNK due to both the structural changes in NColE7 and the competition of protons with the metal ion for the imidazole donor groups of His residues. However, Zn(II) ion was previously shown to be bound to the enzyme during the protein expression [131]. The GST-tag was cleaved off using Pre-session cleavage protease (3C rhinovirus protease). After the

cleavage, the remaining short amino acid sequence consisting of eight amino acid residues at the N-terminus does not affect the structure, the Zn(II) ion/DNA binding or the catalytic activity of the enzyme [131]. The SDS PAGE image revealed that the obtained protein was pure (**Fig. A7** in Appendix). To confirm that all the metal ions were removed, we incubated the enzyme with 10 equivalents of ethylenediamine tetraacetic acid (EDTA), followed by a buffer exchange to 20 mM HEPES (pH 7.7) to remove the strong chelator. This procedure resulted in recovered functional structure of the apoprotein having a single strong metal ion binding site in the active center.

The KGNK-His enzyme was designed to have 23 residues fused to the C-terminus of the 132 a.a long KGNK protein. The fusion tag contains 17 residues as a linker (containing one His residue) and a sequence containing 6×His residues (His-tag) at the C-terminus for immobilized metal ion affinity chromatography. The fused amino acid sequence (23 residues) were shown to affect the catalytic activity and Zn(II) ion binding properties of this enzyme [236].

Metal-ion affinity chromatography is widely used for recombinant protein purification [237]. Terminal 6×His residues (His-tag) attached to the protein coordinates to the Ni(II) ion affinity columns packaging Ni(II)-NTA resin. A buffer solution containing imidazole as a competitor is usually used to elute His-tagged protein from the column. In this work, KGNK-His was expressed by *E. coli* BL21 (DE3) host cells without immunity protein (Im7), which was the first sign of its decreased nuclease activity compared to the KGNK protein. According to the previous results, NColE7 and its mutants, such as KGNK contain 3 His residues as the native metal binding sites in their active center. These binding sites are usually coordinated to a Zn(II) ion, so one His residue of the His-tag may protect the host cell from the DNA cleavage by binding to the fourth coordination site of the tetrahedral Zn(II) ion, thereby, reducing the possibility of the interaction of Zn(II) with the scissile phosphodiester group of the DNA. Thus, the host cells remain viable during the expression of this enzyme even without the Im7 protein. Previously, KGNK-His was purified by batch method, but in this work, it was purified by IMAC on an HPLC system, using a gradient elution with 20 mM Tris-HCl buffer containing ~ 250 mM imidazole (**Fig. A8a** in Appendix) and 250 mM NaCl. The Ni(II) ion affinity column has weak binding to other proteins that have been removed by 50 mM imidazole and 250 mM NaCl. The eluted KGNK-His fractions were detected by 12.5% SDS PAGE (**Fig. A8b** in Appendix), which exhibited a single band at ~17 kDa. The target enzyme was pure enough to use it for further characterization. The IMAC technique carries a disadvantage that Ni(II) ions may partially bind to the metal binding sites of the purified

enzyme, causing ambiguities during the investigation of the metalloenzyme properties. Therefore, 200 eqs of EDTA as a strong chelator was added to the purified protein to remove the traces of Ni(II) or other metal ions. Ultrafiltration was applied to remove the buffer and Ni(II)-EDTA complex and for reducing the volume of the protein solution. The buffer exchange procedure was carried out with 10 mM HEPES, pH 7.7. The yield of the purified protein was determined by UV absorption spectrometry at 280 nm to be ~3 mg/1 g of wet bacterial pellets.

5.2.2. Solution structural studies of NColE7 mutants

5.2.2.1 CD spectroscopic measurements

The structural properties of the purified enzymes (KGNK and KGNK-His) were studied by CD spectroscopy in aqueous solutions to calculate the secondary structure composition and its changes in the presence of native Zn(II) ion, and non-native metal ions such as Ni(II), Cu(II), Cd(II).

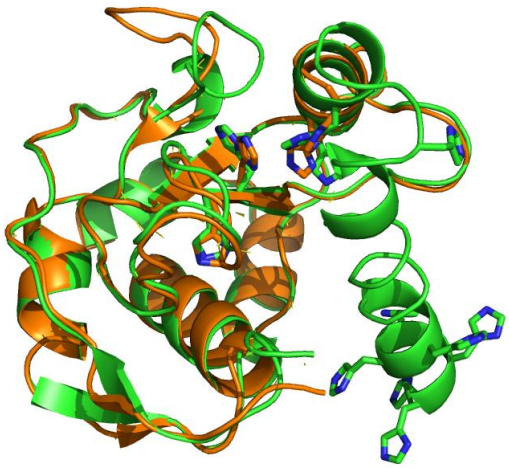

Figure 5.26. Crystal structure of NColE7 (PDB ID:7CEI) was aligned with predicted structure of KNGK-His. The prediction of the protein structures was performed by I-TASSER (online tool: https://zhanggroup.org/I TASSER/). [238-240].

While the secondary structure composition calculated from the CD spectrum of KGNK can be compared to that of NColE7 and thus, to that obtained from its crystal structure, the 23 amino acids at the C-terminus of KGNK-His may affect the structure of the protein. Therefore, a prediction of the 3D structure of KGNK-His was carried out using the I-Tasser on-line tool. The comparison of the predicted structure with the crystal structure of NColE7 shown in **Fig. 5.26** suggested that the secondary structures formed within the common sequence are practically unchanged.

CD spectroscopy in the presence of Zn(II) ion

The identity of the CD spectra of both the KGNK and KGNK-His proteins before and after the above described EDTA treatment suggested that the enzymes were indeed obtained in their apo forms. The Zn(II) ion is a common catalytic metal ion in many hydrolytic enzymes. Due to its properties such as the filled d-shell (d^{10}) it forms complexes in various geometries, and does not participate in redox reactions. The published crystal structures (**Table 2.2**) of NColE7 and its mutants with/without metal ion, DNA, phosphate ion, and Im7 protein exhibited four His residues at the active center, three of which are offered to coordinate metal ions (mostly Zn(II) ion in the available crystal structures). The fourth site in the tetrahedral geometry remains for water molecule, counter ions such as phosphate or sulfate ions or the scissile phosphodiester group of the substrate DNA molecule. Previously, it was shown that the Arg447Gly mutation did not affect the DNA/metal ion binding and the protein structure. The addition of Zn(II) ion to the apo KGNK enzyme caused slight but significant changes in the CD spectrum accompanied by a small change in the intensity and a red shift in the 190 nm peak of ~2 nm [131;143]. In this work, these changes in the CD spectrum of KGNK enzyme (**Fig. 5.27a**) could be reproduced in the presence of one equivalent Zn(II) ion, and seemingly this enzyme was saturated by one equivalent as the addition of further Zn(II) ions did not affect the CD spectrum. This was in line with the available single strong metal binding site.

The K_d value characterizing the Zn(II) binding affinity of KGNK was show to be in the nM order of magnitude [131], while EDTA forms much more stable complex with Zn(II) under the same conditions [241]. This suggests that EDTA can quantitatively remove the Zn(II) ions from the metal binding site of KGNK. Indeed, the addition of equivalent amount of EDTA, independently of the Zn(II) concentration could reverse the changes in the CD signal, and spectra identical to that of the apo-enzyme were obtained (**Fig. 5.27a**).

The changes in the CD spectra of KGNK-His were too small and continuous in the presence of increasing molar ratio of Zn(II) ion to unambiguously analyze and conclude information about the metal ion binding (**Fig. 5.27b**). The number of the metal ion binding sites and in parallel, the number of the bound metal ions increases by the increasing amount of added Zn(II), as it was shown previously by mass spectrometry [236]. This suggests that the coordination of metal ion to the His residues in the affinity tag also causes conformation changes, which makes the assignment of the changes in the CD spectra difficult. We could observe the red shift of the spectrum,

resembling that of the KGNK protein only when excess (~ 5 eq.) of metal ion was added to KGNK-His. This indicated that CD spectroscopy is not sensitive to the effects of Zn(II) binding to the KGNK-His protein, most probably because of mutually cancelling effects of the conformational changes.

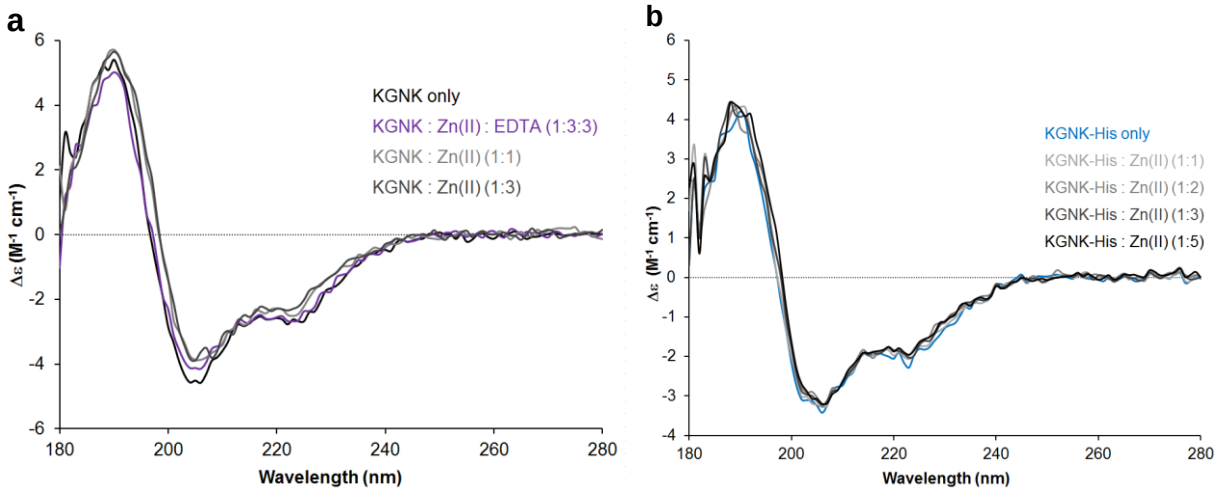

Figure 5.27. Circular dichroism spectra of KGNK **(a)** [P3] and KGNK-His **(b)** in the presence of increasing concentrations of Zn(II) ions ($ZnCl_2$). The recovery of the apo-KGNK via EDTA (violet line) is also shown. The Δε values are related to the amino acid residues. 3-10 mM HEPES, pH 7.7. 18-20 μM apo KGNK-His (pre-treated with EDTA) in the presence of various concentrations of Zn(II) ion. Δε values are related to the amino acid residues.

CD spectroscopy in presence of non-native metal ions

NColE7 and the closely related NColE9 were previously found to behave differently in the presence of various divalent metal ions. It has been shown that these enzymes may bind divalent metal ions other than Zn(II) in their HNH active center, with K_d at ~ μM level [128]. A crystal structure of NColE7 in complex with Ni(II) revealed three His residues bound to the metal ion with a phosphate ion at the fourth binding site for Ni(II) ion (**Fig. 5.28**), but some ambiguity in the metal ion surroundings was also observed [127].

We have selected Ni(II), Cd(II) and Cu(II) for further investigation of the consequences of interaction with KGNK and KGNK-His. Ni(II) ion is the most common component of the immobilized metal ion affinity chromatography (IMAC) technique for protein purification, and traces of it can remain with the protein after the purification. Cu(II) ion is a strong Lewis acid, having high affinity toward imidazole side-chains and thus, could strongly compete with Zn(II) ion, and Cd(II) ion is a d^{10} electron system analogue of Zn(II) ion, but with more soft character.

The structural changes of KGNK upon addition of these non-native metal ions were monitored by CD spectroscopy.

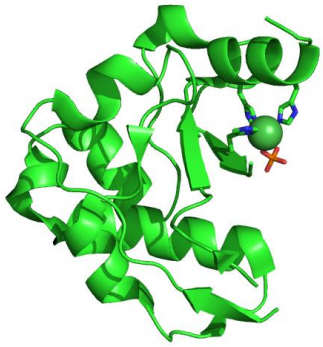

Figure 5.28. Crystal structure of NColE7 mutant in complex with Ni(II) and phosphate ion (PDB ID:1ZNV).

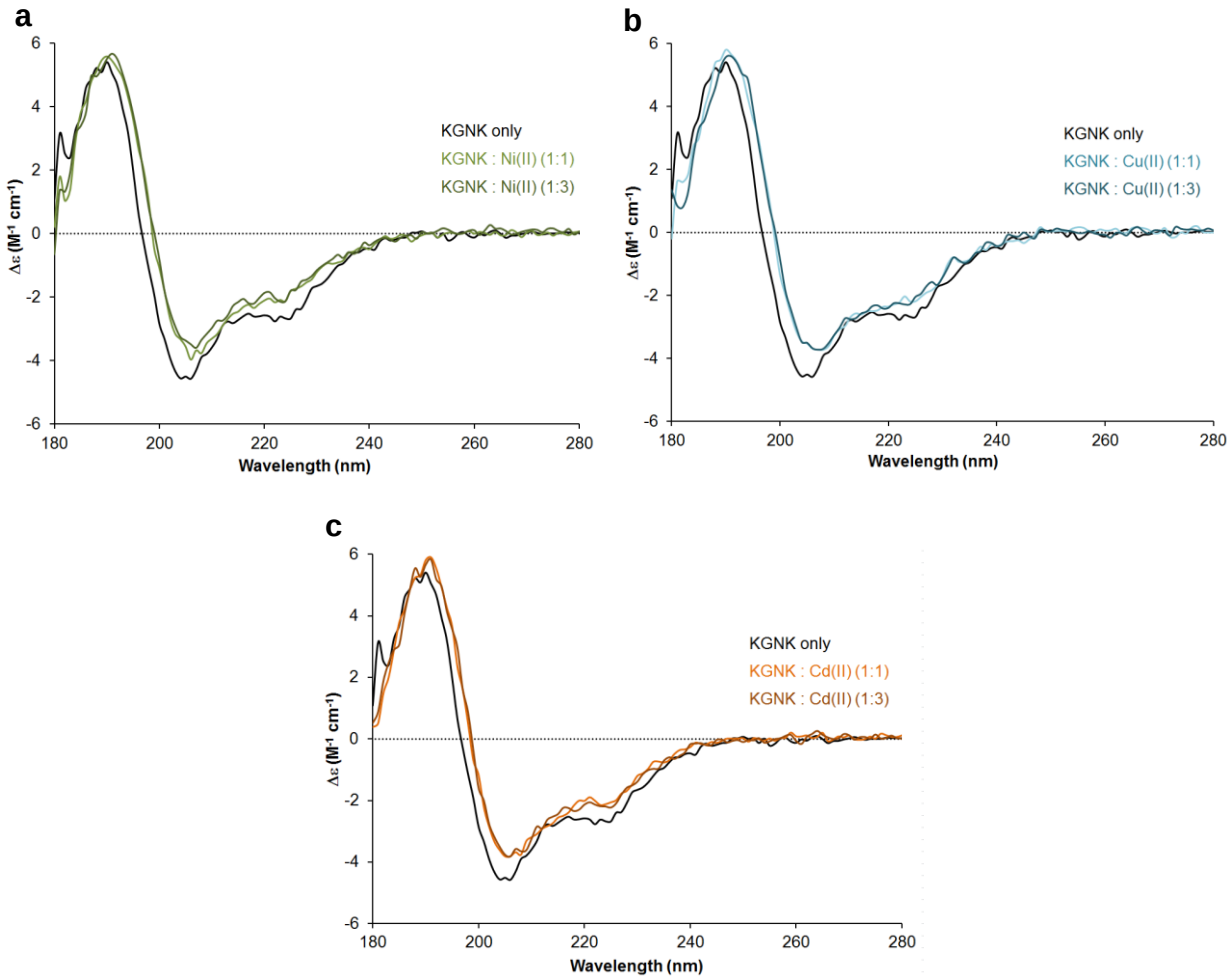

Figure 5.29. Circular dichroism spectra of the KGNK protein in the presence of increasing concentrations of (**a**) Ni(II) ions, (**b**) Cu(II) ions and (**c**) Cd(II) ions. Δε values are related to the amino acid residues [P3].

The addition of either one or three equivalent amounts of Ni(II), Cu(II) or Cd(II) ions to the apo-enzyme caused very similar changes in the CD spectra to that related to the effect of the Zn(II) ion (**Figs. 5.29a,b,c**). In other words, the slight decrease of the intensity was observed along with a red shift of about 2 nm. These changes illustrated that all of the applied metal ions could bind to the KGNK active center, causing a minor change in the secondary structure of the protein. These results were surprising because the structure of the HNH motif in KGNK (as well as in NColE7) offers a tetrahedral metal ion binding site consisting of three His residues which is optimal for Zn(II) ion. However, Ni(II) ion would usually prefer octahedral coordination geometry [242], while Cu(II) ion would prefer square planar coordination geometry [243]. Cd(II) ion could fit into the offered tetrahedral binding site [244], while its affinity towards nitrogen donors of the imidazole ring is lower than those of the other applied metal ions.

CD spectroscopy in presence of anions

As it was shown above, there was red shift about 2 nm in CD spectrum of KGNK upon addition 1.0 or 3.0 eq. of Zn(II), which could be reversed by the addition of EDTA in equivalent amounts compared to the metal ions in each case, resulting in identical CD spectrum to that of the apo-enzyme.

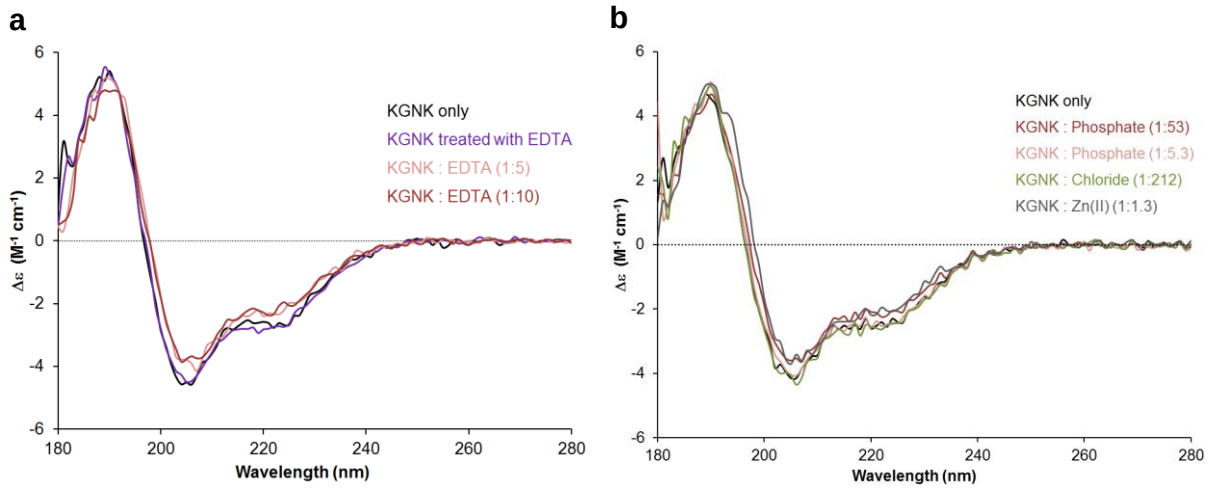

Figure 5.30. (**a**) Circular dichroism spectra of the KGNK enzyme with and without an additional treatment with EDTA and buffer exchange removing the chelator, and well as in the presence of increasing concentrations of EDTA. (**b**) The effect of simple (Cl^-) or complex (HPO_4^{2-}) anions on the KGNK CD spectral shape. Δε values are related to the amino acid residues [P3].

This can be easily explained by the fact that EDTA is a much stronger chelator than the 3 His residues of the KGNK towards the metal ion like Zn(II) ion: the stability constant of EDTA-Zn(II) ion complex is in the order of ~ 10^{16} while 3 His residues of KGNK is in the order of ~ 10^{9}. Such a large difference in the stabilities of the EDTA and KGNK metal complexes with the applied non-native metal ions are also expected. Therefore, no excess of EDTA is needed to inhibit the metalloenzyme catalytic action, as it is usually observed in the literature, unless there is a metal ion excess originally in the reaction mixture.

Similarly, we have supplemented the metallated KGNK solution with an excess of EDTA, and surprisingly, the change in the CD spectrum due to the metal ion coordination could not be reversed. Therefore, we have checked the CD spectrum of the apo KGNK enzyme upon addition of EDTA (**Fig. 5.30a**). This caused changes and a red shift of the CD spectra similar to that observed for the metal ions. This suggested that the negatively charged EDTA may interact with the positively charged residues of the KGNK enzyme otherwise participating in the DNA binding. A similar phenomenon could be suggested, based on the observation upon addition of high excess of phosphate ions also causing a slight change in the CD spectrum of the apo-KGNK similar to that of EDTA (**Fig. 5.30b**). In agreement with these observations, a crystal structure already demonstrated the interaction NColE7 with phosphate ions binding to the positively charged DNA binding sites [144]. In contrast, even a large excess of chloride ions did not cause any change in CD spectrum (**Fig. 5.30b**). This does not necessarily mean that there was no interaction between the enzyme and chloride ions but if bound, these ions could not influence the protein structure.

The above CD spectroscopic results demonstrated that the KGNK enzyme can interact with anionic molecules such as *e.g.*, EDTA and phosphate ion. The catalytic activity inhibition by the Im7 protein is partially based on similar interactions between the acidic side-chains of Im7 protein and basic side-chains of NColE7 or its mutants [133**]**.

5.2.2.2. Mass spectrometric measurements

The purified KGNK and KGNK-His enzymes were characterized by mass spectrometry (MS) approving their molecular masses calculated from the amino acid sequences.

Mass spectrometry of KGNK in the presence of Zn(II) ion

The deconvoluted mass spectrum of KGNK detected the enzyme mainly in its apo form without the addition of metal ions. Nevertheless, in each measurement, the protein already acquired certain amount of Zn(II) ions. This suggested that the used low concentration of the apo-enzyme allowed

for detectable fraction of the protein that could easily bind Zn(II) ions from buffers/reagents/containers/sample holders applied during the experiments, even if these were treated very carefully. A peak with ~20% relative intensity assigned to that of the mono-metallated KGNK with Zn(II) and one with ~80% relative intensity assigned to the apo-enzyme appear in the spectrum shown in **Fig. 5.31a**. In addition, Na^+ and K^+ adducts were also detected in the MS measurements.

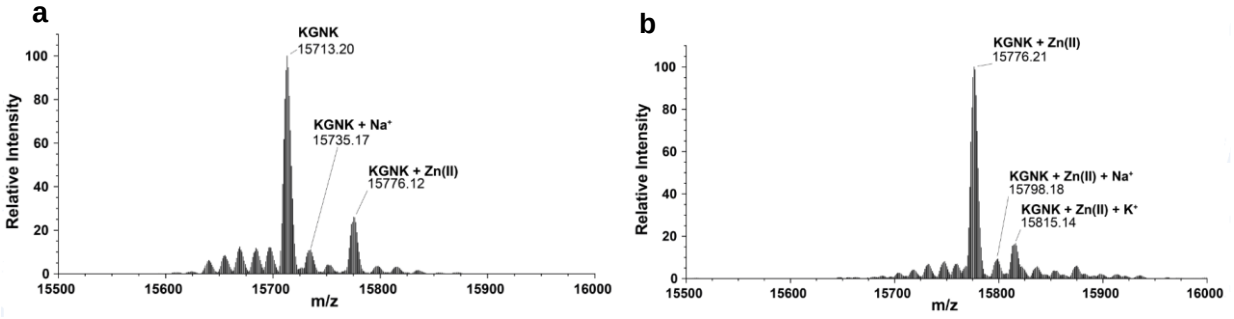

Figure 5.31. The deconvoluted ESI-MS spectra of the (**a**) KGNK protein; (**b**) KGNK + 1 eq Zn(II); the concentration of the KGNK was 3.0 μM [P3].

The expected average molecular masses of the KGNK enzyme in comparison with the obtained ones are collected in the **Table 5.6** below. The MS results showed that the KGNK enzyme was completely metallized by 1 eq. of Zn(II) ion (**Fig. 5.31b**), in good agreement with previously published data.

Mass spectrometry of KGNK in presence of non-native metal ions

The interaction of the KGNK apo-enzyme with Ni(II), Cu(II), and Cd(II) ions was also investigated by mass spectrometry (MS). Upon addition of one equivalent of a non-native metal ion to the apo-enzyme solution, we observed the peak of the metallated KGNK for each selected metal ion (**Fig. 5.32**). The experimentally obtained molecular masses for MH^+ species of Ni(II)-KGNK and Cd(II)-KGNK are collected in **Table 5.6** being in a good agreement with the calculated data. The mass spectrum showed a main peak assigned to Ni(II) coordinated KGNK in the presence of Ni(II) ions as well as a small peak assigned to a potassium adduct of the complex (**Fig. 5.32a**). This means that Ni(II) ion could bind to the apo-enzyme. The MS results revealed a peak related to the KGNK enzyme bound to a Cd(II) ion in the presence of this metal ion (**Fig. 5.32b**). Nevertheless, a peak with smaller relative intensity related to the KGNK apo-enzyme was still detected after the addition

of one equivalent of the Cd(II) ions. Thus, one equivalent of Cd(II) ions could not saturate the available apo-enzyme fully, suggesting that the Cd(II) ions interact more weakly with the enzyme than Ni(II) ions.

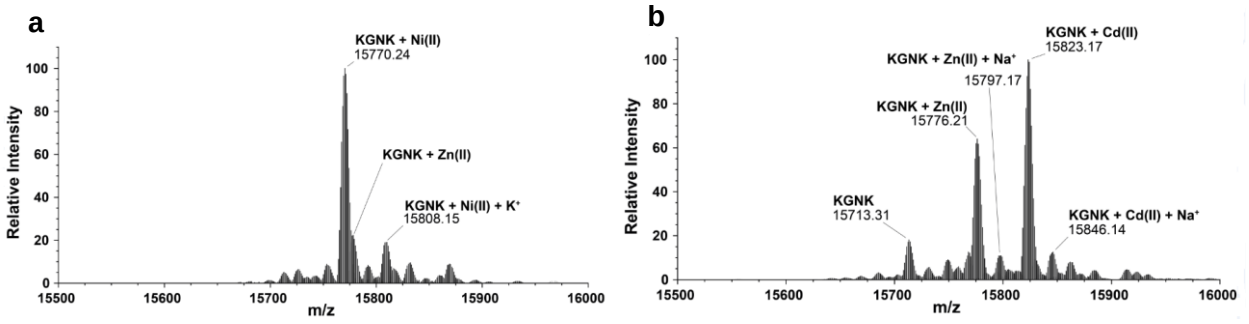

Figure 5.32. Deconvoluted ESI-MS spectra of the (**a**) KGNK + 1 eq. Ni(II) and (**b**) KGNK + 1 eq. Cd(II); concentration of the KGNK was 3.0 μM [P3].

In addition, both in the presence of Ni(II) ions and of Cd(II) ions, the MS data showed a minor peak related to the Zn(II)–KGNK species, although Zn(II) ions were not added to the reaction mixtures. However, this kind of minor metallation with Zn(II) acquired from the environment was already observed in the experiments with apo-enzyme.

Table 5.6. Measured and calculated most abundant MH^+ peaks of KGNK and its metal complexes [P3].

Species	Formula	Calculated Mass of MH^+ (Da)	Measured Mass of MH^+ (Da)
KGNK apo	$C_{690}H_{1101}N_{211}O_{206}S_2$	15,713.19	15,713.20
KGNK+ 1Zn(II)-2H^+	$C_{690}H_{1099}N_{211}O_{206}S_2Zn$	15,776.10	15,776.12
KGNK+ 1Ni(II)-2H^+	$C_{690}H_{1099}N_{211}O_{206}S_2Ni$	15,770.11	15,770.24
KGNK+ 1Cu(II)-2H^+	$C_{690}H_{1099}N_{211}O_{206}S_2Cu$	15,774.10	15,774.23
KGNK+ 1Cd(II)-2H^+	$C_{690}H_{1099}N_{211}O_{206}S_2Cd$	15,823.08	15,823.17

The MS experiments revealed that addition of one equivalent of Cu(II) ion to KGNK enzyme resulted most probably in Cu(II) bound KGNK (**Fig. 5.33**). The measured and calculated molecular masses for the MH^+ species related to the Cu(II)-KGNK complex shown in **Table 5.6** are in good agreement. However, it is rather difficult to distinguish between the Cu(II) and Zn(II) binding to the KGNK enzyme by MS because of the small difference in the molecular masses. For this reason, the isotope distribution pattern of the main peak in the mass spectrum at 15,774 m/z was compared to the simulated isotope pattern of the Cu(II) bound KGNK and Zn(II) bound KGNK

complexes. The observed pattern of the recorded spectrum aligned well with the calculated one for the Cu(II)-enzyme complex, proving that Cu(II) ion could bind to the KGNK apo-enzyme in agreement with the results of the CD spectroscopic investigations shown above.

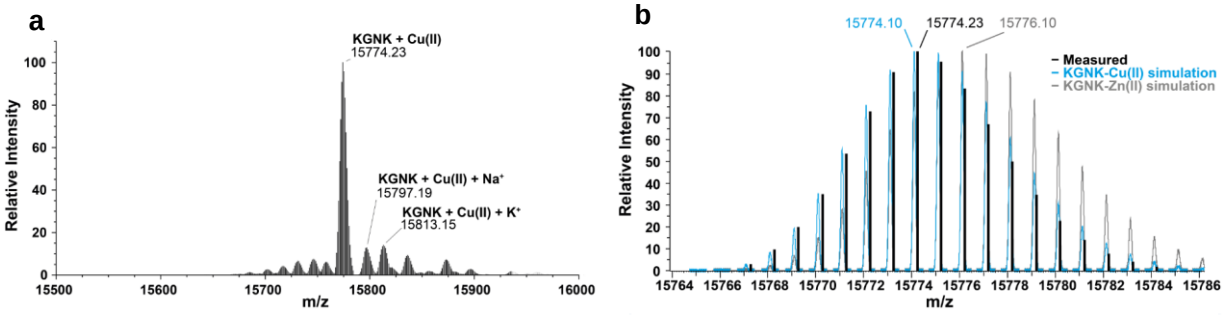

Figure 5.33. Deconvoluted ESI-MS spectra of (**a**) KGNK protein + 1 eq Cu(II); (**b**) comparison of the isotope pattern of the most intense peak of the spectrum recorded in the presence of Cu(II) ions with the simulated spectra of Cu(II)–KGNK and Zn(II)–KGNK complexes; the concentration of the KGNK was 3.0 μM [P3].

The above experiments thus, confirmed that the non-native metal ions could bind to the KGNK active center. It shall be mentioned that in the presence of one equivalent of Cd(II) ions, a small fraction of the apo-enzyme was still observed, also suggesting a weaker binding of this metal ion.

It is worth mentioning that the apo-enzyme possessed a wide range of differently charged species, with two intensity maxima at z = 16 and 10 positive charges, while all of the added metal ions could shift the charge distribution toward a structure exhibiting lower charges **(Fig. 5. 34)**. These observations are in good agreement with previously published results for the NColE2, E7, E8 and E9 proteins (the nuclease domains of the bacterial toxin proteins) upon Zn(II) binding at pH = 7.2 [128]. It was suggested that the apo-enzyme existed in two different conformations one related to a more compact (closed) and the other to an open structure [165;245]. The compact structure is likely more stable than the open one due to the interaction with the Zn(II) ion, as only this is observed in the available crystal structures.

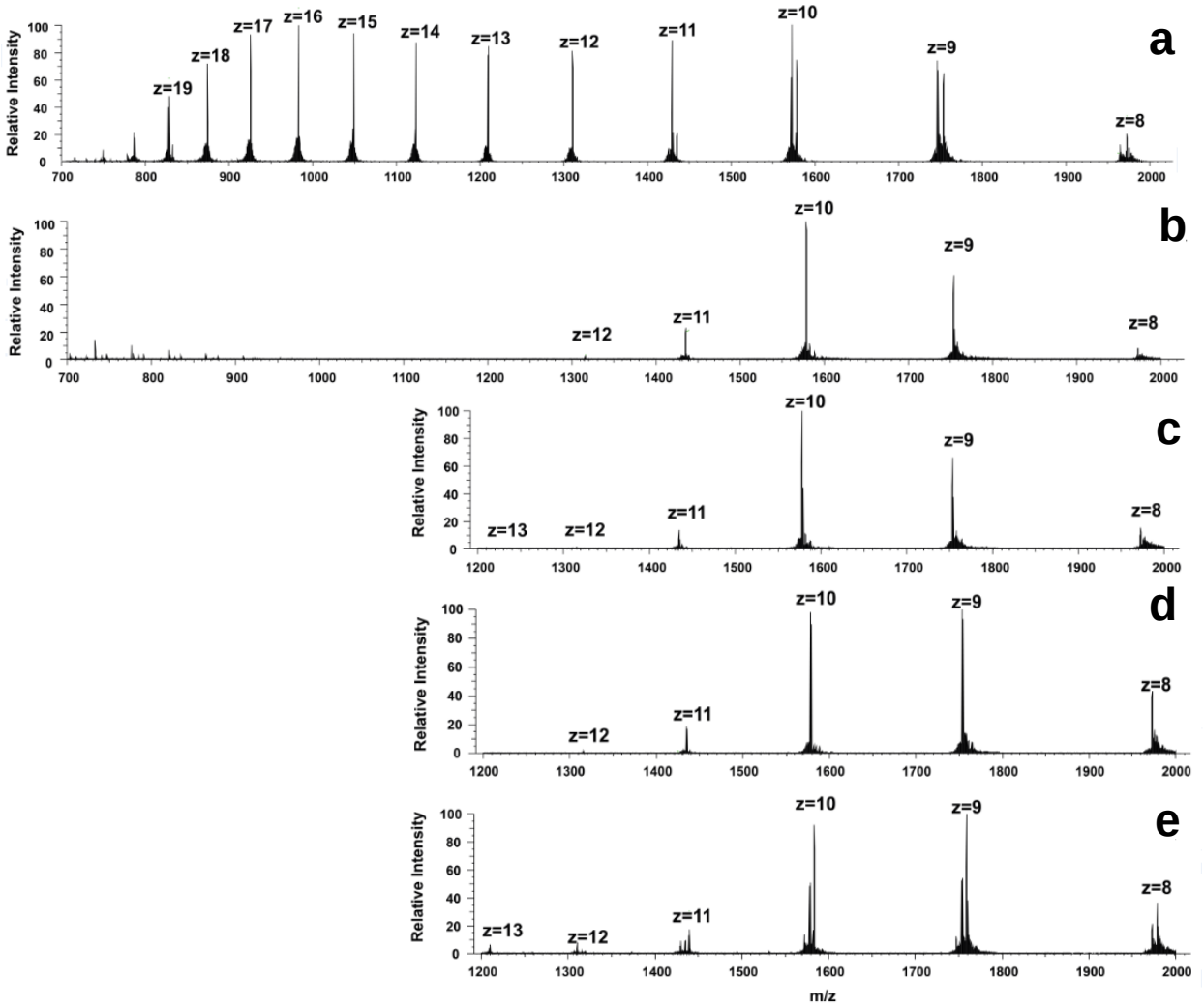

Figure 5.34. The recorded ESI-MS spectra of (**a**) KGNK protein; (**b**) KGNK + 1 eq Zn(II); (**c**) KGNK + 1 eq Ni(II); (**d**) KGNK + 1 eq Cu(II) and (**e**) KGNK + 1 eq Cd(II). Concentration of KGNK was 3 μM [P3].

Competition studies of metal ions towards KGNK monitored by mass spectrometry

Mass spectrometry was utilized to investigate the ability of the applied non-native metal ions to compete with Zn(II) ions for the HNH motif in the KGNK enzyme. One equivalent of the Zn(II) ion was added to the enzyme before supplementing the non-endogenous metal ions *i.e.*, in these experiments, Ni(II), Cu(II) or Cd(II) ions were added to the Zn(II) bound KGNK enzyme. All the mass spectra exhibited a main peak related to the Zn(II) bound KGNK, independently of the nature of the non-native metal ion (**Fig. A9** in Appendix). Thus, none of these metal ions could compete with Zn(II) ion at an equal molar ratio toward the HNH motif. These results are in agreement with

the previous literature data on the high affinity (with a K_d in nM range) of Zn(II) towards the HNH motif of NColE7 [128;131].

According to Irving William series, Cu(II) complexes are characterized by higher stability constants than Ni(II) and Zn(II) complexes involving those formed with the His side chains of the peptides. However, coordination of His side chains in a protein can be different, because the donor groups in a protein may be positioned in a pre-organized geometry, rendering the donor set to select the metal ion with appropriate properties. The tetrahedral coordination geometry offered by the HNH motif of KGNK is a good example of such preorganization, which would prefer Zn(II) over the other applied metal ions in agreement with the MS results.

5.2.3. Catalytic activity of KGNK

The nuclease activity of KGNK was studied using the pUC119 plasmid DNA as a substrate, and the catalytic activity products were monitored by agarose gel electrophoresis (AGE). Generally, a plasmid DNA may produce three forms on the agarose gel image after the electrophoretic run has been finished. These are the compact superhelical (or super-coiled), migrating most efficiently in the gel. The open circular DNA, formed as a consequence of single-strand nicks migrates more slowly in the gel than the linear DNA, formed upon double-strand cleavage (**Fig. 4.8**). The linear form would be preferred over the open circular form in the case of dimerization of the enzyme upon DNA binding and cleavage. In this work, the initial DNA substrate contained mainly the superhelical form of the plasmid.

Based on its similarity to NColE7, KGNK is expected to carry out a series of non-specific cleavages of DNA. This would result the subsequent conversion from superhelical form to open circular and linear forms. The accumulation of large number of cleavages results in the non-specific fragmentation and distribution of different DNA fragments (manifested as a smear) shifting to smaller and smaller sizes with the time of incubation. It was already proven in our laboratory that KGNK is less active than the wild type NColE7 due to the lack of Arg447 that is supposed to have an essential role in proton transfer in the hydrolytic catalysis. The best observation for the catalytic activity was at 2 hours incubation.

5.2.3.1 Catalytic activity in presence of Zn(II) ion and EDTA

The mass spectrometric measurements already revealed that the KGNK enzyme solution may contain some Zn(II) ions acquired from the trace amounts of this metal ion in the environment (buffers/reactants/containers, etc.), as well as the substrate (DNA) solution may also contain a

residual concentration of Zn(II) ions. Previously, it was shown that the Zn(II) bound KGNK enzyme has moderate activity against plasmid DNA [131]. Therefore, the apo-KGNK enzyme with a small fraction of the Zn(II) bound form should not cause a significant DNA cleavage.

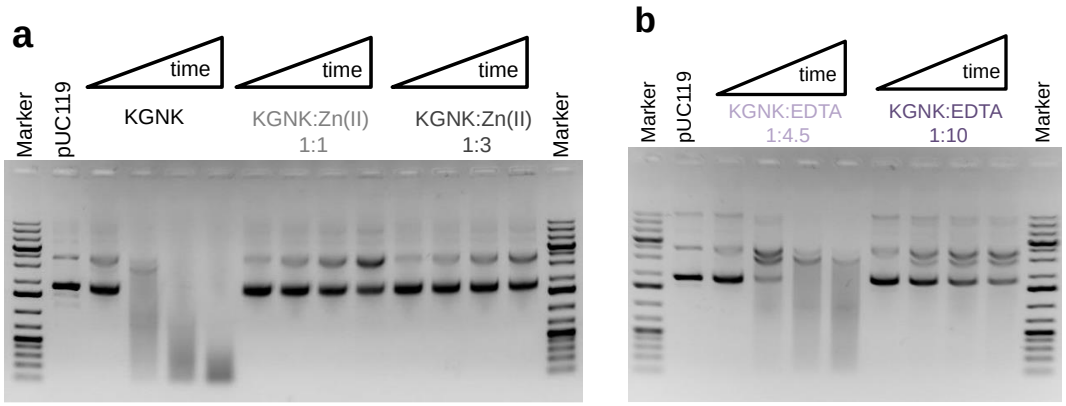

Figure 5.35. Detection of the pUC119 plasmid DNA (c = 74 μM for base pairs (bp), 3162 bp) cleavage by 1 μM KGNK enzyme using 1% (*w*/*v*) agarose gel electrophoresis **a**) in the absence and presence of 1 or 3 equivalents of Zn(II) ions and b) upon addition of EDTA excess. Each well of the agarose gel in a single cleavage experiment represents the catalytic activity after 0, 15, 60, or 120 min, from left to right. Untreated pUC119 DNA was loaded as the negative control [P3]. These conditions were valid for Figures 5.36, 5.37, 5.38 and 5.39.

In contrast, we have found that the apo-enzyme catalyzed the DNA cleavage efficiently without adding metal ion to the reaction mixture (**Fig. 5.35a**). Furthermore, surprisingly the addition one or three equivalents of Zn(II) ions to the apo-enzyme resulted in a decreased activity compared to the apo-enzyme (**Fig. 5.35a**). This may suggest that initially there was a metal ion (impurity) different from Zn(II) that allows for a significant nuclease activity, which can be replaced by the added Zn(II) resulting in a decreased catalytic activity.

Another explanation would be that the apo-enzyme itself can also be active, and an alternative hydrolysis mechanism depending on the role of the His residues in the active center may facilitate the protonation and deprotonation processes by proton transfer. To check this hypothesis, the catalytic activity of the apo-enzyme was checked in the presence of EDTA. Surprisingly, the enzyme activity could only be slightly inhibited by the addition of EDTA at up to 5 equivalents related to the enzyme (**Fig. 5.35b**), while a large excess of EDTA, using more than 10.0 equivalents could inhibit the enzyme. We suggest that this might be attributed to the inhibition by the interaction between the positively charged residue side-chains of the protein with the negatively charged EDTA, as it was already detected by the CD spectroscopy (see above).

Previously, Zn(II) ion was suggested to be essential for the nuclease activity of NColE7 [133;132], but this activity is very much dependent on the concentrations of the enzyme, EDTA and metal ion applied in the reaction. The addition of Zn(II) excess *e.g.*, reduced the catalytic activity [132]. In this work, addition 3 equivalents of the Zn(II) ion to the enzyme caused a slight inhibition of the catalytic process. This might be attributed to the ability of the excess Zn(II) ion to weakly bind to H545 inhibiting the OH^- generation by this His residue.

5.2.3.2 Catalytic activity in the presence of non-native metal ions

Addition one equivalent of Cu(II) ions to the KGNK apo-enzyme caused a similar change to that of Zn(II) ions (**Fig. 5.36a**). It is difficult to conclude at this point, whether the resulting low catalytic activity can be assigned to the Cu(II) bound enzyme, or it is the remnant activity of the small fraction of the apo-enzyme or small fraction of the enzyme bound to an unknown, very active metal ion. Nevertheless, addition of 3 equivalents of the Cu(II) ions caused a slight further decrease of the catalytic activity (**Fig. 5.36a**) suggesting the first option to be unlikely. In the presence of one equivalent of Cd(II) ions more efficient DNA cleavage was observed than with Zn(II) or Cu(II) ions (**Fig. 5.36b**) and less efficient than with the apo-enzyme in the absence of added metal ions. The catalytic activity was further decreased by increasing the excess of Cd(II) ions. These findings are in agreement with the mass spectrometric results showing that Cd(II) ion exhibits weak binding towards the KGNK enzyme. Thus, the remaining activity might be related to the fraction of the apo-enzyme.

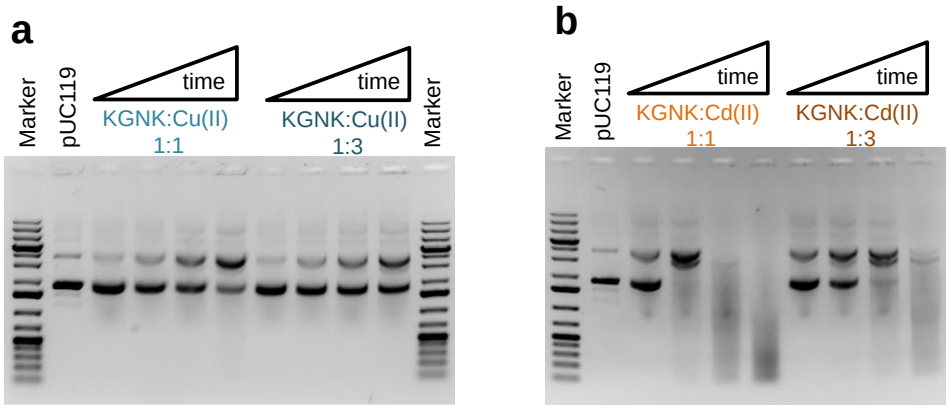

Figure 5.36. Detection of the pUC119 plasmid DNA (c = 74 μM for base pairs (bp), 3162 bp) cleavage by 1 μM KGNK enzyme using 1% (*w*/*v*) agarose gel electrophoresis in the absence and presence of various metal ions. The apo-enzyme in the presence of Cu(II) ions (**a**) and Cd(II) ions (**b**) at 1:1 or 1:3 KGNK/metal ion molar ratios, respectively [P3].

In contrast to the above observations with Zn(II), Cu(II) and Cd(II), the catalytic activity in the presence of Ni(II) ions was much higher than that of the apo-enzyme (**Fig. 5.37a**). It is even more interesting that the excess of the Ni(II) ions did not significantly inhibit this highly active enzyme. This suggests that, while Ni(II) ion may not be the native metal ion, but its presence still results in a highly active metalloenzyme (**Fig. 5.37a**). Ni(II) ion may promote the catalytic activity of the enzyme via different mechanism than those related to the apo-enzyme or the Zn(II) bound KGNK. Ni(II) ion may *e.g.*, promote the deprotonation of a coordinated water molecule, which can serve as an attacking nucleophilic agent for DNA hydrolysis, thus rendering the H545-promoted OH^- generation less or not important. In other words, Ni(II) ion in the octahedral geometry allows for water molecule binding and activation. The crystal structure of Ni(II) bound NColE7 (PDB ID:1ZNV) (**Fig. 5.28**) supports this assumption.

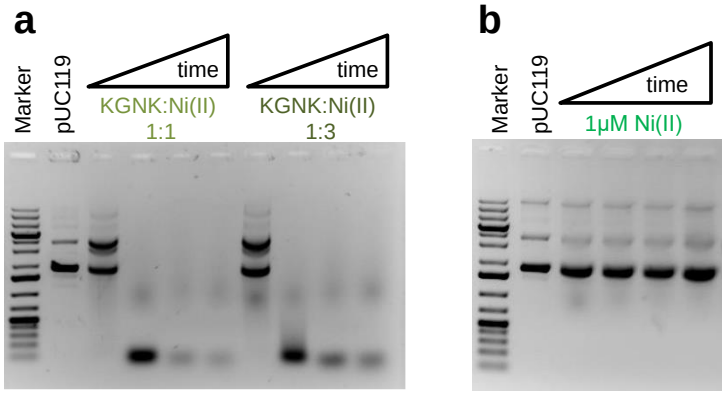

Figure 5.37. Detection of the pUC119 plasmid DNA (c = 74 μM for base pairs (bp), 3162 bp) cleavage by 1 μM KGNK enzyme using 1% (*w*/*v*) agarose gel electrophoresis in the absence and presence of various metal ions. The apo-enzyme in the presence of Ni(II) ion at 1:1 or 1:3 KGNK/metal ion molar ratios, respectively [P3].

Fig. 5.37b also shows that Ni(II) ions themselves cannot initiate significant DNA cleavage in the absence of the enzyme under the applied conditions.

5.2.3.3. The effect of metal ion competition on the catalytic activity

Competition experiments were carried out with the KGNK enzyme using Zn(II) as a strong interacting agent and Ni(II) as a highly active cofactor. Independently of the order of addition of each metal ion to the reaction mixture *i.e.*, first adding Zn(II) ions and then Ni(II) ions, or in the reverse order, identical observations were made as shown in **Fig. 5.38**. The catalytic activity substantially decreased in comparison to that of the Ni(II)-bound enzyme and was rather characteristic of the Zn(II) bound enzyme in both systems. The slight remaining activity may be

related to the presence of a small amount of Ni(II) complex according to the equilibrium relationships, as well as to the small deviations in the concentrations. This illustrated the replacement of the Ni(II) ions by the Zn(II) ions due to the thermodynamic effects *i.e.*, to the higher affinity (with a K_d in nM range) of Zn(II) than the other divalent metal ions towards the HNH motif. These findings are in good agreement with the results of the mass spectrometric experiments carried out under competitive conditions.

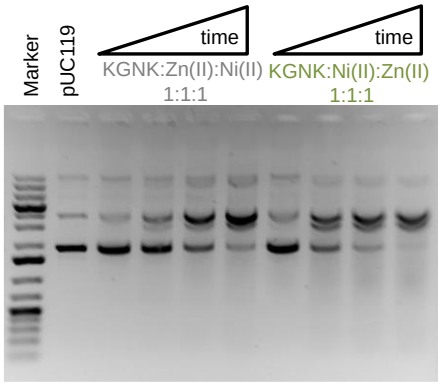

Figure 5.38. Detection of the pUC119 plasmid DNA (c = 74 μM for bp, 3162 bp) cleavage using 1% (*w*/*v*) agarose gel electrophoresis. 1 μM KGNK enzyme was applied under metal ion competition conditions, either supplementing Zn(II) first and then Ni(II) in the reaction mixture or in the opposite order [P3].

These data align well with the results published previously that Zn(II) is more strongly bound to the KGNK protein than the other divalent metal ions by at least three orders of magnitude [128]. From these results, we can conclude that the KGNK mutant enzyme prefers to bind Zn(II) ion, but its catalytic functioning is more efficient in the absence of Zn(II), while it has much higher activity in presence of Ni(II). These observations can be explained by different mechanism of the catalysis applied by KGNK under various conditions, and provides a chance for enzymatic regulation by the metal ion environment.

5.2.4. Catalytic activity of KGNK-His in the presence of non-native metal ions

KGNK-His protein contains two metal binding sites (active site and His-tag). It was previously proven that one imidazole side-chain of the His-tag, bound to the Zn(II) in the active center at the fourth site resulting in inhibition the activity of the enzyme. Mass spectrometric measurements revealed that the enzyme could bind more metal ions [236]. This made it difficult to study the replacement of the various metal ions similarly to the KGNK protein by mass spectrometry, as mixed metal complexes were observed in most cases. On the other hand, the catalytic activity

experiments provided useful information on the metallation of the active center. Starting out from the apo-protein, we have found that similarly to KGNK, the catalytic activity was much higher in the presence of Ni(II) ions (**Fig. 39a**) than that of the apo-KGNK-His and in the presence of the other applied metal ions (Zn(II), Cu(II) and Cd(II)). The excess of the Ni(II) ions did not significantly inhibit the enzyme. This supports our above suggestion, that Ni(II) ions may promote the catalytic activity of the enzyme via an alternative mechanism, such as the deprotonation of a coordinated water molecule, which can serve as an attacking nucleophilic agent for DNA hydrolysis.

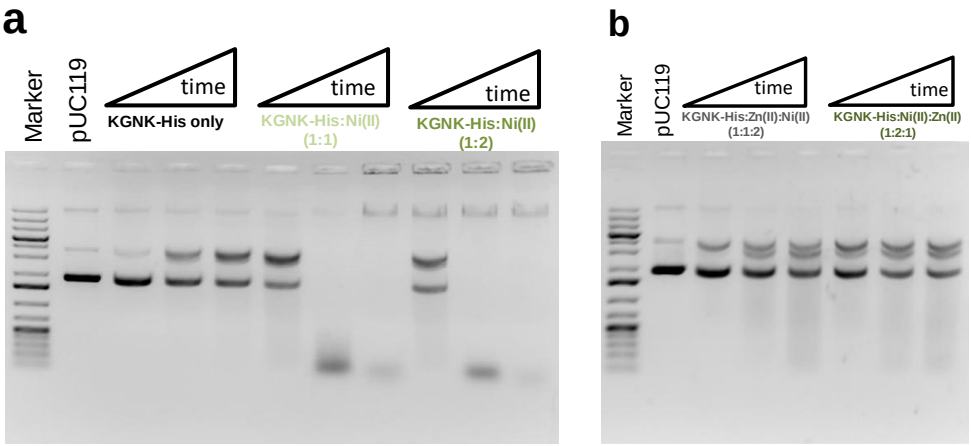

Figure 5.39. Detection of the pUC119 plasmid DNA (c = 74 μM for bp, 3162 bp) cleavage using 1% (*w*/*v*) agarose gel electrophoresis. **a)** 2.8 μM KGNK-His enzyme was applied in the absence and presence of Ni(II) ion at two different molar ratios. **b)** metal ion competition conditions, either supplementing Zn(II) first and then Ni(II) in the reaction mixture or in the opposite order at 1 eq. molar ratio of enzyme, Ni(II), and Zn(II) ions.

The competition experiments carried out between Ni(II) ion and the native metal ion Zn(II) ion toward the metal binding sites (active center and His-tag sites) of the KGNK-His, were carried out with twofold Ni(II) excess (**Fig. 39b**). The catalytic activity substantially decreased in comparison to that of the Ni(II)-bound enzyme, and it was characteristic of the Zn(II) bound enzyme in both systems, independently of the order of addition of each metal ion to the reaction mixture. These results indicated that the catalytic behavior of KGNK-His was very similar to that of KGNK in the presence of Ni(II) ions. We could also demonstrate that none of the non-native metal ions can bind the active center of KGNK-His in the presence of Zn(II) ion.

6. SUMMARY AND FUTURE OUTLOOK

The research work included in this dissertation involved the investigation of two types hydrolytic enzymes. **TEM-1 β-lactamase was studied with the emphasis of its interaction with non-endogeneous, toxic metal ions (Ni(II), Cd(II) and Hg(II)) and their effect on the catalytic activity of the enzyme.** This bacterial enzyme can hydrolyze the β-lactam ring, providing resistance against β-lactam antibiotics. As such it is a frequent target of the researches related to the development of antibiotics resistance posing a serious health threat in humans. TEM-1 β-lactamase is not a metalloenzyme, but it possesses several putative metal ion binding sites, suggesting that it may interact with metal ions affecting its function. The most important achievements of this topic were the following.

We have successfully expressed TEM-1 β-lactamase from the modified pET-21a(+) vector carrying the coding sequence of the DNA binding domain of the His-tagged Nuclear Factor I, in spite of the fact that the gene of TEM-1 β-lactamase is located outside of the multi-cloning site. We purified the protein from the bacterial pellets in its native fold by immobilized metal ion chromatography (IMAC), based on the surface histidine pairs as potential metal binding sites. Our strategy involved two steps of IMAC and single step of anion exchange, providing a yield of 1.9 mg/g of wet bacterial pellet weight, which is comparable to previous purification methods carried out under denaturing conditions.

We could identify the TEM-1 β-lactamase protein by mass spectrometric investigation of the trypsine digested fragments, as well as by intact protein molecular mass measurement. The results proved that purified TEM-1 β-lactamase was a mature enzyme (24-286 a.a.), in which the 23 a.a. signal sequence – required for the export of the protein to periplasm – was already cleaved. In addition, we could identify a mutation of the amino acid in position 82, which proved to be an isoleucine instead of the expected valine in the E.coli TEM-1 β-lactamase. The MS results also proved that the two Cys residues (Cys75 and Cys121) were oxidized in a form of a disulfide bridge.

Analysing the CD spectrum of TEM-1 β-lactamase in solution we could show that he obtained secondary structure composition i.e., the percentage of α-helices, β-sheets, turns, and other conformations is close to that calculated from the published crystal structure. Thus, TEM-1 β-lactamase was folded in solution into its functional structure. We could demonstrate by CD spectroscopy, that the secondary structure of TEM-1 β-lactamase changed only slightly upon interaction with the selected Ni(II), Cd(II) and Hg(II) ions. Since the interaction with Ni(II) was

already proven by the success of the IMAC purification, this supports the binding of Ni(II) and also Cd(II) ion to the surface histidine pairs that are at suitable distance for chelation. The most significant (~20%) decrease of the α-helix content was observed upon increase of the Hg(II):protein concentration ratio up to 10:1. This suggested that Hg(II) is most probably bound close to the methionine thioether groups inside the protein structure.

We have identification the Ni(II) binding sites in TEM-1 β-lactamase. The slight but continuous change of the CD spectra upon increasing the metal ion content did not allow for determination of the number of the bound metal ions. It rather suggested that the enzyme could most likely bind more than one metal ion with not too high affinity. Therefore, mass spectrometric experiments were used to prove that all the studied Ni(II):enzyme molar ratio (2:1-10:1), the major peak was assigned to the monometallated TEM-1 β-lactamase. The relative intensity of the peaks corresponding to the two or three Ni(II)-chelating protein molecules, only slightly increased upon increasing the metal ion excess. This strongly suggested that the sidechain donor atoms of His151 and His156 being at ~3.5 Å distance, are ideal for metal ion binding. Furthermore, Asn152 and Asp155 amino acid residues in their close vicinity may strengthen this interaction.

Upon characterization of the interaction of Hg(II) ion with TEM-1 β-lactamase ESI MS and 199mHg-PAC spectroscopic methods were applied. The results proved that Hg(II) could bind to the TEM-1 β-lactamase weakly. However, no specific Hg(II) adduct could be detected, suggesting that Hg(II) can be bound to one or more similar binding sites. Inspecting the available crystal structures, indeed more similar potential binding sites, composed of methionine side chains complemented with further weakly coordinating amino acid sidechains were identified.

We have revisited the kinetics of the with TEM-1 β-lactamase promoted ampicillin hydrolysis. The hydrolytic process was described by the kinetic analysis of the set of catalytic progress curves recorded at multiple wavelengths, including various concentrations (and concentration ratios) of the enzyme and substrate. These experiments showed that the primary hydrolysis product of ampicillin is converted to second product, which needs also to be considered in the evaluation process. Thus, instead of the usual Michealis-Menten formalism, the full set of the stoichiometric and rate equations were used in the calculations. By this treatment we could determine the kinetic parameters, as well as the molar absorbances with high reliability. We have also identified the $\mathbf{P_1}$ and $\mathbf{P_2}$ hydrolysis products by mass spectrometry as ampicilloic and ampilloic acid, respectively.

We showed that the catalytic activity of TEM-1 β-lactamase was slightly reduced by the gradual increase of concentration of Hg(II). These catalytic progress curves could be fitted allowing the change of the active enzyme concentration, yielding the same kinetic parameter values as in the absence of Hg(II). The decreased active enzyme concentration obtained in this way suggests that the presence of Hg(II) does not affect the substrate binding, but influences the concentration of the catalytically effective enzyme possibly by blocking a fraction of the enzyme molecules. Based on these, we hypothesized that Hg(II) may interact with the sulfur donor atoms of Met residues close to the active center, thereby interfering with the catalytic process.

In contrast to Hg(II), we have found that Ni(II) and Cd(II) ions slightly promoted the enzyme activity. We suggest that the most probable scenario is the binding of the Lewis acid metal ions to the β-lactam ring of antibiotics with a concomitant activation of the substrate for the nucleophilic attack by the enzyme.

We proved that the behavior of bacteria in metal ion containing cultures is affected by numerous factors. We have found that the presence of ampicillin influences the toxic effect of the metal ions through complexation, leading to adducts with lower toxicities than that of the metal ions themselves. While 10 μM Cd(II) did not affect the bacterial growth, neither 10 μM Ni(II) nor 10 μM Hg(II) allowed the bacteria to proliferate. We observed a significant decrease of metal ion toxicity when ampicillin was also present in the above solutions. The differences in the neutralization effect of ampicillin was more pronounced for Hg(II) than for Ni(II), which was suggested to be attributed to different coordination modes of the two metal ions in their ampicillin complexes.

In the future, we plan further studies on TEM-1 β-lactamase involving mutation of the enzyme metal binding sites and thereby, the catalytic activity. This will contribute to better understanding of the effect of metal ion ions, as well as, to regulate its acitivty towards the antibiotics. In our hope, these results will lead to efficient design of future drugs and inhibitors

NColE7 is a bacterial nuclease toxin excreted as part of the defense system during stress or lack of nutrition. NColE7 is a metalloenzyme and cleaves double-stranded DNA non-specifically. The HNH motif, the active center of NColE7 was shown to coordinate Zn(II) ion as a native metal ion. **We studied the structural and catalytic aspects of the interaction of NColE7 mutants with non-endogenous Ni(II), Cu(II), and Cd(II) ions.** The most important achievements of this topic are listed below.

We have successfully purified KGNK-His protein by single step of immobilized metal ion affinity chromatography (IMAC) supplied with HPLC technique with optimized purification conditions. Mass spectrometry demonstrated that the purified KGNK-His was obtained in its apo form and high quality. The yield of the purified protein was ~3 mg/1 g of wet bacterial pellets.

We characterized the interaction of non-native metal ions with NColE7 mutants. We could prove that KGNK enzyme was able to bind single non-native metal ion, such as Ni(II), Cu(II) and Cd(II) ion in its active center. Addition of one equivalent of non-native metal ions caused slight but significant changes in the circular dichroism spectrum, reflected in a red shift of about 2 nm and accompanied by a small change in the intensity similarly to those of the effect of Zn(II). The main MS peak was assigned to the KGNK bound to a single metal ion. We have found that Cd(II) ion is a weaker interacting agent than Ni(II) or Cu(II).

We could demonstrate the interaction of KGNK enzyme with anions, such as phosphate ion or EDTA through changes in CD spectra resulting in a similar red shift to that caused by the metal ions. In contrast, even large excess of chloride ions could not affect the spectrum of KGNK. The above phenomena were attributed to the interaction between the negatively charged complex anions with the positively charged amino acid sidechains of the enzyme.

We have found that addition 1 eq of Zn(II), and Cu(II) ions to the apo-enzyme surprisingly, resulted in a less active enzyme compared to the apo-form. Addition of 1 eq of Cd(II) ions did not decrease the catalytic to the same extent due to the lower affinity towards the catalytic site than those of Zn(II) or Cu(II) ions. Addition of further equivalents of Zn(II), Cu(II), or Cd(II) ions caused further slight inhibition of the enzyme. This can be explained by ability of the excess of these metal ions (Zn(II), Cu(II), and Cd(II) ions) to prevent the His545-mediated OH^- generation via weak coordination to this His residue. We have demonstrated that the enzyme has extremely high activity in the presence of 1 eq of Ni(II) ion, while the excess of the Ni(II) ion could not significantly inhibit this highly active enzyme. We proved that addition Ni(II) ion cannot initiate DNA cleavage in the absence of the enzyme under the applied conditions.

Catalytic activity of NColE7 mutants was observed in the presence of EDTA as chelating agent. We have found that the catalytic activity of both the apo KGNK and the apo KGNK-His enzymes was only slightly inhibited by EDTA addition in equimolar amount – to be enough to remove any metal ion impurity from the enzyme. The enzymes were only inhibited, when ~ 10 eq of EDTA was supplied. Thus, we could demonstrate, that the mutant enzymes exhibited catalytic

activity in their apo-forms under the applied conditions. We suggest that the competition between the negatively charged EDTA and the substrate towards the positively charged amino acid side-chains of the enzyme is responsible for the inhibition at large excess of the chelator.

Competition between non-native metal ions and Zn(II) toward the active site of the NColE7 mutants revealed that none of the foreign metal ions could replace Zn(II) in the enzyme. Based on the MS results (KGNK) and the catalytic activity studies of KGNK, and KGNK-His, we proved that addition 1 eq of Zn(II) to the Ni(II), Cu(II) or Cd(II) bound KGNK resulted in MS peak related of the Zn(II)-bound enzyme, and the catalytic activity was also characteristic for the Zn(II)-bound enzymes. Thus, none of the applied metal ions could compete with Zn(II) ion. The above phenomena were independent of the order of addition of metal ions, reflecting that the thermodynamic relations govern the metal ion binding in the active center of these mutants.

Based on the above results, we suggested that new hydrolytic mechanism operates in the NColE7 mutants in the presence of Ni(II) as a non-native metal ion. We suggest that in apo-KGNK and KGNK-His, the free His residues participate in protonation and deprotonation processes, while in the Ni(II)-bound KGNK or KGNK-His, Ni(II) ion may promote the deprotonation of a coordinated water molecule, which can serve as an efficient attacking agent for DNA hydrolysis.

Future studies are planned, which may reveal a closer look on the individual reaction steps of KGNK promoted DNA hydrolysis. We will try to crystalize KGNK with various metal ions and DNA. Understanding of the catalytic mechanism in detail will allow us to apply KGNK as a regulated catalytic domain of artificial nucleases, based on *e.g.*, the DNA-binding domain of Nuclear factor I (NFI-BD) protein.

7. REFERENCES

[1] A. Judge, L. Hu, B. Sankaran, J. Van Riper, B.V.V. Prasad, T. Palzkill. *Commun. Biol*. 6 (**2023**); 35.
[2] T. Oka, K. Hashizume, H. Fujta. *J. Antibiotics* 33 (**1980**); 1357-1362.
[3] K. Bush, G.A. Jacoby, A.A. Medeiros. *Antimicrob. Agents Chemother*. 39 (**1995**); 1211-1233.
[4] C. Neu Harold. *Appl. Microbiol*. 17 (**1969**); 783-786.
[5] C.C. Sanders, W. E. Sanders. *Antimicrob. Agents Chemother*. 15 (**1979**); 792-797.
[6] T. Naas, S. Oueslati, R.A. Bonnin, M.L. Dabos, A. Zavala, L. Dortet, P. Retailleau, B.I. Iorga. *J. Enzym. Inhib. Med. Chem*. 32 (**2017**); 917-919.
[7] R.P. Ambler. *Phil. Trans. Roy. Soc. Lond. B*. 289 (**1980**); 321-331.
[8] P. Salahuddin, A. Kumar, A.U. Khan. *Curr. Prot. Pept. Sci*. 19 (**2018**); 130-144.
[9] K. Bush, G.A. Jacoby. *Antimicrob. Agents Chemother*. 54 (**2010**); 969-976.
[10] I. Massova, S. Mobashery. *Antimicrob. Agents Chemother*. 42 (**1998**); 1-17.
[11] A. Matagne, J. Lamotte-Brasseur, J.-M. Frere. *Biochem. J*. 330 (**1998**); 581-598.
[12] C.L. Tooke, P. Hinchliffe, E.C. Bragginton, C.K. Colenso, V.H.A. Hirvonen, Y. Takebayashi, J. Spencer. *J. Mol. Biol*. 431 (**2019**); 3472-3500.
[13] J.-M. Ghuysen, J.-M. Frere, M. Leyh-Bouille, H.R. Perkins, M. Nieto. *Phil. Trans*. 289 (**1980**); 285-301.
[14] F.K. Majiduddin, I.C. Materon, T.G. Palzkill. *Int. J. Med. Microbiol*. 292 (**2002**); 127 -137.
[15] M.S. Wilke, A.L. Lovering, N.C.J. Strynadka. *Curr. Opin. Microbiol*. 8 (**2005**); 525-533.
[16] C. Frohlich, J. A. Gama, K. Harms, V.H.A. Hirvonen, B.A Lund, M. W. v.-d. Kamp, P. J. Johnsen. et al., *mSphere*. 6 (**2021**); e00108-21.
[17] J.M. Frere, B. Joris, B. Granier, A. Matagne, F. Jacob, C. Bourguignon-Bellefroid. *Res. Microbiol*. 142 (**1991**); 705-710.
[18] K. Nagshetty, B.M. Shilpa, S.A. Patil, C.T. Shivannavar, N.G. Manjula. *Adv. Microbiol.* 1 (**2021**); 37-62.
[19] I.K. Oshiokhayamhe. *Mathews J. Immunol. Allergy* 7 (**2023**); MJIA10020.
[20] E.P. Abraham, E. Chain. *Nature* 146 (**1940**); 837.
[21] J. Ruiz. *Emerg. Infect. Dis*. 24 (**2018**); 709.
[22] N. Datta, P. Kontomichalou. *Nature* 208 (**1965**); 239-241.
[23] C. Cantu , W. Huang , T. Palzkill. *J. Biol. Chem*. 272 (**1997**); 29144-29150.
[24] A. Liakopoulos, D. Mevius, D. Ceccarelli. *Front. Microbiol*. 7 (**2016**); article 1374.
[25] R.P. Ambler, A.F. Coulson, J.M. Frere, J.M. Ghuysen, B. Joris, M. Forsman, et al., *Biochem. J*. 276 (**1991**); 269-270.
[26] R. Cooksey, J. Swenson, N. Clark, E. Gay, C. Thornsberry. *Antimicrob. Agents Chemother*. 34 (**1990**); 739-745.
[27] M.L.M. Salverda, J. A. G. M. de Visser, M. Barlow. *FEMS Microbiol Rev*. 34 (2010); 1015-1036.
[28] H. Jacquier, A. Birgy, H. Le Nagarda, Y. Mechulam, E. Schmitt, J. Glodt, et al. *PNAS USA*. 110 (**2013**); 13067-13072.
[29] I. Kather, R. P. Jakob, H. Dobbek, F. X. Schmid. *J. Mol. Biol*. 383 (**2008**); 238-251.
[30] A. J. Cumming, D. Khananisho, R. Harris, C.N. Bayer, M.H.H. Nørholm, S. Jamshidi, et al. *ACS Synth. Biol*. 11 (**2022**) 241-253.
[31] A. Birgy, M. Magnan, C.A. Hobson, M. Figliuzzi, K. Panigoni, C. Codde, et al. *Antibiotics* 11 (**2022**); 652.
[32] T. Palzkill. *Front. Mol. Biosci*. 5 (**2018**); 16.
[33] S. Madzgalla, H. Duering, J.C. Hey, S. Neubauer, K.H. Feller, R. Ehricht, et al., *Microorganisms* 9 (**2021**); 1726.
[34] S. Bratulic, F. Gerber, A. Wagner. *PNAS*. 112 (**2015**); 12758-12763.
[35] T.C. Wuerz, S.S. Kassim, K.E. Atkins. *Trav. Med. Infect. Dis*. 37 (**2020**); 101823.
[36] M.I. Zimmerman, K.M. Hart, C.A. Sibbald, T.E. Frederick, J.R. Jimah, C.R. Knoverek, et al., *ACS Cent. Sci*.3 (**2017**); 1311-1321.
[37] E. Dellus-Gur, M. Elias, E. Caselli, F. Prati, M. L. M. Salverda, J. Arjan, et al., *J. Mol. Biol*. 427 (**2015**); 2396-409.
[38] N. Pradel, J. Delmas, L.F. Wu, C.L. Santini, R. Bonnet. *Antimicrob. Agents Chemother*. 53 (**2009**) 242-248.
[39] M. Pohlschröder, E. Hartmann, N.J. Hand, K. Dilks, A. Haddad. *Annu. Rev. Microbiol*. 59 (**2005**); 91-111.
[40] A. Micsonai, F. Wien, L. Kernya, Y. Lee, Y. Goto, M. Refregiers, J. Kardos. *PNAS USA* 112 (**2015**); E3095-E3103.

[41] A. Micsonai, F. Wien, E. Bulyaki, J. Kun, E. Moussong, Y.H. Lee, Y. Goto, M. Refregiers, J. Kardos. *Nucleic Acids Res*. 46 (**2018**); W315-W322.
[42] A. Micsonai, E. Bulyáki, J. Kardos. BeStSel: From Secondary Structure Analysis to Protein Fold Prediction by Circular Dichroism Spectroscopy. Structural Genomics. *Springer*. (**2021**); 175-189.
[43] A. Micsonai, E. Moussong, N. Murvai, A. Tantos, O. Toke, M. Refregiers, F. Wien, J. Kardos. *Front. Mol. Biosci*. 9 (**2022**); Article 863141.
[44] J. Melling, G.K. Scott. *Biochem. J*. 130 (**1972**); 55-62.
[45] J. Fisher, J. G. Belasco, S. Ghosla, J. R. Knowles. *Biochemistry* 19 (**1980**); 2895-2901.
[46] K.V. Venkatachalam, W. Huang, M. LaRocco, T. Palzkill. *J. Biol. Chem*. 269 (**1994**); 23444-23450.
[47] L.A. Eriquez, R.F. Damato. *Antimicrob. Agents Chemother*. 15 (**1979**); 229-234.
[48] S.J. Cartwright, S.G. Waley, *Biochem. J*. 221 (**1984**); 505-512.
[49] E. Bibi. *Biochem. J*. 263 (**1989**); 309-311.
[50] R. Lawung, V. Prachayasittikul, L. Bulow. *Protein Expr. Purif*. 23 (**2001**); 151-158.
[51] J. Yang, N. Naik, J.S. Patel, C.S. Wylie, W. Gu, J. Huang, F.M. Ytreberg, M.T. Naik, D.M. Weinreich, B.M. Rubenstein. *PLoS One*. 15 (**2020**); e0233509.
[52] A. Stratton, M. Ericksen, T. V. Harris, N. Symmonds, T. P. Silverstein. *Protein Sci*. 26 (**2017**); 292-305.
[53] B. Birgersson, T. Drakenberg, G. A. Neville. *Acta Chem. Scand*. 27 (**1973**); 3953-3960.
[54] G. R. Lenz, A.E. Martell. *Biochemistry*. 3 (**1964**); 745-750.
[55] I. Sovago, G. Petocz. *J. Chem. Soc. Dalton Trans*. 7 (**1987**); 1717-1720.
[56] M.P. Latha, V.M. Rao, T.S. Rao, G.N. Rao. *Bull. Chem. Soc. Ethiop*. 21 (**2007**); 363-372.
[57] A.J. Carty, N.J. Taylor. *J. Chem. Soc. Chem. Commun*. 6 (**1976**); 214-216.
[58] D.F. Pyreu, A.M. Ryzhakov, E.V. Kozlovskii, M.S. Gruzdev, R.S. Kumeev. *Inorg. Chim. Acta* 371 (**2011**); 53-58.
[59] C.C.G. Scully, P. Jensen, P.J. Rutledge. *J. Organomet. Chem*. 693 (**2008**); 2869-2876.
[60] M.-H. Yang, C.R. Lohani, H.Ch, K.-H. Lee. *Org. Biomol. Chem*. 9 (**2011**); 2350-2356.
[61] J.T. Rubino, P. Riggs-Gelasco, K.J. Franz. *J. Biol. Inorg. Chem*. 15 (**2010**); 1033-1049.
[62] A.S. Jullien, C. Gateau, C. Lebrun, P. Delangle. *Inorg. Chem*. 54 (**2015**); 2339-2344.
[63] A. Fragoso, P. Lamosa, R. Delgado, O. Iranzo, *Chem. Eur J*. 19 (**2013**); 2076-2088.
[64] A. Miller, D. Dudek, S. Potocki, H. Czapor-Irzabek, H. Kozlowski, M. Rowinska-Zyrek, *Metallomics*. 10 (**2018**) 1631-1637.
[65] S. Potocki, P. Delgado, D. Dudek, A. Janicka-Klos, H. Kozlowski, M. Rowinska-Zyrek, *Inorg. Chim. Acta*. 488 (**2019**); 255-259.
[66] M. Remelli, D. Brasili, R. Guerrini, F. Pontecchiani, S. Potocki, M. Rowinska-Zyrek, J. Watly, H. Kozlowski. *Inorg. Chim. Acta*. 472 (**2018**); 149-156.
[67] J.J. Perona, C.S. Craik. *Protein Sci.* 4 (**1995**); 337-360.
[68] H. Christensen, M.T. Martin, S.G. Waley. *Biochem. J.* 266 (**1990**); 853-861.
[69] N.C. Strynadka, H. Adachi, S.E. Jensen, K. Johns, A. Sielecki, C. Betzel, et al., *Nature* 359 (**1992**); 700-705.
[70] C.C. Chen, T.J. Smith, G. Kapadia, S. Wasch, L.E. Zawadzke, A. Coulson, O. Herzberg. *Biochemistry*. 35 (**1996**); 12251-12658.
[71] C. Damblon, X. Raquet, L.Y. Lian, J. Lamotte-Brasseur, E. Fonze, P. Charlier, et al., *PNAS USA* 93 (**1996**) 1747-1752.
[72] H. Adachi, T. Ohta, H. Matsuzawa. *J. Biol. Chem*. 266 (**1991**); 3186-3191.
[73] W.A. Escobar, A.K. Tan, A.L. Fink. *Biochemistry* 30 (**1991**); 10783-10787
[74] G. Minasov, X. Wang, B.K. Shoichet. *J. Am. Chem. Soc*. 124 (**2002**); 5333-5340.
[75] A.T. Bouthors, N. Dagoneau-Blanchard, T. Naas, P. Nordmann, V. Jarlier, W. Sougakoff. *Biochem. J*. 330 (**1998**); 1443-1449.
[76] J.J. Murtaugh, G.B. Levy. *J. Am. Chem. Soc*. 67(**1945**); 1042.
[77] J.P. Hou, J.W. Poole. *J. Pharm. Sci*. 61 (**1972**); 1594-1598.
[78] A.K. Saz, D.L. Lowery, L.J. Jackson. *J. Bacteriol*. 82 (**1961**); 298-304.
[79] C.J. Perret. *Nature* 174 (**1954**); 1012-1013.
[80] R.P. Novick. *Biochem. J*. 83 (**1962**); 236-240.
[81] N. Citri. *Meth. Med. Res*. 10 (**1964**); 221-232.

[82] N. Citri, N. Garber. *J. Pharm. Pharmacol*. 14 (**1962**) 784-793.
[83] J.F. Alicinio. *Anal. Chem*. 33 (**1961**); 648-649.
[84] G.W. Ross, K.V. Charter, A.M. Harris, S.M. Kirby, M.J. Marshall, C.H. O'Callaghan. *Anal. Biochem*. 54 (**1973**); pages.
[85] S.G. Waley. *Biochem. J*. 139 (**1974**); 789-790.
[86] A. Samuni. *Anal. Biochem*. 63 (**1975**); 17-26.
[87] S. Minami, A. Yotsuji, M. Inoue, S. Mitsuhashi. *Antimicrob. Agents Chemother*. 18 (**1980**); 382-385.
[88] W. Huang, T. Palzkill. *PNAS USA* 94 (**1997**); 8801-8806.
[89] C.H. O'Callaghan, A. Morris, S.M. Kirby, A.H. Shingler. *Antimicrob. Agents Chemother*. 1 (**1972**); 283-288.
[90] A.R. Fersht. Structure and mechanism in protein science: A guide to enzyme catalysis and protein folding. *W.H. Freeman and Company*. (**1999**).
[91] B. Nolting, Protein folding kinetics: Biophysical methods. *Springer*. (**1999**).
[92] S. Schnell, M.J. Chappell, N.D. Evans, M.R. Roussel. *C.R. Biologies* 329 (**2006**); 51-61.
[93] W. Huang, J. Petrosino, M. Hirsch, P.S. Shenkin, T. Palzkill. *J. Mol. Biol*. 258 (**1996**); 688-703.
[94] W.J. Song, F. A. Tezcan. *Science* 346 (**2014**); 1525-1528.
[95] G. Bahr, L.J. Gonzalez, A.J. Vila. *Chem. Rev*. 212 (**2021**); 7957-8094.
[96] N.G. Brown, S. Shanker, B.V.V. Prasad, T. Palzkill. *J. Biol. Chem*. 284 (**2009**); 33703-33712.
[97] V. Stojanoski, D.-C. Chow, L. Hu, B. Sankaran, H.F. Gilbert, B.V.V. Prasad, T. Palzkill, *J. Biol. Chem*. 290 (**2015**); 10382-10394.
[98] V. Sideraki, W. Huang, T. Palzkill, H.F. Gilbert. *PNAS USA* 98 (**2001**); 283-288.
[99] M.A. Stiffler, D.R. Hekstra, R. Ranganathan. *Cell*. 160 (**2015**); 882-892.
[100] D.C. Marciano, N.G. Brown, T. Palzkill. *Protein Sci*. 18 (**2009**); 2080-2089.
[101] M. Galleni, J.-M. Frere. Kinetics of β-lactamases and penicillinbinding proteins. In: Bonomo RA, Tolmasky M, editors. Enzyme-mediated resistance to antibiotics: mechanisms, dissemination, and prospects for inhibition. *ASM Press*. (**2007**).
[102] M.G.P Page. *Clin. Microbiol. Infect*. 14 (**2008**); 63-74.
[103] Punekar NS. ES complex and pre-steady-state kinetics in enzymes: catalysis, kinetics and mechanisms. *Springer*. (**2018**).
[104] I.M. Furey, S.C. Mehta, B. Sankaran, L. Hu, B.V.V. Prasad, T. Palzkill. *J. Biol. Chem*. 296 (**2021**); 100799.
[105] S.C. Mehta, I.M. Furey, O.A. Pemberton, D.M. Boragine, Y. Chen, T. Palzkill. *J. Biol. Chem*. 296 (**2021**); 100155.
[106] J.A. Cowan. *Biometals*. 15 (**2002**); 225-235.
[107] T.J. Lyons, D.J. Eide. Transport and storage of metal ions in biology In Biological Inorganic Chemistry: Structure and Reactivity eds. (Bertini I., Gray H.B., Stiefel E.I.,Valentine J.S.). *University Science Books*. (**2006**); 57-77.
[108] S.J. Lange, L. Que Jr. *Curr. Opin. Chem. Biol*. 2 (**1998**); 159-172.
[109] M. Hernick, C.A. Fierke. *Arch. Biochem. Biophys*. 433 (**2005**); 71-84.
[110] D.H. Kim, S. Mobashery. *Curr. Med. Chem*. 8 (**2001**); 959-965.
[111] E. Jabri, M.B. Carr, R.P. Hausinger, P.A. Karplus. *Science* 268 (**1995**); 998-1004.
[112] M.M. Harding. *Acta Crystallogr. D Biol. Crystallogr*. 55 (**1999**); 1432-1443.
[113] E. Pidcock, G.R. Moore. *J. Biol. Inorg. Chem*. 6 (**2001**); 479-489.
[114] A. Romani, A. Scarpa. *Arch. Biochem. Biophys*. 298 (**1992**); 1-12.
[115] M.C. Dupureur. *Metallomics* 2 (**2010**); 609-620.
[116] W.Q. Yang. *Rev. Biophys*. 44 (**2011**); 1-93.
[117] R. James, C. Kleanthous, G.R. Moore. *Microbiology* 142 (**1996**); 1569-1580.
[118] C. Kleanthous, D. Walker. *TRENDS Biochem. Sci*. 26 (**2001**); 624-631.
[119] P. Elkins, A. Bunker, W.A. Cramer, C.V. Stauffacher. *Structure* 5 (**1997**); 443-458.
[120] K. Schaller, M. Nomura. *PNAS USA*73 (**1976**); 3989-3993.
[121] C. Kleanthous, U.C. Kuhlmann, A.J. Pommer, N. Ferguson, S.E. Radford, G.R. Moore, R. James, A.M. Hemmings. *Nat. Struct, Biol.* 6 (**1999**); 243-252.
[122] T. Boon. *PNAS USA* 68 (**1971**); 2421-2425.
[123] B.W. Senior, I.B. Holland. *PNAS USA* 68 (**1971**); 959-963.
[124] T. Ogawa, K. Tomita, T. Ueda, K. Watanabe, T. Uozumi, H. Masaki. *Science* 283 (**1999**); 2097-2100.

[125] M. Sui, L. Tsai, K. Hsia, L.G. Doudeva, W. Ku, G. Han, H. Yuan. *Protein Sci*. 11 (**2002**); 2947-2957.
[126] Y.S. Cheng, K.C. Hsia, L.G. Doudeva, K.F. Chak, H.S. Yuan. *J. Mol. Biol*. 324 (**2002**); 227-236.
[127] L. Doudeva, D. Huang, K. Hsia, Z. Shi, C. Li, Y. Shen, Y. Cheng, H. Yuan. *Protein Sci*. 15 (**2006**); 269-280.
[128] A.J. Pommer, U.C. Kuhlmann, A. Cooper, A.M. Hemmings, G.R. Moore, R. James, C. Kleanthous. *J. Biol. Chem*. 274 (**1999**); 27153-27160.
[129] U.C. Kuhlmann, G.R. Moore, R. James, C. Kleanthous, A.M. Hemmings. *FEBS Lett*. 463 (**1999**); 1-2.
[130] K.C. Hsia, K.F. Chak, P.H. Liang, Y.S. Cheng, W.Y. Ku, H.S. Yuan. *Structure* 12 (**2004**); 205-214.
[131] E. Nemeth, T. Kortvelyesi, P. W. Thulstrup, H. E. M. Christensen, M. Kozisek, K. Nagata, A. Czene, B. Gyurcsik. *Protein Sci*. 23 (**2014**); 1113-1122.
[132] W. Ku, Y. Liu, Y. Hsu, C. Liao, P. Liang, H. Yuan, K. Chak. *Nucl. Acids Res*. 30 (**2002**); 1670-1678.
[133] T. Ko, C. Liao, W. Ku, K. Chak, H.S. Yuan. *Structure* 7 (**1999**); 91-102.
[134] H. Huang, H.S. Yuan. *J. Mol. Biol*. 368 (**2007**); 812-821.
[135] K.B. Levin, O. Dym, S. Albeck, S. Magdassi, A.H. Keeble, C. Kleanthous , D.S. Tawfik. *Nat. Struct. Mol. Biol*. 16 (**2009**); 1049-1055.
[136] T. Kortemme, L.A. Joachimiak, A.N. Bullock, A.D. Schuler, B.L. Stoddard, D. Baker. *Nat. Struct. Mol. Biol*. 16 (**2009**); 1049-1055.
[137] L.G. Doudeva, H. Huang, K.-C. Hsia, Z. Shi, C.-L. Li, Y. Shen, Y.-S. Cheng, H.S. Yuan. *Protein Sci*. 15 (**2006**); 213-389.
[138] Y. Wang, J.D. Wright, L.G. Doudeva, C. Lim, H.S. Yuan. *J. Am. Chem. Soc*. 131 (**2009**); 17345-17353.
[139] Y. Wang, W. Yang, C. Li, L.G. Doudeva, H.S. Yuan. *Nucl. Acids Res*. 35 (**2007**); 584-594.
[140] A. Czene, E. Nemeth, I.G. Zoka, N.I. Jakab-Simon. T. Kortvelyesi, K. Nagata, H.E.M. Christensen, B. Gyurcsik. *J. Biol. Inorg. Chem*. 18 (**2013**); 309-321.
[141] Z. Shi, K.F. Chak, H.S. Yuan. *J. Biol. Chem*. 280 **(2005**); 24663-24668.
[142] E. Nemeth, M. Kozisek, G.K. Schilli, B. Gyurcsik. *J. Inorg. Biochem*. 151 (**2015**) 143-149.
[143] E. Németh, R.K. Balogh, K. Borsos, A. Czene, P.W. Thulstrup, B. Gyurcsik. *Protein Sci*. 25 (**2016**); 1977-1988.
[144] E. Nemeth, T. Kortvelyesi, M. Kozisek, P.W. Thulstrup, H.E.M. Christensen, M.N. Asaka, K. Nagata, B. Gyurcsik. *J. Biol. Inorg. Chem*. 19 (**2014**); 1295-1303.
[145] A.J. Pommer, S. Cal, A.H. Keeble, D. Walker, S.J. Evans, U.S. Kuhlmann, A. Cooper, B.A. Connolly, A.M. Hemmings, G.R. Moore, R. James, C. Kleanthous. *J. Mol. Biol*. 314 (**2001**); 735-749.
[146] D.C. Walker, T. Georgiou, A.J. Pommer, D. Walker, G.R. Moore, C. Kleanthous, R. James. *Nucl. Acids Res*. 30 (**2002**); 3225-3234
[147] J.A. Gerlt, J.A. Coderre, S. Mehdi. *Adv. Enzymol. Relat. Areas Mol. Biol*. 55 (**1983**); 291-380.
[148] J.H. Eastberg, J. Eklund, *Biochemistry*. 46 (**2007**); 7215-7225.
[149] J.A. Bueren-Calabuig, C. Coderch, E. Rico, A. Jimenez-Ruiz, F. Gago. *ChemBioChem* 12 (**2011**); 2615-2622
[150] C. Garinot-Schneider, A.J. Pommer, G.R. Moore, C. Kleanthous, R. James. *J. Mol. Biol*. 260 (**1996**); 731-742.
[151] E. Németh. PhD dissertation, University of Szeged. (**2014**).
[152] J.P. Hannan, S.B.-M. Whittaker, A.M. Hemmings, R. James, C. Kleanthous, G.R. Moore. *J. Inorg. Biochem*. 79 (**2000**); 365-370.
[153] S.G.N. Grant, J. Jessee, F.R. Bloom, D. Hanahan. *PNAS USA* 87 (**1990**); 4645-4649.
[154] F.W. Studier, A.H. Rosenberg, J.J. Dunn, J.W. Dubendorff. *Methods Enzymol*. 185 (**1990**); 60-89.
[155] K. Bose Textbook on Cloning, Expression and Purification of Recombinant Proteins. *Springer*. (**2022**).
[156] M.A.A. Valones, R.L. Guimaraes, L.A.C. Brandao, P.R.E. de Souza, A. de A.T. Carvalho, S. Crovela. Bras. *J. Microbiol*. 40 (**2009**); 1-11.
[157] P.A. Walker, L.E.-C. Leong, P.W.P. Ng, S.H. Tan, S. Waller, D. Murphy, A.G. Porter. *Bio-Technol*. 12 (**1994**); 601-605.
[158] J. Richey. *Am. Lab*. 14 (**1982**); 104-129.
[159] A. Madadlou,S. O'Sullivan, D. Sheehan. *Methods Mol. Biol*. 681 (**2011**); 439-447.
[160] J.T. Watson, O. D. Sparkman, Introduction to mass spectrometry. 4th addition. *Wiley*. (**2007**)
[161] M. Karas, U. Bahr, T. Dulcks. *Fresenius J. Anal. Chem*. 366 (**2000**); 669-676.
[162] A. Detournay, S. Sauvage, N. Locoge, V. Gaudion, T. Leonardis, et al. *J. Environ. Monit*. 13 (**2011**); 983-990.
[163] R.F. do Nascimento. Advances in chromatographic analysis. *Avidscience*. (**2017**)
[164] I.K. Kaltashov, C.E. Bobst, M. Zhang, R. Leverence, D.R. Gumerov. *Biochim. Biophys. Acta* 1820 (**2012**); 417-426.

[165] E.T. van den Bremer, W. Jiskoot, R. James, G.R. Moore, C. Kleanthous, A.J. Heck, C.S. Maier. *Protein Sci*. 11 (**2002**); 1738-1752.
[166] S.M. Kelly, T.J. Jess, N.C. Price. *Biochim. Biophys. Acta*. 1751 (**2005**); 119-139.
[167] L. Whitmore, B.A.Wallace. *Biopolymers* 89 (**2008**); 392-400.
[168] A.J. Miles, B.A. Wallace. *Chem. Soc. Rev*. 35 (**2006**); 39-51.
[169] A.J. Miles, S.V. Hoffmann, Y. Tao, R.W. Janes, B.A. Wallace. *J. Spectroscopy*. 21 (2007); 245-255.
[170] E. Gasteiger, C. Hoogland, A. Gattiker, S. Duvaud, M. R. Wilkins, R. D. Appel, A. Bairoch. Protein identification and analysis tools on the Expasy server. In The Proteomics Protocols Handbook; J. M. Walker, ed. *Humana Press*. (**2005**); 571-607.
[171] W.S. Rasband, ImageJ 1.46r, U. S. National Institutes of Health. (**1997-2018**) version 1.46r.
[172] C.A. Schneider, W.S. Rasband, K.W. Eliceiri. *Nat. Methods* 9 (**2012**); 671-675.
[173] M.D. Abramoff, P.J. Magalhaes, S.J. Ram. *Biophot. Int*. 11 (**2004**); 36-42.
[174] L. Hemmingsen, M. Stachura, P.W. Thulstrup, N.J. Christensen, K. Johnston. *Hyperfine Interact*. 1997 (**2010**); 255-267.
[175] L. Hemmingsen, K.N. Sas, E. Danielsen. *Chem. Rev*. 104 (**2004**); 4027-4061.
[176] R. Catherall, W. Andreazza, M. Breitenfeldt, A. Dorsival, G.J. Focker, T.P. Gharsa, et al. *J. Phys. G*. 44 (**2017**) pages .
[177] G. Peintler. ZiTa /ChemMech(**2013–2022**): a comprehensive program package for fitting parameters of chemical reaction mechanisms. Department of Physical Chemistry, University of Szeged. Versions 2.1-5.99. (**1989-2022**).
[178] J.H. Miller. Experiments in molecular genetics. *Cold Spring Harbor Laboratory*. (**1972**).
[179] H. Besir. *Methods Mol. Biol*. 1586 (**2017**); 141-154.
[180] K. Nagata, R.A. Guggenheimer, J. Hurwitz. *PNAS USA* 80 (**1983**); 4266-4270.
[181] J. Dekker, J.A.W.M. Van Oosterhout, P.C. Van Der Vliet. *Mol. Cell Biol*. 16 (**1996**); 4073-4080.
[182] A. Bansal, D. Kar1, R.A. Murugan, S. Mallick, M. Dutta, S.D. Pandey, C. Chowdhury, A.S. Ghosh. *Microbiology* 161 (**2015**); 1081-1091.
[183] W.T. Booth, C.R. Schlachter, S. Pote, N. Ussin, N.J. Mank, V. Klapper, L.R. Offermann, C.T. Orcid, B.K. Hurlburt, M. Chruszcz. *ACS Omega* 3 (**2018**); 760-768.
[184] D. Jain, J.Verma, A.S. Ghosh. *Microbiology* 168 (**2022**); 001203.
[185] A. Sosa-Peinado, D. Mustafi, M.W. Makinen. *Protein Expr. Purif*. 19 (**2000**); 235-245.
[186] B. Stec, K.M. Holtz, C.L. Wojciechowski, E.R. Kantrowitz. *Acta Crystallogr*. D61 (**2005**); 1072-1079.
[187] M. Sun, Y. Wang, Q. Zhang, Y. Xia, W. Ge, D. Guo. *BMC Genomics* 18 (**2017**); 279.
[188] A. de Marco, N. Berrow, M. Lebendiker, M. Garcia-Alai, S.H. Knauer, B. Lopez- Mendez, A. Matagne, A. Parret, K. Remans, S. Uebel, B. Raynal. *Nat. Commun*. 12 (**2021**) 2795.
[189] N. Sreerama, R.W. Woody. *Anal. Biochem*. 287 (**2000**); 252-260.
[190] J.G. Lees, A.J. Miles, F. Wien, B.A. Wallace. *Bioinformatics* 22 (**2006**); 1955-1962.
[191] R.K. Balogh, E. Nemeth, N.C. Jones, S.V. Hoffmann, A. Jancso, B. Gyurcsik. *Eur. Biophys. J*. 50 (**2021**); 491-500.
[192] N. Citri, A. Samuni, N. Zyk. *PNAS USA* 73 (**1976**); 1048-1052.
[193] B.A. Lund, T. Christopeit, Y. Guttormsen, A. Bayer, H.K. Leiros. *J. Med. Chem*. 59 (**2016**); 5542-5554.
[194] G. Peintler, I. Nagypal, A. Jancso, I.R. Epstein, K. Kustin. *J. Phys. Chem*. A101 (**1997**); 8013-8020.
[195] S.M. Mitchell, J.L. Ullman, A.L. Teel, R.J. Watts. *Sci. Total Environ*. 466-467 (**2014**); 547-555.
[196] N.V. Sy, K. Harada, M. Asayama, M. Warisaya, L.H. Dung, Y. Sumimura, et al., *Chemosphere* 172 (**2017**); 355-362.
[197] S.M. Raza, Z.A. Alothman, W.S. Mohammad. *J. Chromatogr. Sci*. 52 (**2014**); 1273-1280.
[198] V.A. Robinson-Fuentes, T.M. Jefferies, S.K. Branch. *J. Pharm. Pharmacol*. 49 (**1997**); 843-851.
[199] E. Nagele, R. Moritz. *J. Am. Soc. Mass Spectrom*. 16 (**2005**); 1670-1676.
[200] M. Wilamowski, D.A. Sherrell, Y. Kim, A. Lavens, R.W. Henning, K. Lazarski, et al., *Nat Commun*. 13 (**2022**); 73-79.
[201] P.R. Brown, J.O. Edwards. *Biochemistry* 8 (**1969**); 1200-1222.
[202] P. Perez-Garcia, S. Kobus, C.G.W. Gertzen, A. Hoeppner, N. Holzscheck, C.H. Strunk, et al., *Commun. Biol*. 4 (**2021**);132.
[203] J. Huang, X. Liu, Y. Sun, Z. Li, M.H. Lin, K. Hamilton, et al., *J. Biol. Chem*. 299 (**2023**); 103047.
[204] A.D. Deshpande, K.G. Baheti, N.R. Chatterjee. *Curr. Sci*. 87 (**2004**); 1684-1695.

[205] E. Firnberg, J.W. Labonte, J.J. Gray, M. Ostermeier. *Mol. Biol. Evol*. 31 (**2014**); 1581-1592.
[206] M. Delaire, R. Labia, J.P. Samama, J.M. Masson. *J. Biol. Chem*. 267 (**1992**); 20600-20606.
[207] J.C. Aledo. *Protein Sci*. 28 (**2019**); 1785-1796.
[208] N.E.A. El-Gamel. *J. Coord. Chem*. 63 (**2010**); 534-543.
[209] I. Rasic-Misic, G. Miletic, S. Mitic, M. Mitic, E. Pecev-Marinkovic. *Chem. Pharm. Bull*. 61 (**2013**); 913-919.
[210] Y. Lin, S. Cen. *RSC Adv*. 12 (**2022**); 9786-9792.
[211] N.G. Gensmantel, P. Proctor, M.I. Page. *J. Chem. Soc. Perkin. Trans*. 2 (**1980**); 1725-1732.
[212] N.O. Concha, B.A. Rasmussen, K. Bush, O. Herzberg. *Protein Sci*. 6 (**1997**); 1-6.
[213] C. Kallay, K. Varnagy, G. Malandrinos, N. Hadjiliadis, D. Sanna, I. Sovago, *Inorg. Chim. Acta* 362 (**2009**); 935-945.
[214] I.N. Jakab, O. Lorincz, A. Jancso, T. Gajda, B. Gyurcsik. *Dalton Trans*. (**2008**); 6987-6995.
[215] N.I. Jakab, A. Jancso, T. Gajda, B. Gyurcsik, A. Rockenbauer, *J. Inorg. Biochem*. 102 (**2008**); 1438-1448.
[216] I. Turi, D. Sanna, E. Garribba, G. Pappalardo, I. Sovago. *Polyhedron* 62 (**2013**); 7-17.
[217] J. Watly, A. Hecel, M. Rowinska-Zyrek, H. Kozlowski, *Inorg. Chim. Acta* 472 (**2018**); 119-126.
[218] I. Turi, C. Kallay, D. Szikszai, G. Pappalardo, G. Di Natale, P. De Bona, E. Rizzarelli, I. Sovago. *J. Inorg. Biochem*. 104 (**2010**); 885-891.
[219] A. Jancso, K. Selmeczi, P. Gizzi, N.V. Nagy, T. Gajda, B. Henry. *J. Inorg. Biochem*. 105 (**2011**); 92-101.
[220] A. Grenacs, D. Sanna, I. Sovago. *J. Inorg. Biochem*. 151 (**2015**); 87-93.
[221] V. Joszai, Z. Nagy, K. Osz, D. Sanna, G. Di Natale, D. La Mendola, G. Pappalardo, E. Rizzarelli, I. Sovago. *J. Inorg. Biochem*. 100 (**2006**); 1399-1409.
[222] O Iranzo, P.W. Thulstrup, S. Ryu, L. Hemmingsen, V.L. Pecoraro. *Chem. Eur. J*. 13 (**2007**); 9178-9190.
[223] J.S. Mohler, T. Kolmar, K. Synnatschke, M. Hergert, L.A. Wilson, S. Ramu, et al., *J. Inorg. Biochem*. 167 (**2017**); 134-141.
[224] J.A. Garza-Cervantes, J.F. Meza-Bustillos, H. Resendiz-Hernandez, I.A. Suarez-Cantu, O.A. Ortega-Rivera, E. Salinas, et al., *Front. Bioeng. Biotechnol*. 8 (**2020**); 612.
[225] D. Chudobova, S. Dostalova, I. Blazkova, P. Michalek, B. Ruttkay- Nedecky, M. Sklenar, et al., *Int. J. Environ. Res. Public Health* 11 (**2014**); 3233-3255.
[226] A.D. Wales, R.H. Davies. *Antibiotics* 4 (**2015**); 567-604.
[227] C. Wu, C. Lin, X. Zhu, H. Liu, W. Zhou, J. Lu, et al., *Int. J. Genomics*. 2018 (**2018**); 4989602-498612.
[228] P. Vats, U.J. Kaur, P.J. Rishi. Appl. Microbiol. 132 (**2022**); 4058-4076.
[229] A. Pavlic, I. Gobin, G. Begic, M. Tota, M. Abram, S. Spalj. *Folia Microbiol*. 67 (**2022**); 649-657.
[230] A. M. Garcia, P. G. Navarro, P. J. Martinez de las Parras. *Talanta* 46 (**1998**); 101-109.
[231] S.J. Beard, D.T. Ciccognani, M.N. Hughes, R.K. Poole. *FEMS Microbiol. Lett*. 96 (**1992**); 207-712.
[232] GV. Fazakerley, G.E. Jackson, P.W. Linder. *J. Inorg. Nucl. Chem*. 38 (**1976**); 1397-1400.
[233] A.S. Orabi. *J. Sol. Chem*. 34 (**2005**); 95-111.
[234] M.J. ZaZaworotko, H.H. Hammud, I. Abbas, V.C. Kravtsov, M.S. Masoud. *J. Coord. Chem*. 59 (**2006**); 65-84.
[235] A. Gupta. *Int. Res. J. Pure Appl. Chem*. 3 (**2013**); 441-448
[236] H.A.H. Abd Elhameed, B. Hajdu, A. Jancso, A. Keri, G. Galbacs, E. Hunyadi-Gulyas, B. Gyurcsik. *J. Inorg. Biochem*. 206 (**2020**); 111013.
[237] F.H. Arnold. *Biotechnology* 9 (**1991**); 151-156.
[238] X. Zhou, W. Zheng, Y. Li, R. Pearce, C. Zhang, E.W. Bell, G. Zhang, Y. Zhang. *Nat. Protocols* 17(**2022**); 2326-2353.
[239] W. Zheng, C. Zhang, Y. Li, R. Pearce, E.W .Bell, Y. Zhang. *Cell Reports Methods* 1 (**2021**); 100014
[240] J. Yang, Y. Zhang. *Nucl. Acids Res*. 43 (**2015**); W174-W181
[241] A. Kręzel, W. Maret. *Arch. Biochem. Biophys*. 611 (**2016**); 3-19.
[242] D.R. Eaton, K. Zaw. *J. Am. Chem. Soc*. 94 (**1972**); 4394-4395.
[243] E. Garribba, G. Micera. *J. Chem. Educ*. 83 (**2006**); 1229-1232.
[244] J. Pons, J. Garcia-Anton, R. Jimenez, X. Solans, M. Font-Bardia, Josep Ros. *Inorg. Chem. Commun.* 10 (**2007**); 1554-1556.
[245] T.J. Ewald van den Bremer, A.H. Keeble, W. Jiskoot, R.E.J. Spelbrink, C.S. Maier, A.V. Hoek, et al., *Protein Sci*. 13 (**2004**); 1173-1434.

ACKNOWLEDGEMENTS

I am sincerely grateful, and I would like to say special thanks to my supervisor, Associate Prof. Dr. Béla Gyurcsik, for his consistently excellent supervision, his interesting scientific discussions, letting me be a member of his unique research group, the opportunities to work with collaborators in Hungary and abroad (Denmark, Germany, and Japan), as well as his effective help in applications and publishing papers.

I am grateful to Prof. Dr. Tamás Gajda, the leader, as well as to all the members of the Bioinorganic Research Group at the University of Szeged and Dr. Éva Enyedy, the head as well as all the members of the Molecular and Analytical Chemistry Department at University of Szeged, for their help and for the nice working atmosphere. Special thank goes to Dr. Jancsó Attila, Dr. Bálint Hajdu and PhD student Annamária Tóth, as well as to chemistry MSc students Viktória Egyed and Benjamin Fógel for their useful work on the TEM-1 β-lactamase and NColE7 mutants.

I would like to thank my family for their support and encouragement throughout this time: my wife (Israa T. J. Almusawi), my son (Ahmed Z. H. Nafaee), and my daughter (Asawer Z. H. Nafaee) for their continuous, unlimited help, support, patience, and motivation. I especially thank my father (Hasan A. Nafaee), my mother (Ameena Sareea), all my brothers, my sister, and my close friends for their patience and unconditional support.

I would like to thank our collaborators for the possibility to study and work in their excellent laboratories, for the professional help that I got during my research visits, and for their contributions to improve our manuscripts:

Dr. Éva Hunyadi-Gulyás, ESI-MS, Hungarian, Biological Research Center

Dr. Gábor Peintler, kinetic calculations and evaluation, University of Szeged

Dr. Søren Vrønning Hoffmann and Dr. Nykola C. Jones, SR-CD spectroscopy, University of Aarhus.

Dr. Stephan Niebling, Dr. Angelica Struve Garcia, Dr.Katharina Veith, Dr. Osvaldo Burastero, and Dr. Maria Garcia-Alai, Characterization of Membrane Proteins, EMBL Hamburg

Dr. Kato Kohsuke, Dr. Atsushi Kawaguchi, Dr. Kyosuke Nagata, providing, design and cloning genes, University of Tsukuba

I would like to say a special thanks to the Tempus Public Foundation and the Stipendium Hungaricum Scholarship at the University of Szeged for their financial support in covering the expenses of tuition, health insurance, and monthly salary.

I am grateful to and would like to thank the Ministry of Higher Education and Scientific Research (MOHER), the Scholarship and Cultural Relations Directorate (SCRD) in Iraq, the Embassy of the Republic of Iraq in Budapest, and the Iraqi Regional Cultural Attche in Bucharest, Romania.

I would like to express my sincere gratitude to the University of Babylon, College of Pharmacy, for financial support during my PhD study.

Last but not least, I would like to greatly acknowledge the financial support provided by the Hungarian National Research, Development, and Innovation Office (GINOP-2.3.2-15-2016-00038, GINOP-2.3.2-15-2016-00001, GINOP-2.3.2-15-2016-00020, and 2019-2.1111-TET-2019-00089).

PUBLICATION LIST

The Hungarian Scientific Bibliography (MTMT) identifier: **10069594**

Full papers related to the dissertation

P1. Z.H. Nafaee, É. Hunyadi-Gulyás, B. Gyurcsik: Temoneira-1 β-lactamase is not a metalloenzyme, but its native metal ion binding sites allow for purification by immobilized metal ion affinity chromatography, *Protein Expression and Purification*, DOI: 10.1016/j.pep.2022.106169; 201 (2023) 106169. **IF= 1.6 - Q3**

P2. Z.H. Nafaee, V. Egyed, A. Jancsó, A. Tóth, A.M. Gerami, T.T. Dang, J. Heiniger-Schell, L. Hemmingsen, É. Hunyadi-Gulyás, G. Peintler, B. Gyurcsik: Revisiting the hydrolysis of ampicillin catalyzed byTemoneira-1 β-lactamase, and the effect of Ni(II), Cd(II) and Hg(II). *Protein Science*, DOI: 10.1002/pro.4809; 32 (2023) e4809. **IF= 8.1 - Q1, D1**

P3. Z.H. Nafaee, B.Hajdu, É. Hunyadi-Gulyás, B. Gyurcsik: Hydrolytic mechanism of a metalloenzyme is modified by the nature of the coordinated metal ion, *Molecules*, DOI: 10.3390/molecules28145511; 28 (2023) 5511. **IF= 4.6 - Q1**

ΣIF= 14.3

Two further manuscripts are in progress for publication: (i) the first article is related to His-tagged NColE7-R447G (KGNK-His), and (ii) the second is a literature review related to nuclease domains of colicin E7 and E9.

APPENDIX

Section A1. Role of metal ions in metallo-β-lactamases

Class B metallo-β-lactamases (MBLs) are different from the serine β-lactamases in structures and catalysis mechanism [A1-A3]. MBLs utilize Zn(II) ion to promote the hydrolysis of β-lactam antibiotics through direct attack by a hydroxide ion that is generated by the Lewis acid Zn(II) ion in the active center [A4;A5]. MBLs encompass a His-Xaa-His-Xaa-Asp motif that forms a metal binding site located at the interface of two β-sheets of the protein [A1;A3]. There are three distinct MBL subfamilies termed B1, B2 and B3, [A6] they have low sequence identity about 20% [A7]. B1 enzymes are the most important clinically. They possess a binuclear Zn(II) ion center comprising His-His-His residues (termed Zn1) and an Asp-Cys-His metal site, termed Zn2 [A3]. B3 enzymes possess a binuclear Zn(II) center: Zn1 coordinating to His-His-His residues and Zn2 coordinating to His-His-Asp residues [A1] The active site of B2 enzymes is a mononuclear Zn(II) ion center coordinating to Asn-His-Asp [A8]. In the binuclear enzymes (B1 and B3) (**Fig. A10**), metal ion coordination is completed by a bridging water molecule connecting the two metal ions.

Section A2. The steps of the catalytic mechanism of TEM-1 β-lactamases

The class-A β-lactamase catalysis mechanism includes two stages: acylation and de-acylation. The acylation mechanism of the class A enzymes remains a source of debate. Two main pathways were proposed supported by experimental evidences from crystallographic studies of enzyme complexes, computational simulations and biochemical investigations of enzyme mutants (**Scheme A2**) [A9-A15]. These agree that the activated Ser70 nucleophile attacks the β-lactam carbonyl carbon. Both Lys73 (part of the SXXK motif) and the deprotonated sidechain of a Glu166 are close to Ser70 in the active center, being able to fulfill general base function activating the serine residue [A16]. Therefore, it is under debate, [A17], whether the removed proton is transferred to the transiently deprotonated side chain (amine group) of Lys73 or to a water molecule that is coordinated by Ser70 and Glu166 [A17- A19].

In deacylation step (**Scheme A3**), the general base (the side chain of an amino acid) activates the deacylating water moleculeby deprotonation, the deprotonated water attack the carbonyl group of penicilloate-enzyme resulting in the penicilloate-enzyme complex(deacylation transition state), then this complex is rearranged, and Ser residue leaves the complex with alcoholic oxygen producing the hydrolysis of the β-lactam antibiotic (product) and the regeneration of the enzyme (native enzyme) [A10;A18;A19].

The identity of bases B1 and B2 are different in various β-lactamases. The residues Ser70, Glu166, and Asn170 are conserved in over 150 class A β-lactamases [A20]. Asn170 forms hydrogen bonds with Glu166 and coordinates the hydrolytic water involved in the deacylation step. Ser70 and Glu166 of class A β-lactamases are invariant because of their direct role in catalysis, while Asn170 is conserved in over 96% of class A β-lactamase sequences, (numbering of amino acids according to [A21]).

Crystal structures provide static images of many points of the reaction mechanism. Combined with mutation and catalytic studies, these experiments with various substrates revealed that Asn170 has important role in β-lactam hydrolysis. On the other hand, Asn170Gly or Ala mutants were very efficient in the hydrolysis of the substrates containing a primary amine group within the R substituent (see **Scheme A3** in the dissertation), such as ampicillin and cephalexin, which is close to the side chain Asn170 in the covalent acyl-intermediate. While Asn170Gly mutant was inefficient to activate the water molecule by Glu166 for deacylation step, the amine group of the ampicillin substrate can take over the role of Asn170 amine group to coordinate to the hydrolytic water [A10]. Thus, Asn170Gly mutant hydrolyzes ampicillin efficiently because of substrate-assisted catalysis. This was also proven by using penicillin-G, lacking this amine group, instead of ampicillin as substrate, leading to decreased activity of the mutant enzyme (**Fig. A11**).

Section A3. The domains structure of colicins

Colicins are sensitive to the surface receptors of *E. coli* cells. Based on the cell surface receptor, colicins are classified into two groups. (i) Group A colicins bind to the BtuB receptor protein that is an essential component of the vitamin B_{12} transport system (**see Fig. A12**) and then utilize the Tol-dependent translocation system (TolA, TolB, TolQ, TolR, and Pal proteins) such as colicin endonucleases (colicin Es);. (ii) Group B colicins utilize the Ton-dependent translocation system such as colicins B and Ia [A22]

Colicins Es are ~60 kDa proteins consisting of three domains: translocation, receptor binding, and nuclease (cytotoxic) domains (**Fig. A12**). Each domain is implicated in one of the three stages of bacterial cell killing. The C-terminal is the nuclease domain responsible for cytotoxicity [A23;A24]. The function of the central domain is binding to the receptor [A24;A25]. The N-terminal domain mediates translocation of the cytotoxic C-terminal domain across the outer bacterial membrane [A26;A27]. Thus, the cytotoxic effect involves colicin E binding to a receptor

of the bacterium, translocation across the outer membrane, periplasm, and inner membrane of the bacterium and finally, the nuclease action of the C-terminal domain (**Fig. A12**). [A28]

Tables A1-A3.

Table A1: Conditions of the cell culture assays for studying the effect of the metal ions on E. coli cells transformed with the modified pET-21a(+) [P2].

Experiments №	1	2 – 4	5	6,7	8,9	10,11
Starting McFarland value	~1.0	~1.0	~1.0	~2.3	~2.3	~2.3
Ampicillin (μM)	0 or 270	0 or 270	0 or 270	0 or 270	–	10 or 100
Kanamycin (μM)	–	–	–	–	0 or 83	0 or 83
IPTG (mM)	–	–	0 or 1.0	0 or 1.0	–	–
Ni(II) (μM)	1000	1.0 or 10.0	1.0 or 10.0	1.0 or 10.0	1.0 or 10.0	–
Cd(II) (μM)	1000	1.0 or 10.0	1.0 or 10.0	1.0 or 10.0	1.0 or 10.0	–
Hg(II) (μM)	500	1.0 or 10.0	1.0 or 10.0	1.0 or 10.0	1.0 or 10.0	5.0 – 100.0

Table A2: Table of LC-MSMS analysis results for protein identification. The marked gel bands in **Fig. 5.1.b** were cut out of the gel, digested by trypsin and then subjected to the LC-MS-MS analysis. Peak lists were generated with Proteome Discoverer software and subjected to database search on Protein Prospector (version: 6.3.1) [P1].

Rank	Acc #	NFI-BDH_Total			Protein MW	Species	Protein Name
		Num Unique	Peptide Count	% Cov			
1	P62593	90	382	86.0	31515.5	ECOLX	Beta-lactamase TEM
2	P0A7V0	38	74	92.9	26743.9	ECOLI	30S ribosomal protein S2
3	P62707	33	72	94.0	28556.6	ECOLI	2,3-bisphosphoglycerate-dependent phosphoglycerate mutase
4	P0A7V3	37	68	85.8	25983.4	ECOLI	30S ribosomal protein S3
5	P0A910	31	54	77.5	37201.1	ECOLI	Outer membrane protein A
6	P0AEK4	30	48	67.9	27864.2	ECOLI	Enoyl-[acyl-carrier-protein] reductase [NADH] FabI
7	Q8X8V9	23	38	80.1	29416.9	ECO57	D-methionine-binding lipoprotein MetQ
8	P0A7V8	22	36	78.2	23469.3	ECOLI	30S ribosomal protein S4
9	Q0TH01	20	27	69.4	25878.7	ECOL5	RNA chaperone ProQ
10	P0ABA8	21	31	52.3	31577.7	ECO57	ATP synthase gamma chain
11	P07014	21	29	66.8	26770.1	ECOLI	Succinate dehydrogenase iron-sulfur subunit
12	P0A9D8	22	32	75.9	29892.3	ECOLI	2,3,4,5-tetrahydropyridine-2,6-dicarboxylate N-succinyltransferase
13	P0A7L0	18	34	53.4	24729.8	ECOLI	50S ribosomal protein L1
14	P69805	15	22	54.1	30955.8	ECOLI	PTS system mannose-specific EIID component
15	P02931	15	18	48.9	39333.6	ECOLI	Outer membrane porin F
16	P0AGE9	17	23	46.4	29777.7	ECOLI	Succinate--CoA ligase [ADP-forming] subunit alpha
17	P0AEZ3	16	18	59.6	29614.3	ECOLI	Septum site-determining protein MinD

18	P0A9Q1	13	19	42.0	27292.3	ECOLI	Aerobic respiration control protein ArcA
19	P0AA16	14	17	61.1	27353.9	ECOLI	Transcriptional regulatory protein OmpR
20	P61889	14	15	66.3	32337.6	ECOLI	Malate dehydrogenase
21	P13645	13	14	25.9	58827.5	HUMAN	Keratin, type I cytoskeletal 10
22	P0A927	11	18	49.0	33589.3	ECOLI	Nucleoside-specific channel-forming protein Tsx
23	P0A794	14	15	56.8	26384.5	ECOLI	Pyridoxine 5'-phosphate synthase
24	P37440	14	17	59.3	27850.2	ECOLI	Oxidoreductase UcpA
25	P69442	16	20	62.1	23586.2	ECO57	Adenylate kinase
26	P12758	13	14	75.1	27159.3	ECOLI	Uridine phosphorylase
27	P04264	15	17	22.7	66039.2	HUMAN	Keratin, type II cytoskeletal 1
28	P45523	12	15	55.9	28882.2	ECOLI	FKBP-type peptidyl-prolyl cis-trans isomerase FkpA
29	P15770	12	14	51.1	29413.9	ECOLI	Shikimate dehydrogenase (NADP(+))
30	P0AFH2	10	13	27.5	33443.5	ECOLI	Oligopeptide transport system permease protein OppB
31	P0AEU0	12	15	54.2	28483.6	ECOLI	Histidine-binding periplasmic protein
32	P0A8K1	11	12	40.7	35934.7	ECOLI	Phosphatidylserine decarboxylase proenzyme
33	Q0SX30	10	11	49.0	27749.1	SHIF8	Deoxyribose-phosphate aldolase
34	P04846	12	13	54.0	29423.8	ECOLI	Lipoprotein 28
35	P0A877	9	9	51.5	28724.4	ECOLI	Tryptophan synthase alpha chain
36	P39831	9	14	43.5	27249.2	ECOLI	NADP-dependent 3-hydroxy acid dehydrogenase YdfG
37	P37902	11	11	33.8	33420.5	ECOLI	Glutamate/aspartate import solute-binding protein
38	P07109	11	13	51.4	28653.3	ECOLI	Histidine transport ATP-binding protein HisP
39	P0A858	8	8	46.7	26972.0	ECOLI	Triosephosphate isomerase
40	P0A722	9	11	41.6	28080.2	ECOLI	Acyl-[acyl-carrier-protein]--UDP-N-acetylglucosamine O-acyltransferase
41	P04951	8	8	40.7	27614.7	ECOLI	3-deoxy-manno-octulosonate cytidylyltransferase
42	P0ABP8	9	10	34.3	25950.2	ECOLI	Purine nucleoside phosphorylase DeoD-type
43	P0AE08	7	7	37.4	20761.6	ECOLI	Alkyl hydroperoxide reductase C
44	P0A9B2	8	8	33.5	35532.8	ECOLI	Glyceraldehyde-3-phosphate dehydrogenase A
45	P0AEM9	10	11	32.0	29039.4	ECOLI	L-cystine-binding protein FliY
46	P0ADS6	10	10	39.4	26635.5	ECOLI	Uncharacterized protein YggE
47	P0AAF6	8	8	44.2	27022.3	ECOLI	Arginine transport ATP-binding protein ArtP
48	P04036	8	9	25.6	28756.9	ECOLI	4-hydroxy-tetrahydrodipicolinate reductase
49	P76034	8	9	40.2	27602.9	ECOLI	Uncharacterized HTH-type transcriptional regulator YciT
50	P31680	6	7	29.9	30579.7	ECOLI	Co-chaperone protein DjlA
51	P27836	9	9	39.8	27928.4	ECOLI	UDP-N-acetyl-D-mannosaminuronic acid transferase
52	Q0TEA4	6	7	26.2	27975.1	ECOL5	Phosphoadenosine phosphosulfate reductase
53	P60438	7	7	32.1	22243.7	ECOLI	50S ribosomal protein L3

54	P76422	8	8	44.0	28633.9	ECOLI	Hydroxymethylpyrimidine/phosphomethylpyrimidine kinase
55	P0AFH6	5	9	15.2	33022.2	ECOLI	Oligopeptide transport system permease protein OppC
56	P0AFP4	6	7	32.3	29410.4	ECOLI	Uncharacterized oxidoreductase YbbO
57	P0A9V1	6	7	36.1	26800.9	ECOLI	Lipopolysaccharide export system ATP-binding protein LptB
58	P0A6P1	7	8	22.6	30423.2	ECOLI	Elongation factor Ts
59	P60422	9	9	34.1	29860.7	ECOLI	50S ribosomal protein L2
60	P0AC02	6	6	23.7	27829.6	ECOLI	Outer membrane protein assembly factor BamD
61	P0A7Y0	9	9	33.2	25550.2	ECOLI	Ribonuclease 3
62	P0A9D4	6	6	26.4	29316.9	ECOLI	Serine acetyltransferase
63	P10346	6	7	32.5	26731.2	ECOLI	Glutamine transport ATP-binding protein GlnQ
64	P0AG55	7	7	37.3	18903.9	ECOLI	50S ribosomal protein L6
65	P0AFB1	6	6	25.9	33621.0	ECOLI	Lipoprotein NlpI
66	P37774	6	6	32.4	27677.2	ECOLI	L-cystine transport system ATP-binding protein YecC
67	P67175	5	7	12.6	26436.8	ECOL6	Probable transcriptional regulatory protein YebC
68	P0AE18	5	5	25.8	29331.1	ECOLI	Methionine aminopeptidase
69	P0AG93	4	5	13.9	35382.7	ECOLI	Protein translocase subunit SecF
70	P66679	5	6	28.2	25312.1	ECOL6	Ribonuclease PH
71	P0C0S1	4	4	15.7	30896.3	ECOLI	Small-conductance mechanosensitive channel
72	B1IXV6	4	4	32.5	26585.7	ECOLC	Ubiquinone biosynthesis O-methyltransferase
73	P0ABJ1	6	6	20.0	34911.6	ECOLI	Cytochrome bo(3) ubiquinol oxidase subunit 2
74	P0A9N4	3	3	18.7	28204.6	ECOLI	Pyruvate formate-lyase 1-activating enzyme
75	P09414	5	5	14.7	55976.7	RAT	Nuclear factor 1 A-type
76	P0AFM6	5	6	18.5	25493.2	ECOLI	Phage shock protein A
77	P0ACL0	4	4	19.8	28048.1	ECOLI	Glycerol-3-phosphate regulon repressor
78	P0A7S9	5	5	53.4	13099.5	ECOLI	30S ribosomal protein S13
79	P0ACN4	6	6	21.8	29269.9	ECOLI	HTH-type transcriptional repressor AllR
80	P46125	3	4	10.2	32191.0	ECOLI	Inner membrane protein YedI
81	P0AB38	4	4	33.3	22515.8	ECOLI	Penicillin-binding protein activator LpoB
82	P0ABK5	4	4	24.1	34489.9	ECOLI	Cysteine synthase A
83	P0A840	3	3	17.8	26900.7	ECOLI	5'/3'-nucleotidase SurE
84	P0AA43	6	7	29.0	25865.5	ECOLI	Ribosomal small subunit pseudouridine synthase A
85	P22255	5	5	27.6	27176.1	ECOLI	3'(2'),5'-bisphosphate nucleotidase CysQ
86	P0A7R9	3	3	22.5	13845.0	ECOLI	30S ribosomal protein S11
87	Q83IU1	4	4	18.7	28378.9	SHIFL	CDP-diacylglycerol pyrophosphatase
88	P02938	3	5	49.4	8239.2	SERMA	Major outer membrane lipoprotein
89	P31057	4	4	29.2	28237.7	ECOLI	3-methyl-2-oxobutanoate hydroxymethyltransferase
90	P0A8Y5	4	5	20.0	29721.4	ECOLI	Sugar phosphatase YidA
91	P59437	3	3	13.7	29698.2	SHIFL	N-acetylmannosamine kinase

92	P16528	3	3	15.7	29739.6	ECOLI	Transcriptional repressor IclR
93	P0AEN1	4	4	14.6	26242.2	ECOLI	NAD(P)H-flavin reductase
94	P0A8U2	4	4	14.3	29991.9	ECOLI	UPF0294 protein YafD
95	P0A903	3	3	13.4	36842.7	ECOLI	Outer membrane protein assembly factor BamC
96	P0CE47	5	6	15.0	43283.9	ECOLI	Elongation factor Tu 1
97	P22524	4	4	15.4	26974.7	ECOLI	Chromosome partition protein MukE
98	P0A7Z4	3	3	10.0	36512.0	ECOLI	DNA-directed RNA polymerase subunit alpha
99	P60955	2	3	11.3	33108.3	ECOLI	Phosphatidylglycerol--prolipoprotein diacylglyceryl transferase

Table A3: Sample preparation for ^{199m}Hg PAC measurements [P2].

Stock solutions	**Sample 1**	**Sample 2**
Hot Hg(II)	140 µL	
Cold Hg(II) (100 µM $HgCl_2$ solution)	13.5 µL	28.5 µL
500 mM HEPES buffer (pH 7.4)	10 µL	
~23.1 µM TEM-1 β-lactamase in 20 mM Tris-HCl (pH 7.5)	65 µL	
0.1 M $HClO_4$	23 µL	
H_2O (and acid/base for pH adjustment)	56 µL	41 µL
V_{total}	307.5 µL	
Sucrose	0.3075 g	
V_{final}	500 µL	
density of 50 % (w/w) sucrose solution	1.23 g/mL	

Schemes A1-A3.

```
atgtattctccgctctgtctcacccaggatgagtttcatcctttcattgaagcacttctg
 M  Y  S  P  L  C  L  T  Q  D  E  F  H  P  F  I  E  A  L  L
ccccatgtccgcgccttcgcctacacatggttcaacctgcaggcccgaaagcggaaatac
 P  H  V  R  A  F  A  Y  T  W  F  N  L  Q  A  R  K  R  K  Y
ttcaaaaaacatgagaagcgcatgtcgaaagaagaggagagggccgtgaaggatgaactg
 F  K  K  H  E  K  R  M  S  K  E  E  E  R  A  V  K  D  E  L
ctaagcgagaagcccgaggtcaagcagaagtgggcttcccgacttctggccaagttacgg
 L  S  E  K  P  E  V  K  Q  K  W  A  S  R  L  L  A  K  L  R
aaagatatccgacccgagtaccgagaggattttgttcttacagttacagggaaaaaacct
 K  D  I  R  P  E  Y  R  E  D  F  V  L  T  V  T  G  K  K  P
ccatgctgtgttctttccaaccctgatcagaaaggcaagatgcggagaattgactgcctc
 P  C  C  V  L  S  N  P  D  Q  K  G  K  M  R  R  I  D  C  L
cgccaggcagataaagtatggaggttggacctcgtcatggtgatcttgttcaaaggtatt
 R  Q  A  D  K  V  W  R  L  D  L  V  M  V  I  L  F  K  G  I
ccgctggaaagtactgatggcgagcgccttgtaaagagtccacagtgctctaatccaggg
 P  L  E  S  T  D  G  E  R  L  V  K  S  P  Q  C  S  N  P  G
ctctgtgtccag/caccccatcacatagggtttctgtaaaggaactcgatttatatttggca
 L  C  V  Q  /  H  P  H  H  I  G  V  S  V  K  E  L  D  L  Y  L  A
tactttgtacatgcagcagattcaagtcaatctgaaagtcccagccagccaagtgaagct
 Y  F  V  H  A  A  D  S  S  Q  S  E  S  P  S  Q  P  S  E  A
gacattaaggaccagccagaaaatggacatttgggcttccaggacagctttgtcacatca
 D  I  K  D  Q  P  E  N  G  H  L  G  F  Q  D  S  F  V  T  S
ggtgttttcagtgtgactgagctagtaagagtgtcacaaacaccaatagctgcagggacc
 G  V  F  S  V  T  E  L  V  R  V  S  Q  T  P  I  A  A  G  T
gaattcccgggtcgactcgagcaccaccaccaccaccactga
 E  F  P  G  R  L  E  H  H  H  H  H  H  -
```

Scheme A.1. The genes of Nuclear factor I DNA binding domain variants (NFI-BD and NFI-BDH) inserted in the pET-21a(+) vector as verified by DNA sequencing. The translated amino acid sequence is also shown below the DNA sequence. The Q164H mutation site leading to NFI-BDH is highlighted by red characters. The map of pET-21a(+) vector including the NdeI and XhoI sites and the TEM-1 β-lactamase gene is shown in **Fig. A3** [P1].

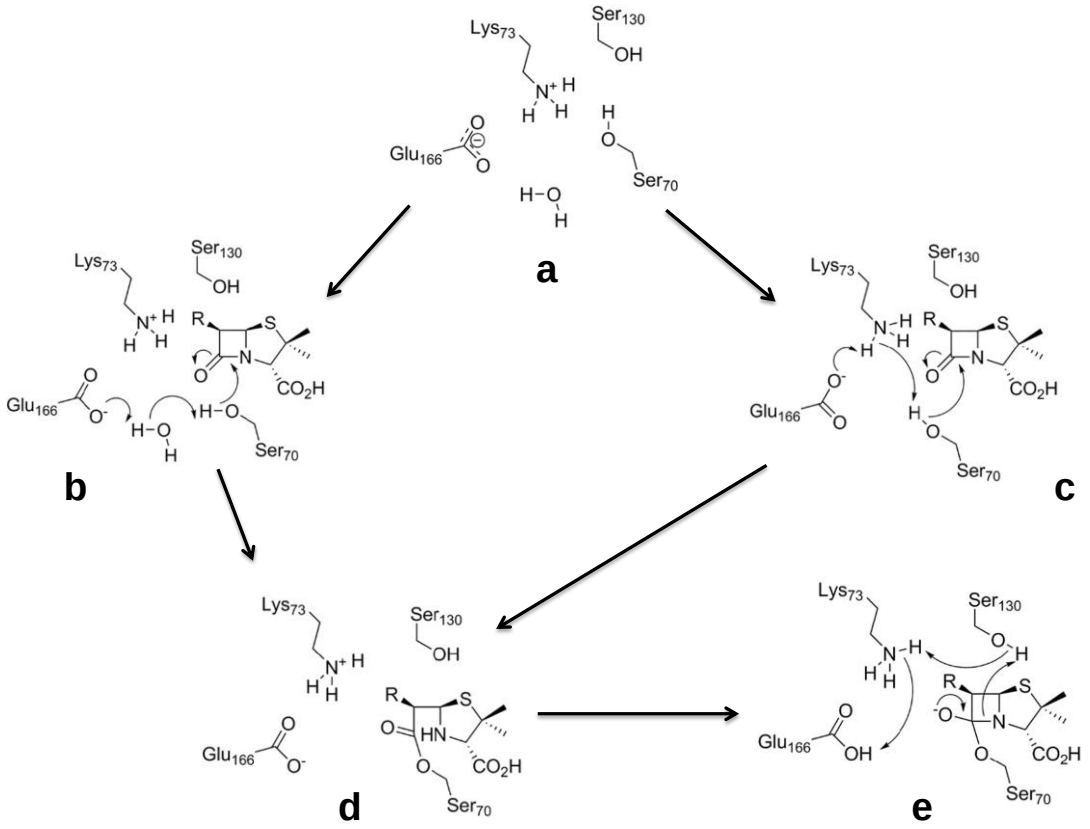

Scheme A.2. Acylation mechanisms of β-lactamases class A. **a**) Enzyme active site shows protonated Lys73, Ser70, Ser130, and deprotonated Glu166. **b**) Ser70 is activated for nucleophilic attack on the β-lactam carbonyl by Glu166 via a water molecule. **c**) Alternatively, Lys73 is neutralized by deprotonated Glu166, and then Ser70 is activated by neutralized Lys73. (numbering of amino acids according to [A21]) **d**) Proton transfer in the transition state acyl-enzyme intermediate, Ser130 provides the proton for the N-atom of the β-lactam ring. **e**) Acylenzyme intermediate with opened β-lactam ring [A12].

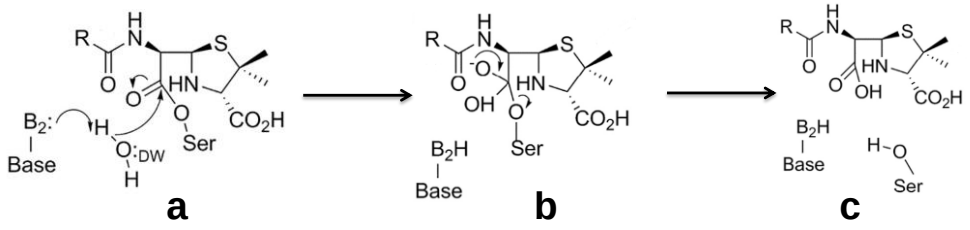

Scheme A2. Deacylation mechanisms of β-lactamases class A. **a**) The general base B2 activates the deacylating water molecule (DW) for nucleophilic attack at the carbonyl carbon atom of the acylenzyme complex. **b**) The intermediate complex is rearranged. **c**) The alcoholate oxygene of the leaving the Ser is protonated by the conjugate acid of the general base. This step yields the free penicilloate product [A12].

Figures A1-A12.

```
1zg4    HPETLVKVKDAEDQLGARVGYIELDLNSGKILESFRPEERFPMMSTFKVLLCGA
1tem    HPETLVKVKDAEDQLGARVGYIELDLNSGKILESFRPEERFPMMSTFKVLLCGA
1erm    HPETLVKVKDAEDQLGARVGYIELDLNSGKILESFRPEERFPMMSTFKVLLCGA
3dtm    HPETLVKVKDAEDQLGARVGYIELDLNSGKILESFRSEERFPMMSTFKVLLCGA

   VLSRIDAGQEQLGRRIHYSQNDLVEYSPVTEKHLTDGMTVRELCSAAITMSDNTAANLL
   VLSRIDAGQEQLGRRIHYSQNDLVEYSPVTEKHLTDGMTVRELCSAAITMSDNTAANLL
   VLSRVDAGQEQLGRRIHYSQNDLVEYSPVTEKHLTDGMTVRELCSAAITMSDNTAANLL
   ILSRIDAGQEQLGRRIHYSQNDLVEYSPVTEKHLTDGMTVRELCSAAITMSDNTAANLL

LTTIGGPKELTAFLHNMGDHVTRLDRWEPELNEAIPNDERDTTMPVAMATTLRKLLTGEL
LTTIGGPKELTAFLHNMGDHVTRLDRWEPELNEAIPNDERDTTMPVAMATTLRKLLTGEL
LTTIGGPKELTAFLHNMGDHVTRLDRWEPELNEAIPNDERDTTMPAAMATTLRKLLTGEL
LTTIGGPKGLTAFLHNMGDHVTRLDRWEPELNEAIPNDERDTTTPVAMATTLRKLLTGEL

LTLASRQQLIDWMEADKVAGPLLRSALPAGWFIADKSGAGERGSRGIIAALGPDGKPSRI
LTLASRQQLIDWMEADKVAGPLLRSALPAGWFIADKSGAGERGSRGIIAALGPDGKPSRI
LTLASRQQLIDWMEADKVAGPLLRSALPAGWFIADKSGAGERGSRGIIAALGPDGKPSRI
LTPASRQQLMDWMEADKVAGPLLRSVLPAGWFIADKSGAGERGSRGIVAALGPDGKPSRI

                  VVIYTTGSQATMDERNRQIAEIGASLIKHW
                  VVIYTTGSQATMDERNRQIAEIGASLIKHW
                  VVIYTTGSQATMDERNRQIAEIGASLIKHW
                  VVIYTTGSQATMDELNRQIAEIGASLIKHW
```

Figure A1. The sequences of various TEM-1 β-lactamases differing by few amino acid residues (PDB ID: 1ZG4, 1TEM, 1ERM, 3DTM) [P1].

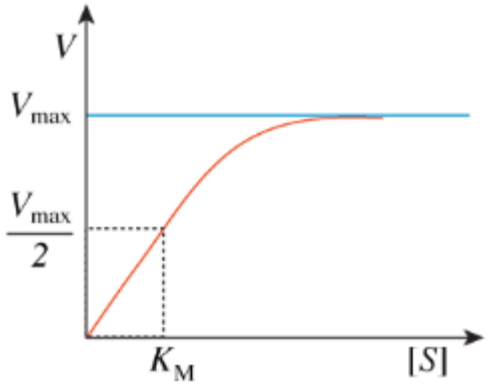

Figure A2 Michaelis-Menten graph, [S]: substrate concentration, *V*: velocity, V_{max}: the maximum velocity.

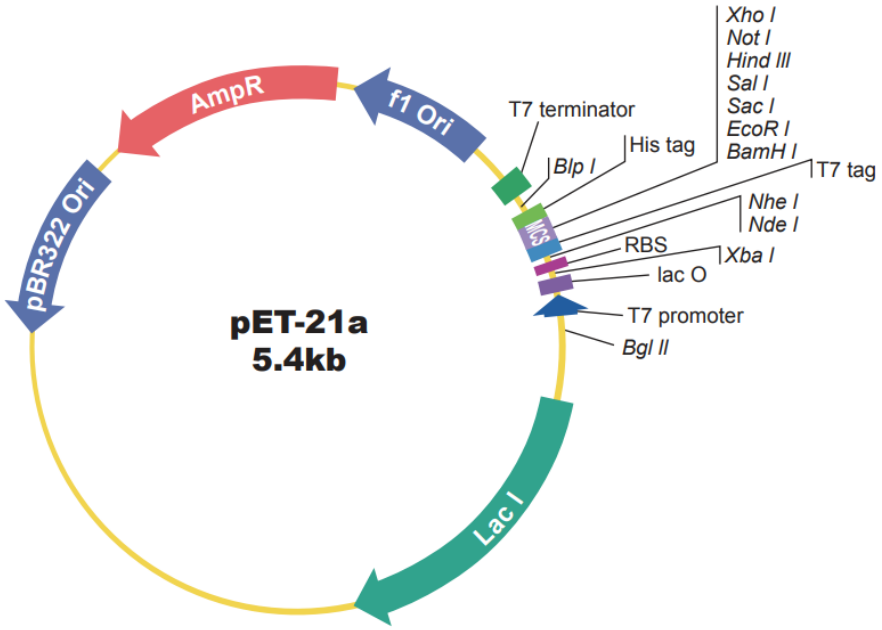

Figure A3. Map of the pET-21a(+) plasmid that illustrates the multi-cloning site (MCS), antibiotic resistance site (the *AmpR* ampicillin resistance gene aids to control the growth of bacteria in the culture media supplied with ampicillin: only the cells that have the resistance gene together with the plasmid can survive.), promoter sites and the ORI sites. The map is taken from (https://www.genscript.com).

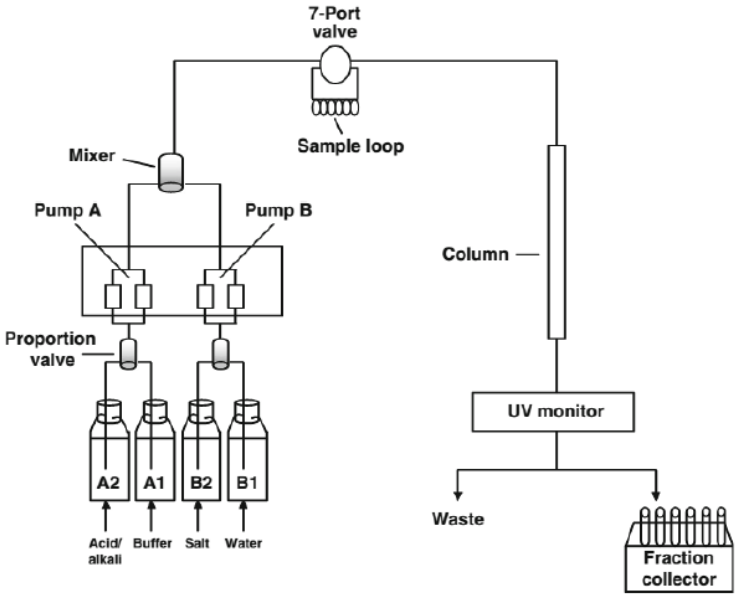

Figure A4. The scheme of the ÄKTA system used for protein purification. Taken from [A29]

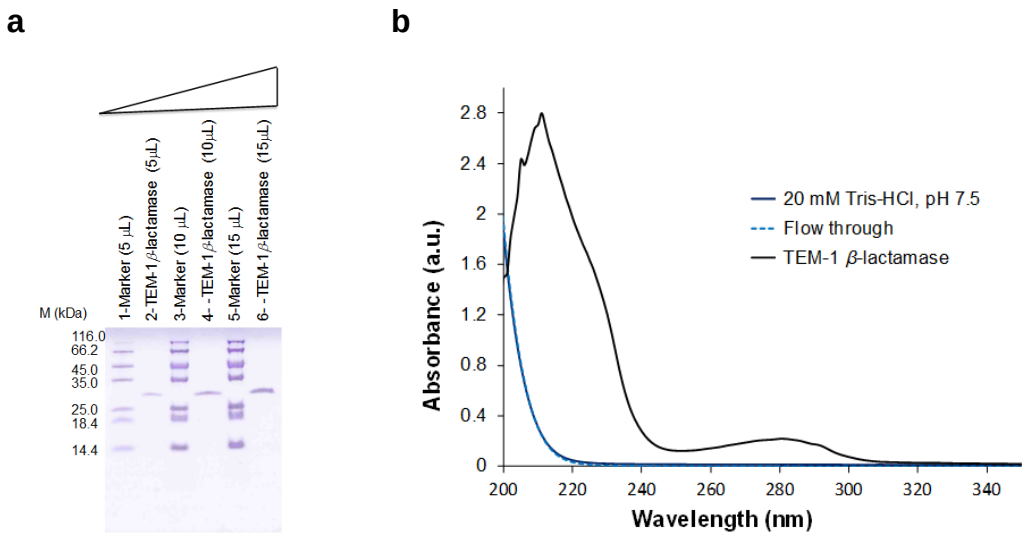

Figure A5. a) SDS-PAGE image of the marker (wells no.1, 3, and 5), and pure TEM-1 β-lactamase (wells no. 2, 4, and 6) loaded in increasing quantities. Marker proteins served the reference values (5 µL of the Thermo Fisher Scientific #26610 marker contains 0.5-1 µg of proteins in each band, based on the information provided by the manufacturer). **b)** UV absorbance spectra of pure TEM-1 β-lactamase in 20 mM Tris-HCl, pH 7.5, the 20 mM Tris-HCl, pH 7.5 buffer used for buffer exchange, and the final flow through fraction of this procedure (1.0 cm quartz cell) [P1].

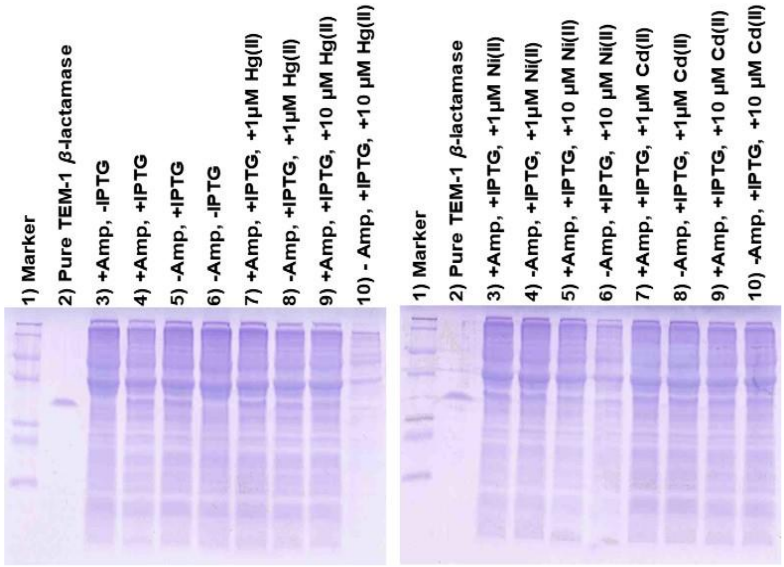

Figure A6. SDS PAGE monitoring of the TEM-1 β-lactamase (28919.0 Da) overexpression induced by IPTG at 1 mM concentration in *E. coli* BL21 (DE3) bacterial cells, transformed by the modified pET-21a(+) vector in the presence or absence of ampicillin and various concentrations of the metal ions: Hg(II), Cd(II), and Ni(II) [P2].

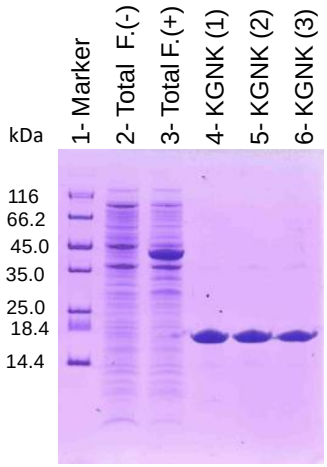

Figure A7. Expression and purification of KGNK based on the pGEX-6p-1(+)-KGNK DNA carrier in *E. coli* BL21(DE3). (1) marker, (2 and 3) total GST-target protein fractions lysates (-) absence (IPTG) and (+) presence of inducer using 0.5 mM IPTG respectively. (4) Pure KGNK in 20 mM HEPES (batch no. 1), (5) Pure KGNK in 20 mM HEPES (batch no. 2), (6) Pure KGNK in 25 mM ammonium bicarbonate.

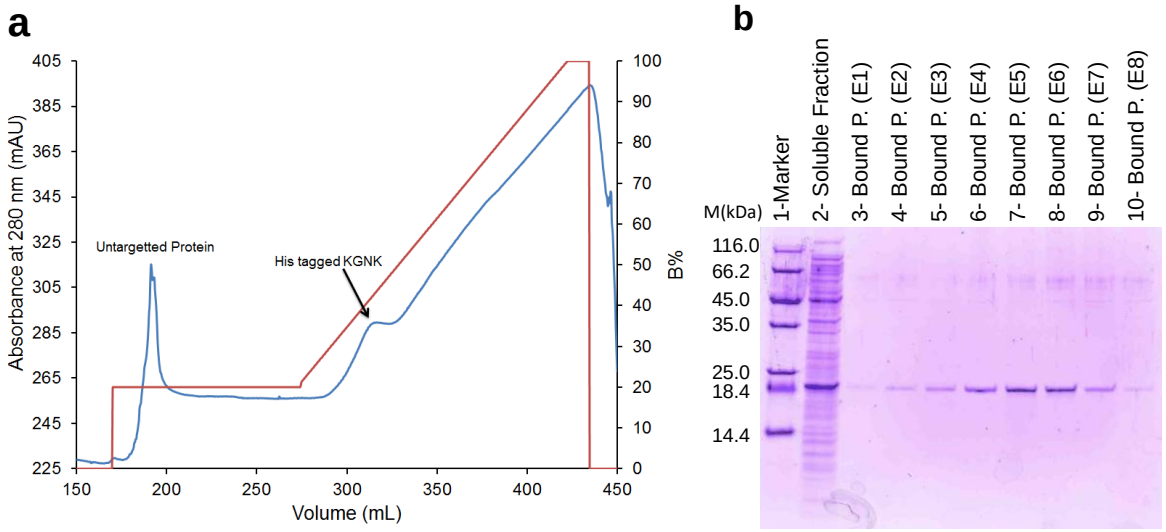

Figure A8. (**a**) Chromatogram of the immobilized Ni(II) ion affinity HPLC purification of KGNK-His. (**b**) SDS-PAGE monitoring of the purification steps: 1 marker, 2 soluble fraction, 3-10 elution fractions (E3–E10).

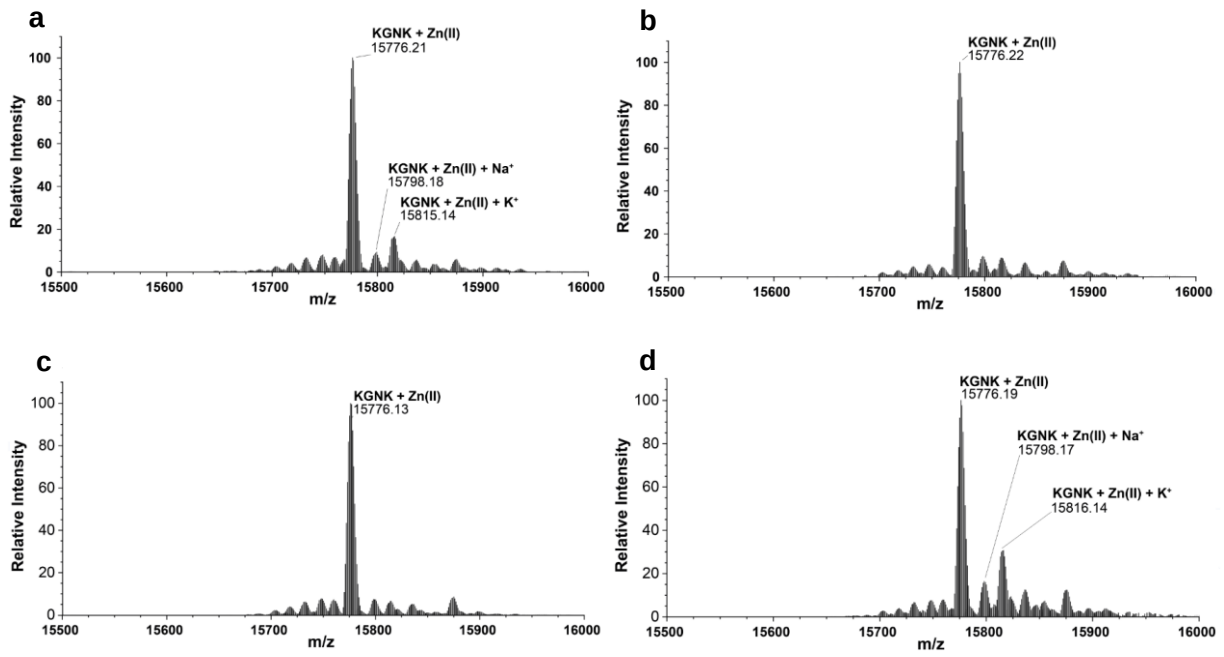

Figure A9. Deconvoluted ESI-MS spectra of KGNK protein in the presence of (**a**) 1 eq Zn(II); (**b**) 1 eq Zn(II) + 1 eq Cu(II); (**c**) 1 eq Zn(II) + 1 eq Ni(II) and (**d**) 1 eq Zn(II) + 1 eq Cd(II); the concentration of the KGNK was 3.0 μM [P3].

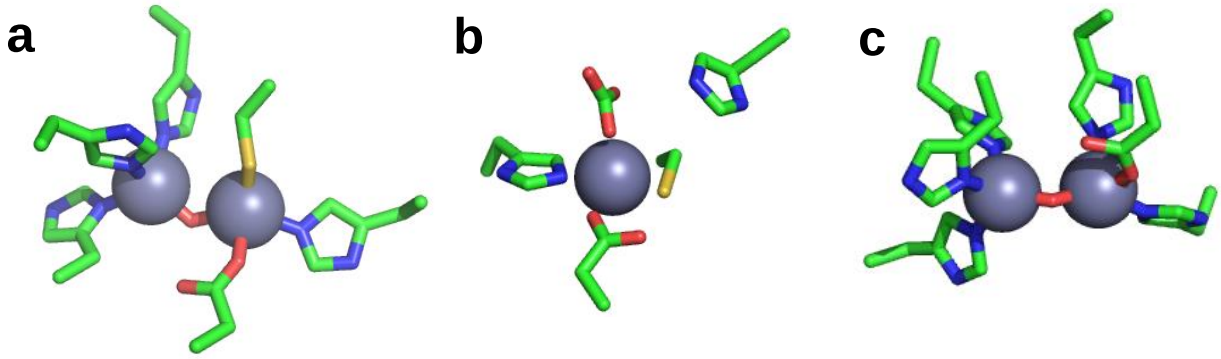

Figure A10. Metal ion binding sites of B1, B2, and B3 subclasses of metallo-β-lactamases. Zn(II) ions are represented by grey spheres. **a**) Zn(II) ions in the active site of the subclass B1 CcrA enzyme (Protein Data Bank identification code (PDB ID): 1ZNB). **b**) Binding residues of *A. hydrophila* mono-zinc carbapenemase CphA enzyme of subclass B2 MBLs (PDB ID: 1X8G). **c**) Amino acid residues coordinating Zn(II) ions in pathogen *S. maltophilia* L1 enzyme of subclass B3 MBLs (PDB ID: 1SML).

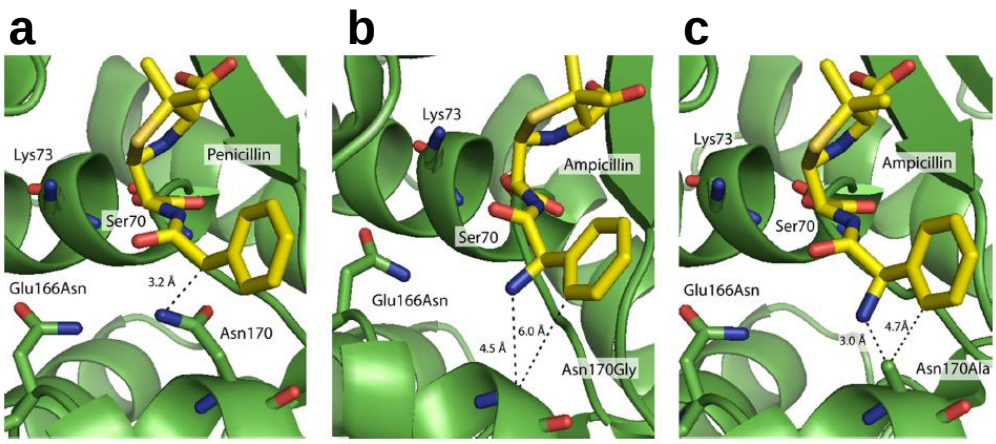

Figure A11. Molecular modelling of the TEM-1 β-lactamase acyl-intermediate. **a**) The acyl-intermediate with the enzyme covalently bonded to penicillin G illustrating that Asn170 is close to the substrate and Asn166 (PDB ID: 1FQG). **b**) Ampicillin acyl-Asn170Gly mutant enzyme are modelled into the acyl-intermediate structure. **c**) Ampicillin acyl-Asn170Ala mutant enzyme model from **b** [A19].

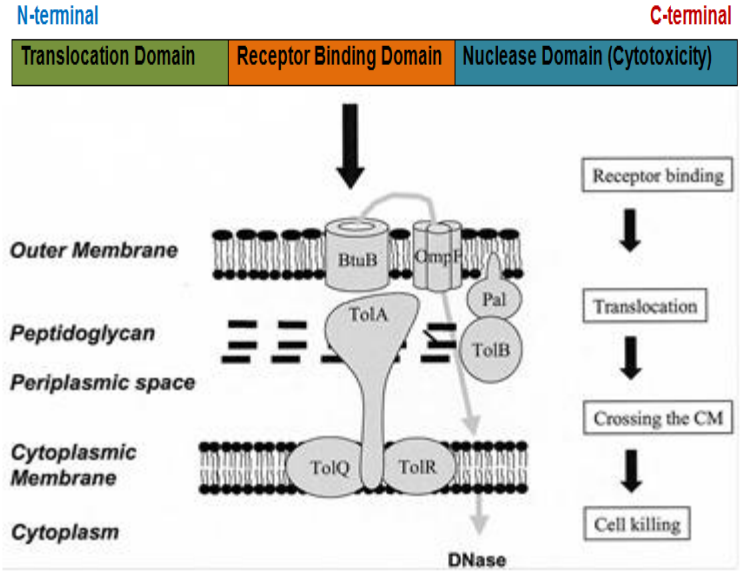

Figure A12. Diagram of the colicin E action including the receptor-binding, translocation, and cell killing steps. Proteins of the Tol-dependent translocation system that interact with colicin Es are also shown [A22].

Protocols A1-A6

Protocol A1. Expression of TEM-1 β-lactamase

BL21 (DE3) *E. coli* cells were transformed by pET-21a(+) ligated NFI-BDH gene by heat shock. The cells were grown on the standard LB nutrition plate (1g of Tryptone, 0.5g yeast extract, 1.0 g NaCl, and 1.5 g agar-agar dissolved in 100 mL water spread on Petri dishes) containing 0.1 mg/ml Amp. A bacterial colony was transferred into 5.0 mL of LB medium (1.0 g of Tryptone, 0.5 g yeast extract, and 1.0 g NaCl in 100 mL water) containing 0.1 mg/mL Amp, and then it was incubated at 37 °C for 12 h. After reaching OD_{600} ~ 2, 200 µL of this culture was transferred into 500 mL of LB medium (100 µg/mL ampicillin). Incubation followed for 3 h at 37 °C. When the OD_{600} of the culture reached ~0.6, protein expression was induced by adding 1.0 mM IPTG at final concentration and the bacterial culture was incubated for 16 h at 24 °C. The bacterial cells were harvested by centrifugation at 16500×g at 4 °C for 25 min.

Protocol A2. Expression of the NColE7 mutants

BL21 (DE3) *E. coli* cells were transformed either by pGEX-6P-1-KGNK, or by pET-21a-KGNK plasmids. The cells were grown on standard nutrition LB plate supplemented with Amp at 0.1 mg/ml concentration. A bacterial colony from both plates was transferred into 5 mL of LB media containing 0.1 mg/mL Amp and incubated at 37 °C for 12 h. After reaching OD_{600} ~ 2, about 200 µL of both cultures were transferred into 250 mL LB media containing 0.1g/mL Amp and then incubated for 3 h at 37 °C. When the OD_{600} of the culture reached ~0.6, protein expression was induced by adding 0.4-0.5 mM IPTG at final concentration and the bacterial culture was incubated for 3-4 h at 37 °C. The cells were harvested by centrifugation at 16500×g at 4 °C for 25 min.

Protocol A3. Purification of TEM-1 β-Lactamase

TEM-1 β-lactamase was purified in two steps of immobilized metal ion affinity chromatography (Ni(II)-loaded Sepharose 6 Fast Flow resin in XK 16/20 column) and in a subsequent step of anion exchange chromatography (HiPrep Q sepharose FF anion exchanger) with an ÄKTA HPLC explorer system. IMAC column (sepharose 6 FF resin chelated with Ni(II) packed in XK 16/20 column) was equilibrated with 1 × PBS, pH 7.3, then soluble fraction of the lysate containing TEM-1 β-lactamase was loaded. The column loaded with lysate was washed with 4–5 column volumes (CVs) of 100% buffer A1 (1 × PBS). The protein was eluted by increasing the percentage of buffer B1 (500 mM imidazole in 1 × PBS) with a following gradient: 0-50% in 1.5 CV (6 min); 50% for

2.0 CV (8 min); 50-100% in 1.5 CV (6 min) and then kept at 100% for 2.5 CV (10 min). The elution buffer in the fractions containing the protein was exchanged to 1× PBS using an Amicon Ultra 15 mL centrifugal filter. In the second IMAC step, the loaded sample was washed with 5 CVs of buffer A2 (1 × PBS, 250 mM NaCl). The TEM-1 β-lactamase was then eluted with an increasing percentage of buffer B2 (250 mM imidazole in 1 × PBS) in the eluent. The buffer of the eluted fractions was exchanged to 20 mM Tris-HCl, pH 7.5 using an Amicon Ultra 15 mL centrifugal filter. The last purification step was an anion exchange, the loaded protein was washed with 5 CVs of 20 mM Tris- HCl, pH 7.5 (buffer A3) and then eluted with a gradient of 1000 mM NaCl in 20 mM Tris-HCl (buffer B3), pH 7.5 as follows: 0–60% in 4.5 CV (18 min); 60% for 2.5 CV (10 min) and then 100% for 4 CV (16 min). The elution buffer of the pooled fractions was finally exchanged to 20 mM Tris-HCl, pH 7.5 by ultrafiltration.

Protocol A4. Purification of NColE7-KGNK

NColE7-KGNK was purified single step of GST affinity chromatography and cation exchange (Sepharose SP FF 16/10) chromatography with an ÄKTA HPLC explorer system. GST column was equilibrated with 1 × PBS, pH 7.3, and then soluble fraction of the lysate containing NColE7-KGNK was loaded. The column loaded with lysate was washed with 4–5 column volumes (CVs) of 100% buffer A1 (1 × PBS). The fusion proteins were cleaved on column with human rhinovirus C3 protease (Pre-scission protease) to remove the GST tag. Next 20µM of 10 mM C3 protease in 1x PBS was loaded on the column and incubation overnight at 4 ºC or 2 hours at RT followed by the elution with 1 x PBS. The eluted fractions were contained NColE7-KGNK in complex with the immunity protein. The pH of the mixture was adjusted to 3.0 after a 3x dilution with a 20 mM Gly/HCl buffer and then the components were loaded on a cation exchange column equilibrated with 20 mM Gly/ HCl pH 3.0. A gradient elution was 0-2 M NaCl in 1xPBS in 30 x CV. The immunity protein was eluted at pH 8.0 with 1x PBS containing 2M NaCl. The NColE7-KGNK was concentrated by 15 mL Amicon ultrafilter with 3 kDa and the buffer was exchanged to 20 mM HEPES, pH 7.7. The buffer of the purified product was exchanged to 20Mm HEPES (N-2-hydroxyethylpiperazine-N-2-ethane sulfonic acid) pH 7.7 using an Amicon ultra 15 mL centrifugal filter.

Protocol A5. Purification of His-tagged NColE7-KGNK

His-tagged NColE7-KGNK was purified in single step of immobilized metal ion affinity chromatography (Ni(II)-loaded Sepharose 6 Fast Flow resin in XK 16/20 column) with an ÄKTA HPLC explorer system. IMAC column (sepharose 6 FF resin chelated with Ni(II) packed in XK 16/20 column) was equilibrated with 20 mM Tris-HCl containing 400 mM NaCl, pH 7.5, then soluble fraction of the lysate containing targeted protein was loaded. The column loaded with lysate was washed with 5 column volumes (CVs) of 100% buffer A1 (20 mM Tris-HCl + 400 mM NaCl, pH 7.5). The second wash was by 0-10% 3.5 CV (14 min) of buffer B1 (500 mM imidazole in 20 mM Tris-HCl + 400 mM NaCl, pH 7.5) with a following gradient elution 10-100% in 7.5 CV (30 min) of buffer B and then kept at 100% for 1 CV (5 min). The elution buffer in the fractions containing the protein was concentrated to 5 mL by 15 mL Amicon Ultrafilter 3kDa and concentration was estimated by nanodrope to be 32 μM then 65 uL of 0.5 M EDTA was added to 5 mL targeted protein +10 mL 20 mM HEPES pH 7.7 followed incubation at 4C for 30 min. The buffer was exchanged to 20 mM HEPES pH 7.7 by15 mL Amicon Ultrafilter 3kDa.

Protocol A6. PAC measurements

Radioactive mercury was produced and collected in 150 μL of frozen milliQ water, as described previously [A30]. The following solutions were used for sample preparation (**Table A3**): 300 μL of 23.1 μM TEM-1 β- lactamase as stock solution in 20 mM Tris-HCl, pH 7.5; 100 μM $HgCl_2$ as stock solution; 10mM HEPES buffer solution, pH 7.4; and stock solutions for pH adjustment (1.0 M NaOH, 1.0 M $HClO_4$, 0.1 M NaOH, 0.1 M $HClO_4$). Sample 1 contains 3.0 μM enzyme and 2.7 μM $HgCl_2$ in 10 mM HEPES, pH 7.4, and 50 % (w/w) sucrose while sample 2 contains 3.0 μM enzyme and 5.7 μM $HgCl_2$ in 10 mM HEPES, pH 7.4, and 50 % (w/w) sucrose.Two PAC setups were used: the digital DIGIPAC [A31] equipped with six 1.5”×1.5” LaBr3(Ce) detectors and the analogue PERM [A32] equipped with six 1”×1” $CeBr_3$ detectors. Time resolutions were by averaging the time values that were obtained during determination of time zero (t_0) channels for the 30 individual spectra of detector pairs. The time resolutions were 0.6 ns and 0.5 ns. Time-per-channel calibrations of 0.04883 ns and 0.05068 ns were used for the digital and analog PAC setups, respectively. The purpose of the calibration was to give the same recorded frequency for the $Hg(II)(Cys)_2(s)$ sample for the two instruments. The recorded data was analyzed by the Winfit program (provided by Prof. T. Butz) using 600 data points. However, the first 10 points were excluded because the time zero (t_0) determination was uncertain near time zero. In

addition, a Lorentzian line shape was used to calculate the line broadening. It was given by the parameter δ, due to a static distribution of EFGs. Fourier transformation of the data and fitted results were performed using 600 points after mirroring 300 data points and a Keiser-Bessel function with the window parameter equal to 4.

For nuclear spin I = 5/2 (in case the intermediate nuclear state for which the NQI is measured in ^{199m}Hg PAC) and randomly oriented, static, identical Hg(II) ion sites, the so-called perturbation function [A33; A34] is given by the following:

$$A_{22}^{eff} G_{22}(t) = A_{22}^{eff} (a_0 + a_1 \cos(\omega_1 t) + a_2 \cos(\omega_2 t) + a_3 \cos(\omega_3 t))$$

where A_{22}^{eff} is the effective anisotropy, and a_i and ω_i depend on the NQI [A32; A35].

The experimental equivalent of $A_{22}^{eff}G_{22}(t)$, $R(t)$, is constructed as [A34]:

$$R(t) = 2\frac{W(180°, t) - W(90°, t)}{W(180°, t) + 2W(90°, t)}$$

where $W(180°,t)$ and $W(90°,t)$ are the geometrical mean of coincidence spectra recorded with 180° and 90° between detectors, after subtraction of random coincidences and adjustment to the same time = 0 for all 30 coincidence time traces. The data presented in the dissertation have been base-line shifted to zero. This has no effect on the fitted parameters.

References related to the Appendix

[A1] J. H. Ullah, T. R.Walsh, I. A. Taylor, D. C. Emery, C. S. Verma, S. J. Gamblin, J. Spencer. *J. Mol. Biol*. 284 (**1998**); 125-136.
[A2] A. Carfi, S. Pares, E. Duee, M. Galleni, C. Duez,, J. M. Frere, O. Dideberg. *EMBO J*. 14 (**1995**); 4914-4921.
[A3] N.O. Concha, B. A. Rasmussen, K. Bush, O. Herzberg. *Structure* 4 (**1996**); 823-836.
[A4] M. W. Crowder, J. Spencer, A. J. Vila. *Acc. Chem. Res*. 39 (**2006**); 721-728.
[A5] Z. Wang , W. Fast, A. M. Valentine, S. J. Benkovic. *Curr. Opion. Chem. Biol*. 3 (**1999**); 614-622.
[A6] M. Galleni, J. Lamotte-Brasseur, G. M. Rossolini, J. Spencer, O. Dideberg, J. M. Frere. *Antimicrob. Agents and Chemother*. 45 (**2001**); 660-663.
[A7] P. Nordmann, L. Poirel, T. R. Walsh, D. M. Livermore. *Trends Microbiol*. 19 (**2011**); 588-595.
[A8] G. Garau, C. Bebrone, C. Anne, M. Galleni, J. M. Frere, O. Dideberg. *J. Mol. Biol*. 345 (**2005**); 785-795.
[A9] A. Matagne, J.-M. Frere. *Biochim Biophys Acta* 1246 (**1995**); 109-127.
[A10] N.C. Strynadka, H. Adachi, S.E. Jensen, K. Johns, A. Sielecki, C. Betzel, et al., *Nature* 359 (**1992**); 700-705.
[A11] C. Damblon, X. Raquet, L.Y. Lian, J. Lamotte-Brasseur, E. Fonze, P. Charlier, et al., *PNAS USA*. 93 (**1996**) 1747-1752.
[A12] C.L. Tooke, P. Hinchliffe, E.C. Bragginton, C.K. Colenso, V.H.A. Hirvonen, Y. Takebayashi, J. Spencer. *J. Mol. Biol*. 431 (**2019**); 3472-3500.
[A13] A. Egorov, M. Rubtsova, V. Grigorenko, I. Uporov, A. Veselovsky. *Biomolecules* 9 (**2019**); 854.
[A14] X. Wang, G. Minasov, J. Blazquez, E. Caselli, F. Prati, B. K. Shoichet. *Biochemistry* 42 (**2003**); 8434-8444.
[A15] G. Minasov, X. Wang, B.K. Shoichet. *J. Am. Chem. Soc*. 124 (**2002**); 5333-5340.
[A16] M. Hernick, C.A. Fierke. *Arch. Biochem. Biophys*. 433 (**2005**); 71-84.
[A17] C.C. Chen, T. J. Smith, G. Kapadia, S. Wasch, L.E. Zawadzke, A. Coulson, O. Herzberg. *Biochemistry* 35 (**1996**); 12251-12258.
[A18] C.Jelsch, L. Mourey, J. M. Masson, J. P. Samama. *Proteins* 16 (**1993**); 364-383.
[A19] N.G. Brown, S. Shanker, B.V.V. Prasad, T. Palzkill. *J. Biol. Chem*. 284 (**2009**); 33703-33712.
[A20] D.C. Marciano, N.G. Brown, T. Palzkill. *Protein Sci*. 18 (**2009**); 2080-2089.
[A21] R.P. Ambler, A.F. Coulson, J.M. Frere, J.M. Ghuysen, B. Joris, M. Forsman, et al., *Biochem. J*. 276 (**1991**); 269-270.
[A22] R. James, C. N. Penfold, G. R. Moore, C. Kleanthous. *Biochimie* 84 (**2002**); 381-389.
[A23] Y. Ohno-Iwashita, K. Imahori. *Biochemistry* 19 (**1980**); 652-659.
[A24] K.R. Brunden, W.A. Cramer, F.S. Cohen. *J. Biol. Chem*. 259 (**1984**); 190-196.
[A25] C.N. Penfold, C. Garinot-Schneider, A.M. Hemmings, G.R. Moore, C. Kleanthous, R. James, *Mol. Microbiol*. 38 (**2000**); 639-649.
[A26] C. Garinot-Schneider, C.N. Penfold, G.R. Moore, C. Kleanthous, R. James. *Microbiology* 143 (**1997**); 2931-2938.
[A27] E. Bouveret, A. Rigal, C. Lazdunski, H. Benedetti. *Mol. Microbiol*. 23 (**1997**); 909-920.
[A28] C.J. Lazdunski, E. Bouveret, A. Rigal, L. Journet, R. Lloubes, H. Benedetti. *J. Bacteriol*. 180 (**1998**); 4993-5002.
[A29] A. Madadlou,S. O'Sullivan, D. Sheehan. *Methods Mol. Biol*. 681 (**2011**); 439-447.
[A30] A. Jancso, J. G. Correia, R. K. Balogh, J. Schell, M. L. Jensen, D. Szunyogh, et al., *Nucl. Inst. Meth. Phys. Res*. 1002 (**2021**); 165154.
[A31] M. Jager, K. Iwig, T. Butz. *Rev Sci Instr*. 82 (**2011**); 065105.
[A32] T. Butz , S. Saibene, T. Fraenzke, M. A. Weber. *Nucl. Instr. Meth. Phys. Res*. A284 (**1989**); 417-421.
[A33] H. Frauenfelder, R. M. Steffen . Alpha-, beta and gamma-ray spectroscopy. *North-Holland Pub. Co*. (**1965**); 997.
[A34] L. Hemmingsen, K.N. Sas, E. Danielsen. *Chem. Rev*. 104 (**2004**); 4027-4061.
[A35] T. Butz. *Hyperfine Interact*.73 (**1992**); 387-388.

Abbreviations

3D	three dimensional
AC	affinity chromatography
AGE	agarose gel electrophoresis
Amp	ampicillin
BL21, DH10B	names of *Escherichia coli* (*E. coli*) strains
bp	base pairs
CD	circular dichroism
Colicins E2, E7, E8, and E9	colicin endonucleases 2, 7, 8, and 9
CV	column volume
DEAE-C (DE-52)	diethylaminoethyl diethylaminoethyl cellulose
DNA	deoxyribonucleic acid
DSB	double strand break
dsDNA	double strand DNA
EcoRI, FokI, NdeI, XhoI	names of restriction endonuclease enzymes
EMSA	electromobility shift assay
eq.	equivalent
ESBLs	extended-spectrum β-lactamases
ESI	electrospray ionization
FF	fast flow
GST	glutathione-S-transferase
HEPES	(4-(2-hydroxyethyl)-1-piperazineethanesulfonic acid)
His-tag	6×histidine residues sequence
HPLC	high performance liquid chromatography
Im7	immunity protein 7 is natural inhibitor protein of colicin E7
IMAC	immobolized metal ion affinity chromatography
I-PpoI	intron-encoded endonuclease from *Ph. polycephalum*
IPTG	isopropyl β-D-1-thiogalactopyranoside
Kan	kanamycin
KGNK	446-KGNK-449 part of the mutant NColE7 sequence
KGNK-His	446-KGNK-449 part of the NColE7 sequence with 6 His residues on C-terminus
LB	lysogeny broth or commonly Luria-Bertani medium
M9	minimal growth medium
MBLs	metallo-β-lactamases
Mono-Q	strong anion exchanger prepacked with MonoBeads in a tricorn-column
MS	mass spectrometry
NColE7	nuclease domain of colicin Endonuclease 7
NFI-BD	Nuclear factor I binding domain
NFI-BDH	NFI-BD mutant: histidine instead of glutamine at position 164
Q-sepharose	quaternary ammonium (Q) strong anion exchange groups
QSS	quasi-steady state
RMSD	root mean square deviation
RNA	ribonucleic acid
Sephadex G-75	gel filtration resin for desalting and buffer exchange of large biomolecules
SOS	save our souls
SRCD	synchrotron radiation circular dichroism
TAE	tris(hydroxymethyl) aminomethane, acetic acid and ethylenediaminetetraacetic acid
Taq	thermus aquaticus
TEM	temoneira
TOF	time of flight
Tris-HCl	tris (hydroxymethyl) aminomethane-hydrochloric acid
UV	ultraviolet
Vis	visible
BES-β-lactamase	Brazil extended-spectrum β-lactamase
GES-β-lactamase	Guiana-extended spectrum β-lactamase

IBC-β-lactamase	integron-associated class A β-lactamase with extended-spectrum
PER-β-lactamase	Pseudomonas extended resistant β-lactamase
SFO-β-lactamase	Serratia fonticola β-lactamase
TLA-β-lactamase	Tlahuica β-lactamase
VEB-β-lactamase	Vietnam extended-spectrum β-lactamase
A	adenine
C	cytosine
G	guanine
T	thymine
A, Ala	alanine
C, Cys	cysteine
D, Asp	aspartic acid
E, Glu	glutamic acid
F, Phe	phenylalanine
G, Gly	glycine
H, His	histidine
I, Ile	ioleucine
K, Lys	lysine
L, Leu	leucine
M, Met	methionine
N, Asn	asparagine
P, Pro	proline
Q, Gln	glutamine
R, Arg	arginine
S, Ser	serine
T, Thr	threonine
V, Val	valine
W, Trp	tryptophan
Y, Tyr	tyrosine